Design and Simulation of Vehicle-to-Load System with Nissan Leaf

Tolga Osmancık

A Thesis

in

The Department

of

Electrical and Computer Engineering

Presented in Partial Fulfillment of the Requirements

for the Degree of

Master of Applied Science (Electrical and Computer Engineering) at

Concordia University

Montréal, Québec, Canada

December 2023

CONCORDIA UNIVERSITY
SCHOOL OF GRADUATE STUDIES

This is to certify that the thesis prepared

By: Tolga Osmancık

Entitled: Design and Simulation of Vehicle-to-load System with Nissan Leaf

and submitted in partial fulfillment of the requirements for the degree of

Master of Applied Science (Electrical and Computer Engineering)

complies with the regulations of this University and meets the accepted standards with respect to originality and quality.

Signed by the final examining committee:

_____ Chair
Dr. Chunyan Lai

_____ Internal Examiner
Dr. Mohsen Ghafouri

_____ Supervisor
Dr. Pragasen Pillay

Approved by: _____
Dr. Yusef R. Shayan, Chair
Department of Electrical and Computer Engineering

_____
Dr. Mourad Debbabi, Dean,
Faculty of Engineering and Computer Science

ABSTRACT

Design and Simulation of Vehicle-to-Load System with Nissan Leaf

Tolga Osmancık

The fact that the Global Warming problem poses a more significant threat to our society every day has pushed us to use energy more efficiently and cleanly. Using power more efficiently in every aspect of our lives can pave the way for achieving the goal of reducing global gas emissions and saving the planet. This can be done by applying various approaches. One of the most effective ways is to use electric car technology, which is one of the best ways not to cause more carbon emissions and to increase energy efficiency and savings.

This study aims to design and simulate a vehicle-to-load system using an electric vehicle, Nissan Leaf, to power emergency independent loads of the Future Building Laboratory (FBL). The FBL is a solar research house at the Loyola Campus of Concordia University, Montréal, Canada. This research facility is built to investigate numerous renewable energy systems that can help achieve the net-zero energy goal for a typical detached single-family dwelling in Québec. It has integrated renewable energy sources such as solar, solar-thermal, and wind, allowing the opportunity to test different power management scenarios.

In this research, the vehicle-to-load system of the FBL and Nissan Leaf is designed and simulated in MATLAB software, considering the house's rated load and the real-life system's exact ratings. The design reflects the actual characteristics of the load, EV battery, and power electronic elements in interaction. The simulation is a straightforward model of the actual system.

The last step is to validate the simulation results. The simulation model was tested experimentally at the PEER group laboratory at Concordia University, using the available converters, devices, and a real-time DSP microcontroller. Various experiments are conducted to observe the system's performance in real conditions. All time-domain and frequency-domain results match the ones obtained via simulation.

Methods for enabling the discharging feature of EVs that utilize CHAdeMO are studied and explored. The structure of the CHAdeMO connector and charging sequence are explained. Possible integration methods for Vehicle-to-Home are also explored.

Acknowledge

I want to express my genuine gratitude to my supervisor, Professor Pragasen Pillay, who provided this opportunity to me so that I could further explore science under his valuable supervision.

I would like to sincerely acknowledge the guidance of Dr. Akrem Aljehaimi and Dr. Mathews Boby throughout this research.

I also cordially thank my colleagues who created a home-like atmosphere in the PEER group laboratory. Nazanin, Amir, Sumeet, Yupeng, Gayathri, Mohanraj, Tamanwe, Neetusha, Bassam, Zahra, Talha, Tshamala, and Gabriel.

Finally, I would like to express my heartfelt appreciation to my parents Hülya and Oktay, and my beloved sister Dilara.

Table of Contest

List of Figures

List of Tables

Nomenclature

A	Ampere
AC	Alternative Current
Ah	Ampere-Hour
C	Capacitor
C_{bin}	Initial Current Capacity
DC	Direct Current
EMI	Electromagnetic Interference
EMS	Energy Management System
EV	Electric Vehicle
F	Farad
f	Frequency
FBL	Future Building Laboratory
h	Hour
H	Henry
hp	Horsepower
Hz	Hertz
I	Current
I_{nc}	Nominal Current Capacity
I_{batt}	Battery Current
kW	Kilowatt
kWh	Kilowatt-Hour
LC	Inductor- Capacitor
Min	Minute
mm	Millimetre
N_c	Number of Cells
N_{cs}	Number of Cells connected series
OCV	Open Circuit Voltage

P_{batt}	Battery Power
PCC	Point of Common Coupling
PHEV	Plug-in Hybrid Electric Vehicles
PWM	Pulse Width Modulation
R	Resistance
R_{batt}	Battery Resistance
RC	Resistance-Capacitor
SOC	State of Charge
UPS	Uninterruptable Power Supply
V	Voltage
V2G	Vehicle-to-Grid
V2H	Vehicle-to-House
V2L	Vehicle-to-Load
V2X	Vehicle-to-Everything
V_{batt}	Battery Voltage
V_{nb}	Nominal Voltage of the Battery Pack
V_{nc}	The Nominal Voltage
V_{oc}	Open Circuit Voltage
V_{occell}	Open Circuit Voltage of Cell
W	Watt
Wh	Watt-Hour

1 Introduction

1.1 Introduction

This section seeks to answer the question of why this research is conducted. A brief explanation of emergency power, bidirectional charging, and electrical cars are given, followed by the importance of energy efficiency. Next, the case study of this thesis is explained in detail.

1.2 Emergencies and Back-up Power

Six time zones, three oceans, mountains, plains, forests, and tundra are all features of North America. It experiences a variety of weather patterns, from Arctic to mild, apparently never-ending rain to drought, paralyzing cold to heat waves. With so many different types of weather and landforms, the potential for extreme weather and geological events is a constant reality.

When a natural hazard affects people to the extent that the community involved needs assistance dealing with the harm that has occurred to people, and possibly the surrounding property and environment, the event becomes known as a disaster [1]. These disasters are causing emergencies and power loses. Outages due to weather-related reasons such as storms and severe weather, cold and ice, hurricanes, tornadoes, etc. have doubled since 2003 [2]. Figure 1-1 shows the power outages data of north America due to extreme weather in 28 years.

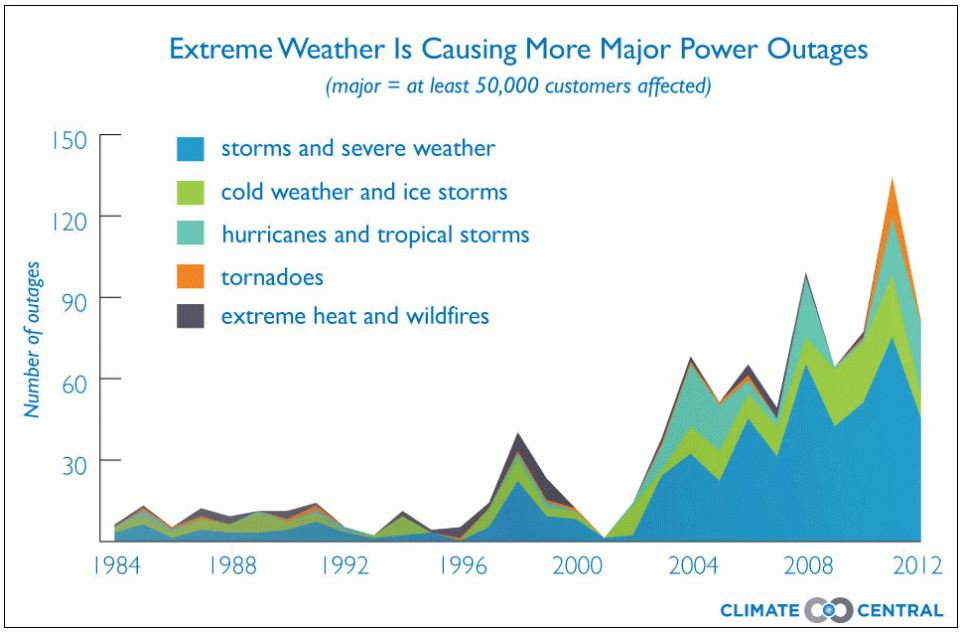

Figure 1-1: Analysis of 28 years of power outage data of North America [2].

The necessity for emergency backup power is more crucial than ever in our technologically advanced and networked society. Unexpected occurrences like bad weather, natural disasters, or equipment malfunctions can result in extensive power outages, which could impair vital services and pose serious hazards to public safety, health, and economic stability. Critical facilities, such as hospitals, data centers, communications networks, and emergency response centers, can maintain their essential operations and guarantee that life-saving machinery, crucial data, and crucial communication lines remain functional during emergencies by having an emergency backup power system. Furthermore, backup power systems can lessen how long-lasting power outages affect homes and businesses, giving communities a sense of security and readiness as they handle challenging conditions.

1.3 Backup Power Options

There are several backup power options available to ensure a constant supply of electricity during power outages. Some of the most common options include:

- Generators. Generators are engines that transform mechanical energy into electrical energy. They can run on a variety of fuels (including natural gas, diesel, and propane) and come in a variety of sizes [3].
- Uninterruptible Power Supply (UPS). When the main power supply fails, a UPS system supplies temporary power to a device. It is typically made up of a battery and an inverter that converts DC power to AC power [3].
- Solar Panels with Battery Storage. Solar panels use sunshine to create electricity, and when combined with battery storage, they may offer backup power during disruptions [3].
- Fuel Cells. A chemical reaction, often including hydrogen and oxygen, generates energy in fuel cells. They provide a clean and efficient backup power supply [4].
- Flywheel Energy Storage. Flywheel systems store kinetic energy in a rotating mass, which can be converted back into electrical energy when needed [5].
- Thermal Energy Storage. This system stores energy in the form of heat, which can be later converted into electricity using a heat engine or a thermoelectric generator [6].

Each of these options has its advantages and disadvantages. Therefore, it is essential to consider factors such as cost, availability, efficiency, and environmental impact when selecting a backup power solution.

1.4 Electrical Vehicle as a Backup Power

Electric vehicles (EVs) have the ability to act as a backup power supply in case of emergencies in addition to being a sustainable form of mobility. EVs with sizable battery packs have the capacity to store a lot of energy that can be utilized in power outages. This idea, also referred to as "vehicle-to-grid" or "vehicle-to-home," enables electricity to be extracted from a car's battery and utilized to power a house or other electrical equipment. This ground-breaking approach not only ensures a steady supply of electricity during blackouts but also supports a stable grid and effective energy management. The significance of electric vehicles as backup power sources is anticipated to grow as their uptake rises, underscoring the many advantages of switching to more environmentally friendly modes of transportation.

Using an electric car as a backup power source is an emerging concept, known as Vehicle-to-Home (V2H) or Vehicle-to-Grid (V2G). With this setup, the electric vehicle's battery can be used to power your home during an outage or to provide electricity back to the grid, as needed. Here's how it works.

I. Bi-directional Charging: Electric vehicles (EVs) require a bidirectional charger that allows power to flow to and from the vehicle's battery. This allows the EV to take power from the grid for charging and send it back to the home or grid as needed [7].
II. Power Inverter: A power inverter is necessary to convert the DC power from the EV's battery to AC power, which is used by most household appliances [7].
III. Energy Management System (EMS): An EMS helps manage the power flow between the electric vehicle, home appliances, and the grid. This system ensures that the EV's battery is used efficiently and prevents overloading [7].

Using an electric car as a backup power source has several advantages:

- Eco-friendly: EVs generate zero emissions when providing backup power, making them environmentally friendly [8].
- Cost-effective: If you already own an electric car, using it as a backup power source can save you the cost of purchasing a separate generator or other backup power system [8].

However, there are some limitations:

- Limited Capacity: The EV's battery capacity may not be sufficient to power an entire home for an extended period, especially if the car is needed for driving during the outage [9].
- Battery Degradation: Frequently using an EV's battery as a backup power source may cause faster battery degradation over time [8].

In summary, using an electric car as a backup power source can be a viable and eco-friendly option, but it's essential to consider the limitations and ensure you have the necessary equipment to support the setup.

1.5 V2G, V2H and V2L Technologies

1.5.1 V2G Technology

Vehicle to Grid (V2G) concept is one of the smart grid technologies, which involves the EV to improve the power system operation. V2G concept allows the energy exchange between EV and the power grid. A bidirectional charger is an advanced EV charger capable of charging and discharging energy from an electric vehicle battery. The AC/DC converter is used to rectify the AC power from the power grid to the DC power during the EV charging mode and inverts the DC power to the AC power before injecting back to power grid in the discharging mode [8]. This bi-directional energy transfer has the potential to improve grid stability, reduce peak demand, and increase the utilization of renewable energy sources. As the number of EVs on the road grows, V2G technology can turn them into a vast, distributed energy storage system, effectively leveraging their batteries during periods of low demand or high renewable generation. In return, EV owners could benefit from reduced charging costs or even generate revenue by participating in demand-response programs [8]. Although technical and regulatory challenges still need to be addressed, V2G technology holds significant promise for transforming the energy landscape and promoting sustainable transportation. The system is shown in Figure 1-2.

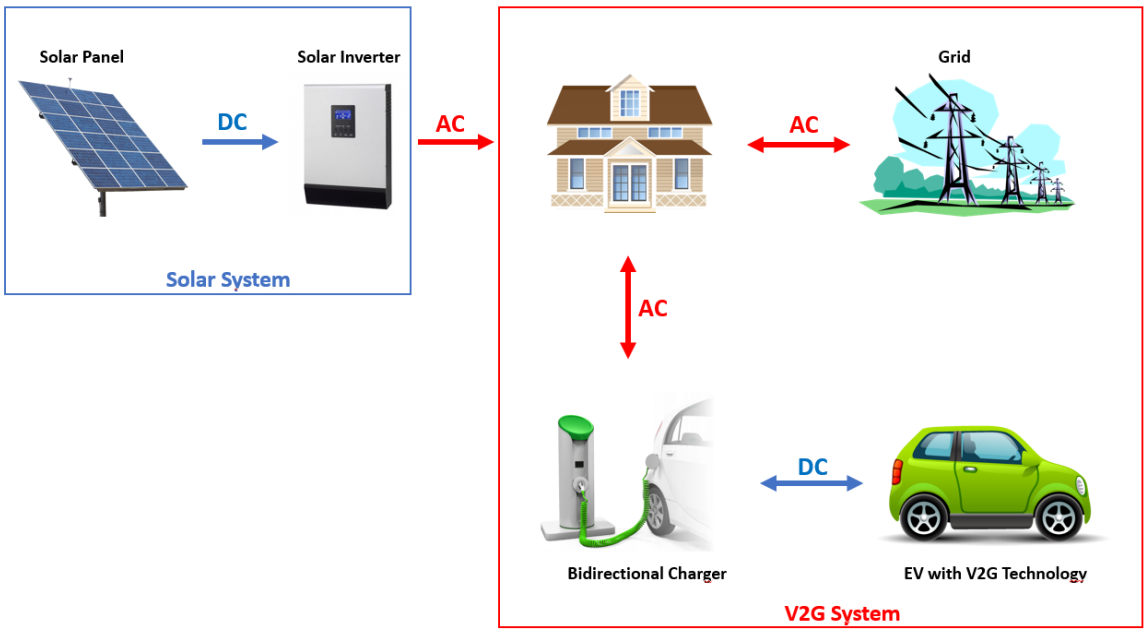

Figure 1-2: Vehicle to Grid system with solar system.

1.5.2 V2H Technology

During power outages or times of heavy electricity demand, electric cars (EVs) can serve as a backup power source for households thanks to vehicle-to-home (V2H) technology. A stable and sustainable power source is made possible by V2H systems, which enable the energy stored in an EV's battery to be transported back to the home's electrical grid through a bi-directional charger [10]. Utilizing electric vehicles' energy storage capabilities, V2H not only improves energy resilience but also helps to optimize energy use, lower power prices, and facilitate the integration of renewable energy sources like V2G systems [10]. Additionally, the development of smart grids and the creation of a more effective and sustainable energy ecology are both greatly aided by this technology. [9].

1.5.3 V2L Technology

Electric vehicles (EVs) can serve as mobile power sources for a variety of electrical gadgets and appliances thanks to vehicle-to-load (V2L) technology. Electric vehicles might become important energy assets thanks to V2L technology, making the energy grid more adaptable and durable. Additionally, V2L enables EVs to store excess solar or wind-generated electricity and release it when needed, maximizing the use of renewable energy and minimizing dependency on conventional power systems. [9].

1.6 Electrical Vehicles with V2H or V2G Technology

Vehicle-to-Grid (V2H) technology allows electric vehicles (EVs) to supply electricity back to the grid or directly to homes during power outages or peak demand periods. Several EV manufacturers have been working on V2H technology, and some of the electric cars that support or are expected to support V2H include:

- Nissan Leaf: Nissan has been a pioneer in V2H technology, and the Nissan Leaf has been compatible with V2H systems in Japan for years. However, availability in other markets may vary [11].
  Battery: 60 kWh
  Range: 342 km
- Mitsubishi Outlander PHEV: Mitsubishi's plug-in hybrid electric vehicle, the Outlander PHEV, also supports V2H technology in some markets [12].
  Battery: 20 kWh
  Range: 61 km
- F-150 Lightning: Unlike the Leaf's V2G charging, which is targeted toward fleets, the 2022 Ford F-150 Lightning offers V2H for individual owners through its available Intelligent Backup Power charging system. Using an 80 A charger with up to 131 kWh of electric energy storage [13].
- The 2022 Hyundai Ioniq 5 and Kia EV6: Each offer V2L capability with high-current outlets that can power appliances or provide backup power when needed. Their shared vehicle platform uses an Integrated Charging Control Unit that supplies up to 3.6 kilowatts of power to charge large items like electric bikes or camping equipment [13].

Please note that the availability of V2H technology may vary depending on the market, and not all electric vehicles with V2H capabilities may be available in every region. Additionally, V2H technology requires compatible charging equipment and local grid infrastructure, which may not be present in all areas.

1.7 Future Buildings Laboratory (FBL)

Future Buildings Laboratory (Figure 1-3), which is in Loyola Campus, is a research facility for buildings of the Future. The exact location of the house is shown in Figure 1-4. The house also supports electrical vehicles. There is also an electrical vehicle with vehicle to grid system. Via this vehicle, it is

planned to investigate the possibility of supplying power to Future Buildings Laboratory. In addition, it is planned to investigate the possibility of evacuation of people in distress by providing energy to elevators such as in old age residences.

Figure 1-3: Future Buildings Laboratory (FBL).

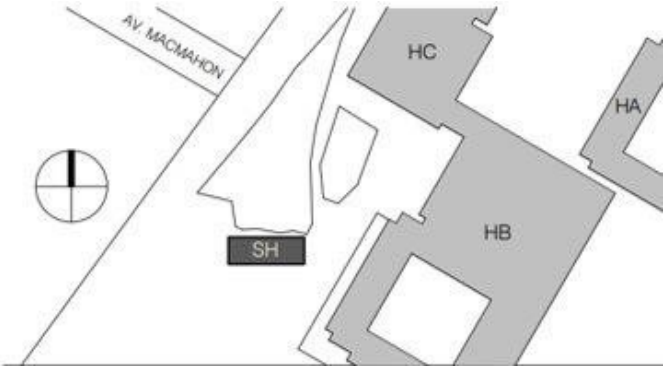

Figure 1-4: Location of the FBL in Loyola Campus shown as SH building in the map.

1.8 Thesis Limitations

Unfortunately, the purchased 2018 Nissan Leaf for the solar house project had an accident and went total loss. For this reason, the experimental results at the Future Building Laboratory couldn't be performed with an electric vehicle. However, the EV replacement purchase has been done, and the new Nissan Leaf is expected to arrive by the end of November 2023. This will allow testing the designed inverter and the presented V2L and V2H approaches with the Nissan Leaf at the solar house.

1.9 Thesis Organization

The thesis is organized as follows.

Chapter 2. This chapter reviews the future building laboratory regarding the installed solar system, electrical aspects of building, and load characteristics used in this thesis.

Chapter 3. In this chapter, electric car battery types are examined. Calculations of the car battery to be used are made. Finally, battery model and simulation are done.

Chapter 4. In this chapter, all parts of the simulation are studied and designed. Inverter, LC filter, and control parts are explained. Transfer functions are calculated and control parameters are obtained. Finally, system simulation is carried out.

Chapter 5. In this chapter, a V2L circuit is built in the laboratory. The built circuit is tested and the results are compared with the simulation results.

Chapter 6. In this chapter, the various V2L and V2H methods using Nissan Leaf at the solar house were explored. The CHAdeMO working principle and the enabling of EVs' discharging feature were dissuaded and explained.

Chapter 7. Conclusion and future work.

1.10 Contribution

Out of this thesis, a conference paper has been published in IEEE power electronics and drive system conference.

T. Osmancik, A. M. Aljehaimi and P. Pillay, "An Electric Vehicle Circuit for Powering Independent Loads," *2023 IEEE 14th International Conference on Power Electronics and Drive Systems (PEDS)*, Montreal, QC, Canada, 2023, pp. 1-5, doi: 10.1109/PEDS57185.2023.10268828.

Moreover, this research work has been scored the First poster award for M.A.Sc. Program at "The department of electrical and computer engineering 7th graduate student research conference (GSRC 2023)".

2 Future Buildings Laboratory

2.1 Introduction

In this chapter, the installed solar system in the FBL, electrical aspects of the building, and used load characteristics are brought into further details.

2.2 Building Specifications

The FBL has 103 m^2 of ground floor area consisting of 6 cells (among which 4 are test cells), electrical room, mechanical room, and 24 m^2 of mezzanine area. Figures 2-1 and 2-2 show the maps of the ground floor and the mezzanine. The house has Building Integrated Photovoltaics in one of the test cells and Semi-Transparent Photovoltaics in three other test cells. The roof of the house has three racks for the installation of PV panels in the future. The house also supports electrical vehicles, fuel cells, and wind turbines.

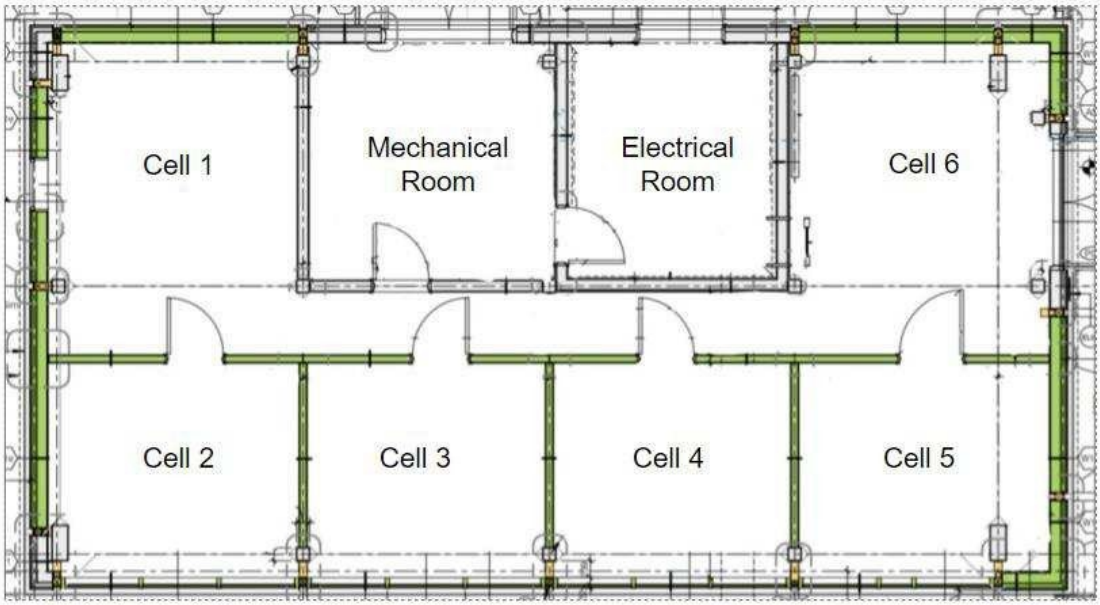

Figure 2-1: Map of the ground floor.

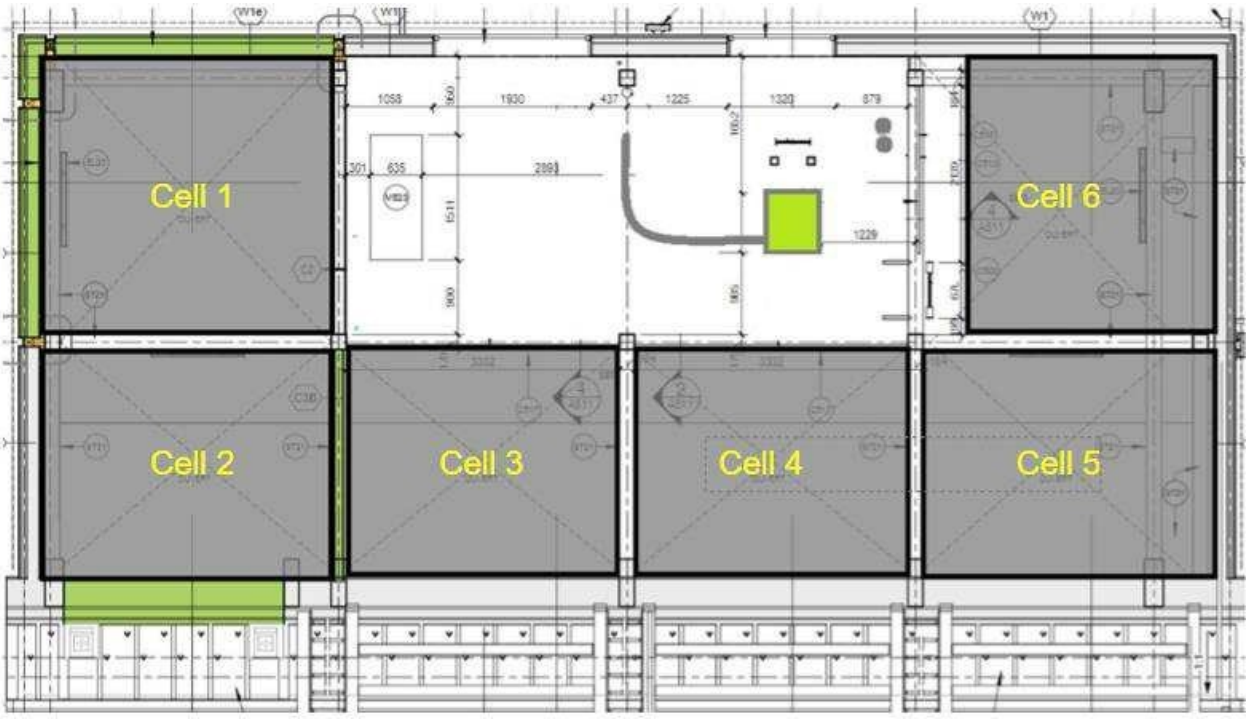

Figure 2-2: Map of the mezzanine.

2.3 Solar System

The details of the solar power system are brought along with the characteristics of the devices used.

2.3.1 Solar power system and devices

Based on the specifications of the house such as its size, load, resources, etc., a commercial system was designed to benefit from the solar energy captured via PV panels. The knowledge of the house's original electrical system was needed to find the best way of connecting the solar power system. A block diagram of the original system is shown in Figure 2-3. The grid input of 600 V and 225 A is connected to the Δ-Y 600-120/208 V, 150 kVA transformer. The stepped-down voltage is connected to the distribution panel which then feeds the loads. The total load of the house is 70 kVA.

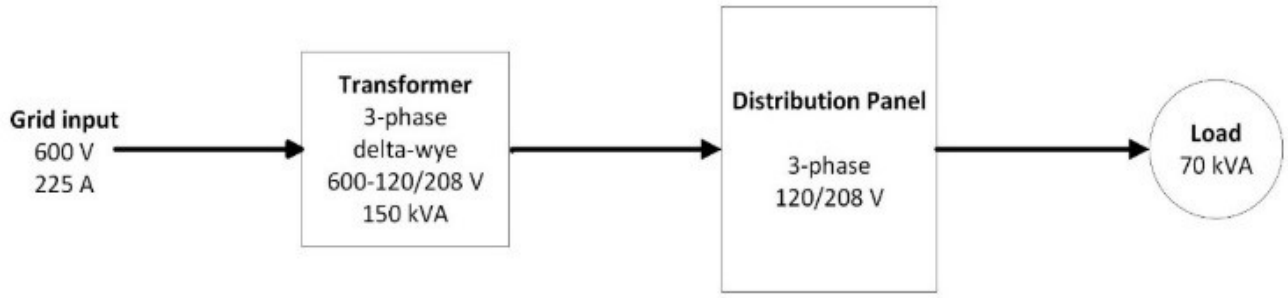

Figure 2-3: Block diagram of the electrical system of the house.

The connection is done in a way that there will be no interference with the original system. The system consists of three grid-following inverters, three grid-forming inverters, and six batteries. The connection of the solar power devices is illustrated by the block diagram in Figure 2-4. The output of each grid-following inverter is connected to two lines at the PCC, and the output of each grid-forming inverter is connected to a single line. So, the three inverters of each type will make a three-phase connection at the PCC to feed the three-phase load. The system was sized by an electrician and the devices were ordered accordingly.

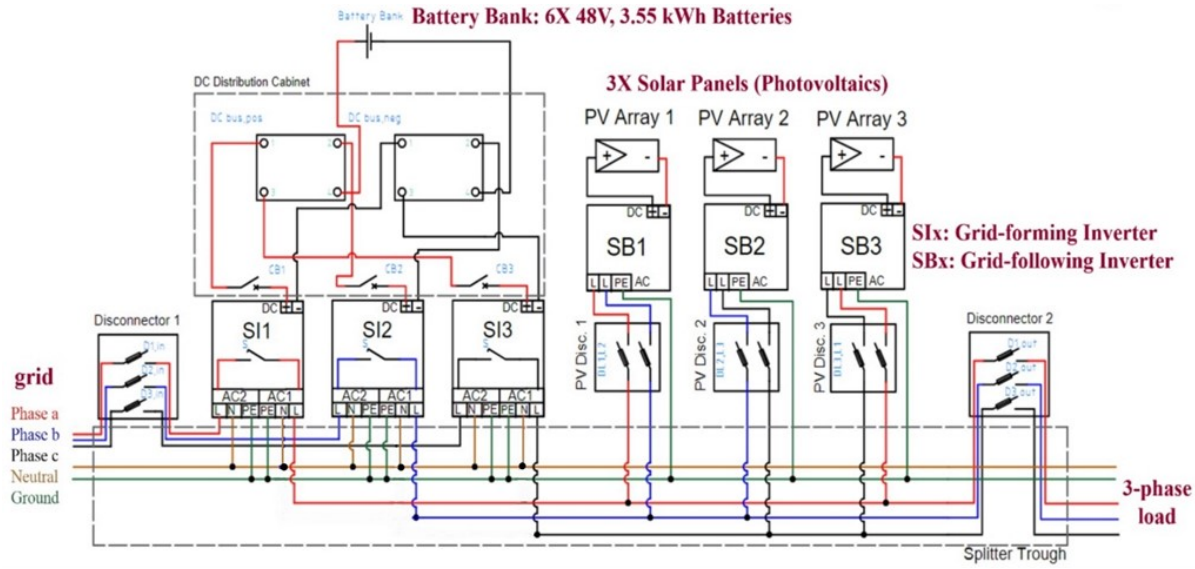

Figure 2-4: Block diagram of the connections of solar power system devices.

The system to be created is planned to be connected to the grid forming inverter as a single phase while the FBL's system operates independently of the grid. The loads connected to the grid forming inverter through single phase will be powered by the vehicle-to-house system created.

2.4 House Load

As will be discussed in the following sections, the aim of this thesis is to use the electric car battery during emergency to provide sufficient power to the household and office appliances used within the FBL to continue their operation. For this reason, the household load is examined in this section. These appliances are shown in Table 2-1.

Table 2-1 Load Table

Load type	Qty.	Power (W)	Usage Time (h)	Consumption (Wh/day)
Laptop	8	70	6	3360
Fridge	1	125	7	875
Fluxstream Strip 4’	2	45	8	720
Fluxstream Strip 8’	1	90	8	720
Wall Mount Led	1	35	8	280
Led High Bay (375mm)	1	87	8	696
Led High Bay (610mm) 16L	1	125	8	1000
Led High Bay (610mm) 20L	1	142	8	1136
Exit Signaling	1	12	8	96
Dual Headlight	1	3	8	24
Kettle	3	1000	0.25	750
Microwave	1	1300	0.2	260
Smart Phone	1	10	1	10

Exit Signaling Combined With Double Headlight	1	60	8	480
TOTAL				10407 Wh
PEAK				3104 W

2.5 Transient and steady-state current of house appliances

For better understanding of the house loads and to examine the maximum power to supply, the transient current for some house loads is examined.

2.5.1 Microwave

Microwave was operated with grid power. Transient and steady state currents were observed. Transient current has been observed as high as 65 A. The measured waveforms captured by the oscilloscope are shown in Figures 2-5, 2-6, and 2-7.

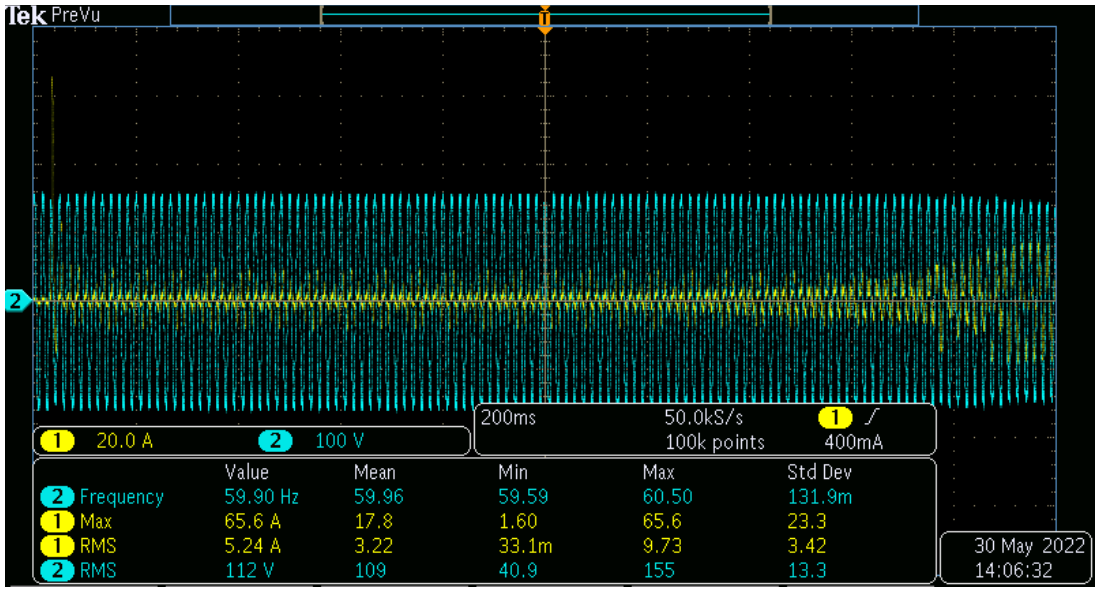

Figure 2-5: Microwave's current/voltage measurement.

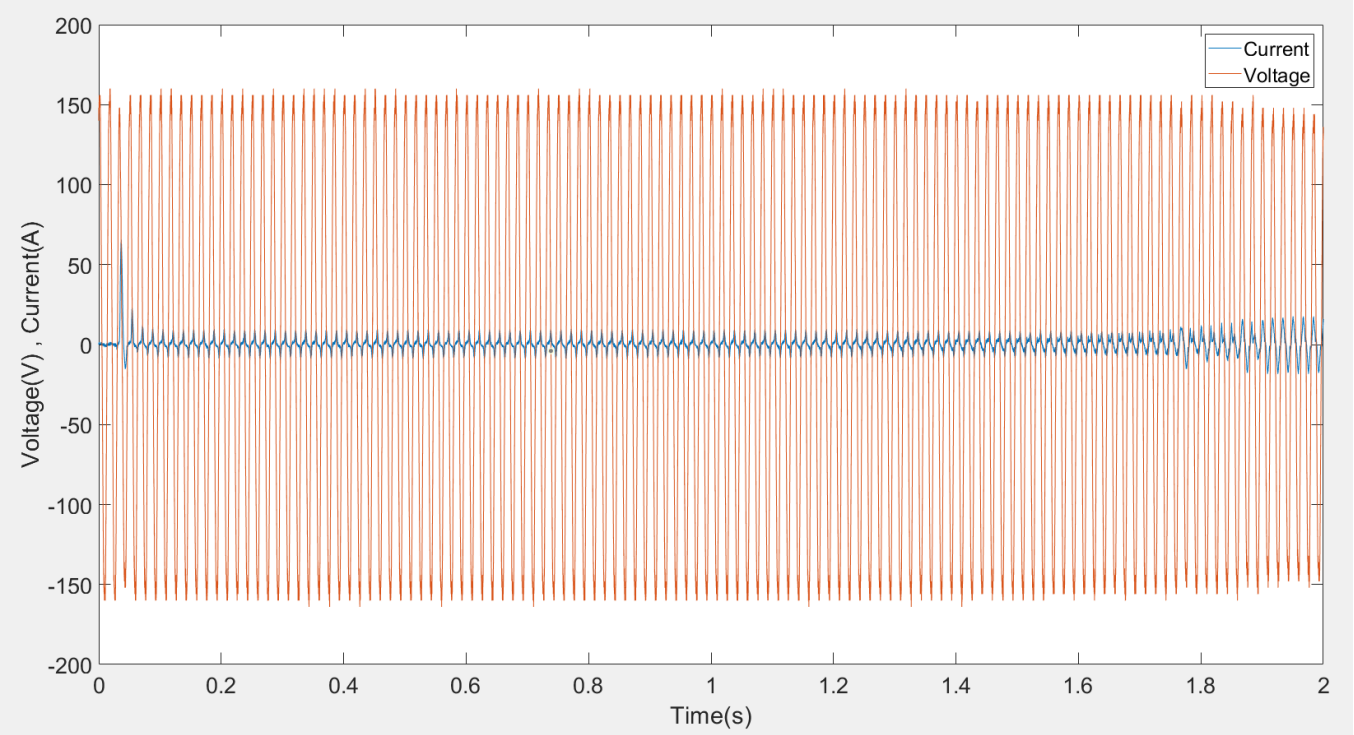

Figure 2-6: Microwave's current and voltage vs time.

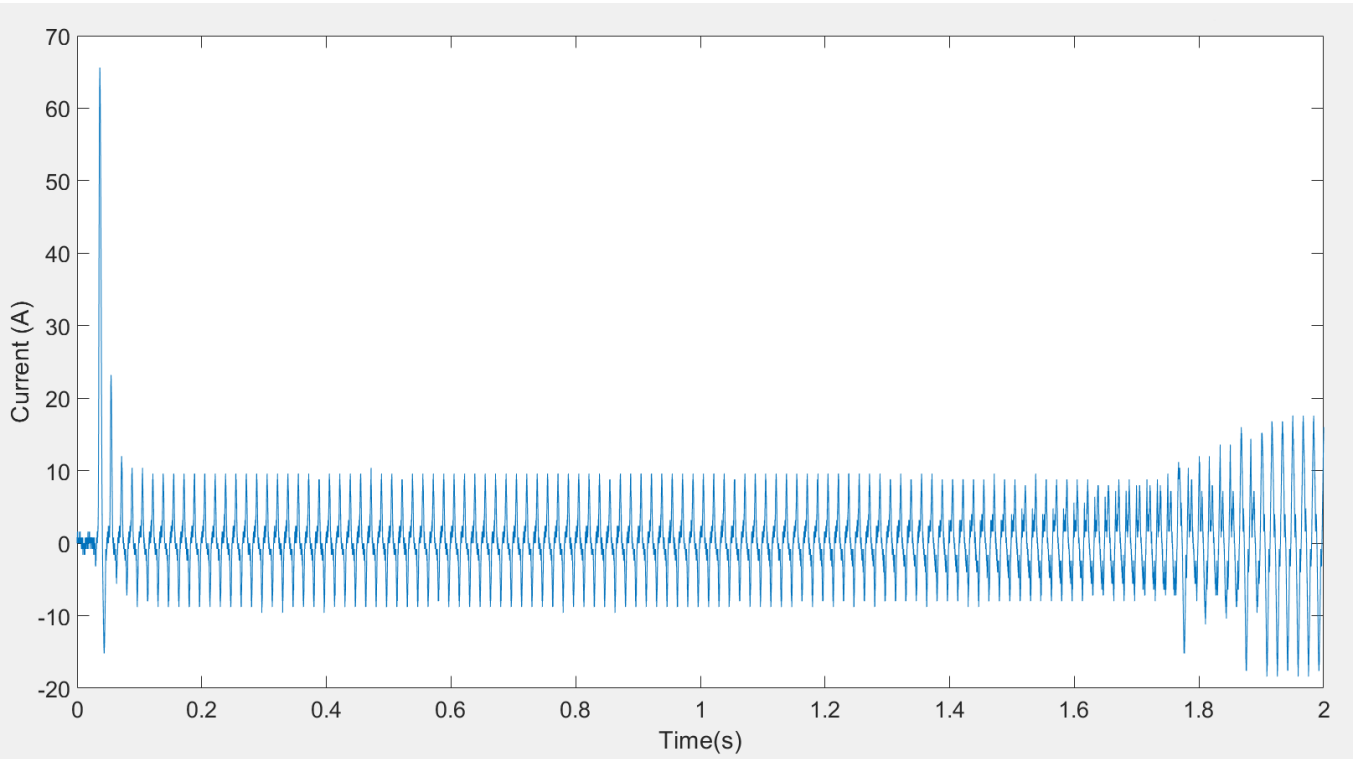

Figure 2-7: Microwave's current vs time.

2.5.2 Kettle

The kettle, which has a resistive structure, was operated with grids power, and transient and steady state currents were observed. The results captured by the oscilloscope are shown in Figures 2-8, 2-9 and 2-10.

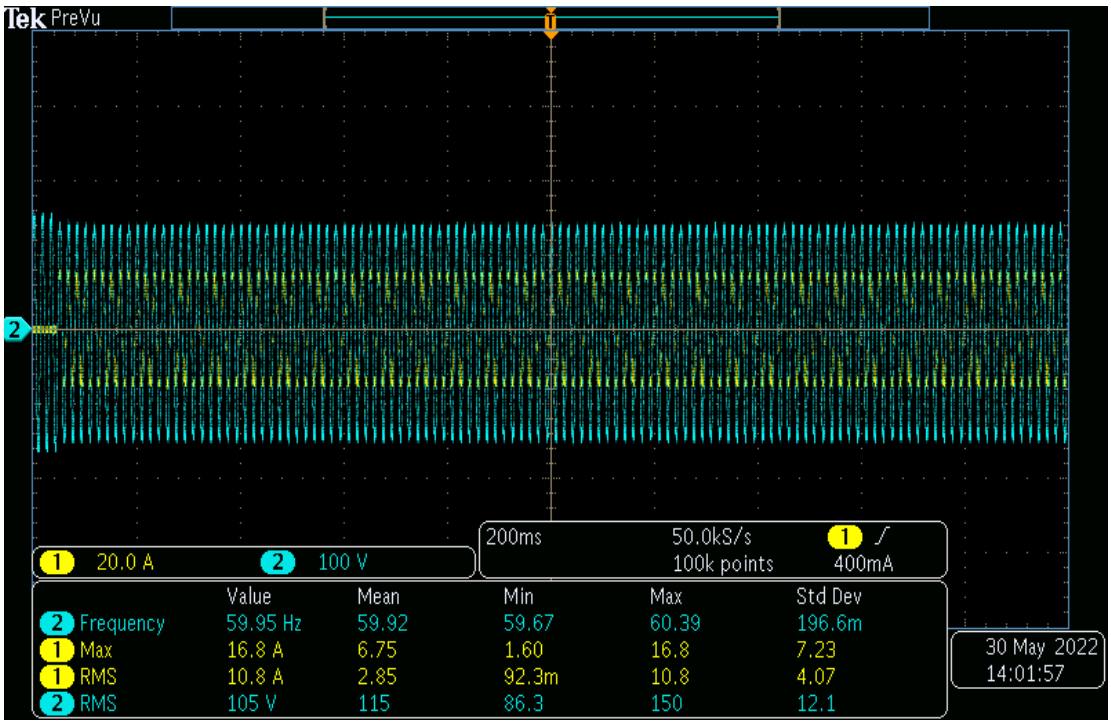

Figure 2-8: Kettle's current and voltage measurement by oscilloscope.

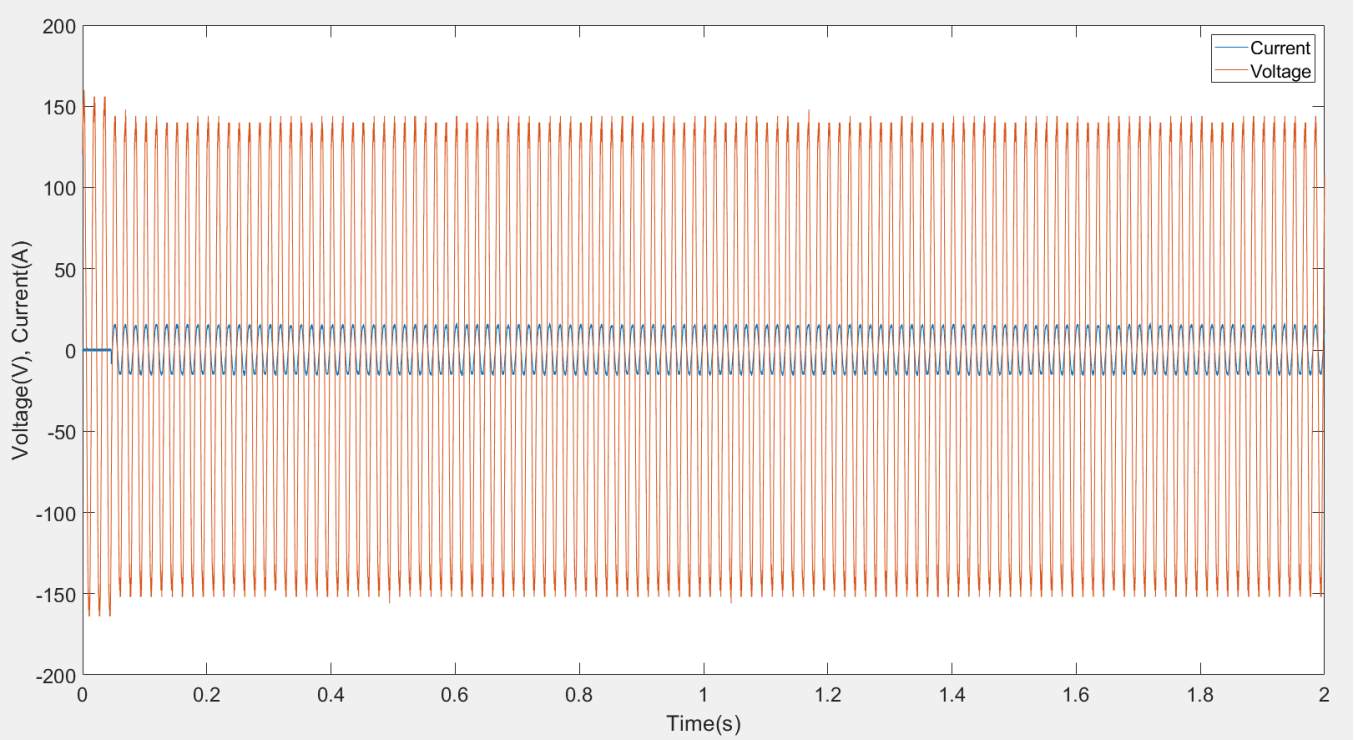

Figure 2-9: Kettle's current and voltage vs time.

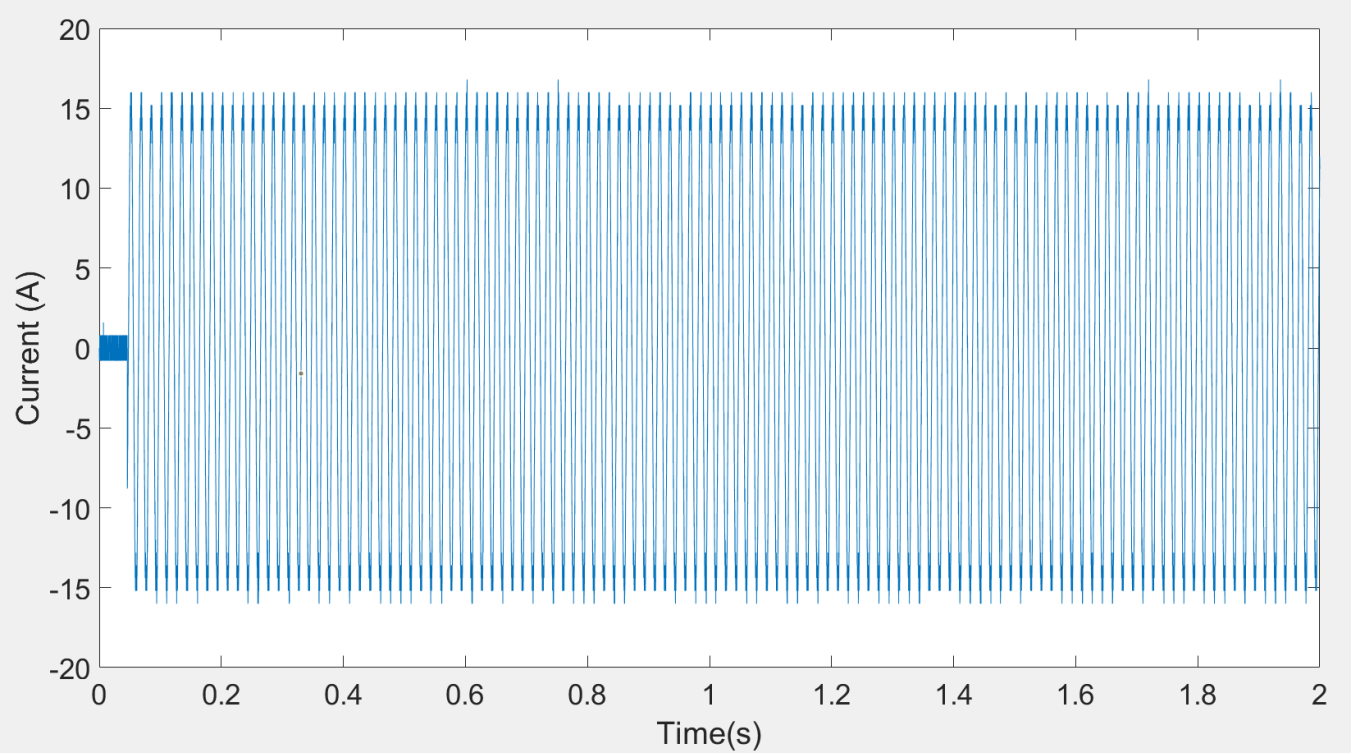

Figure 2-10: Kettle's current vs time.

2.5.3 Laptop

Transient and steady-state currents are observed. The results are shown in Figures 2-11, 2-12, and 2-13.

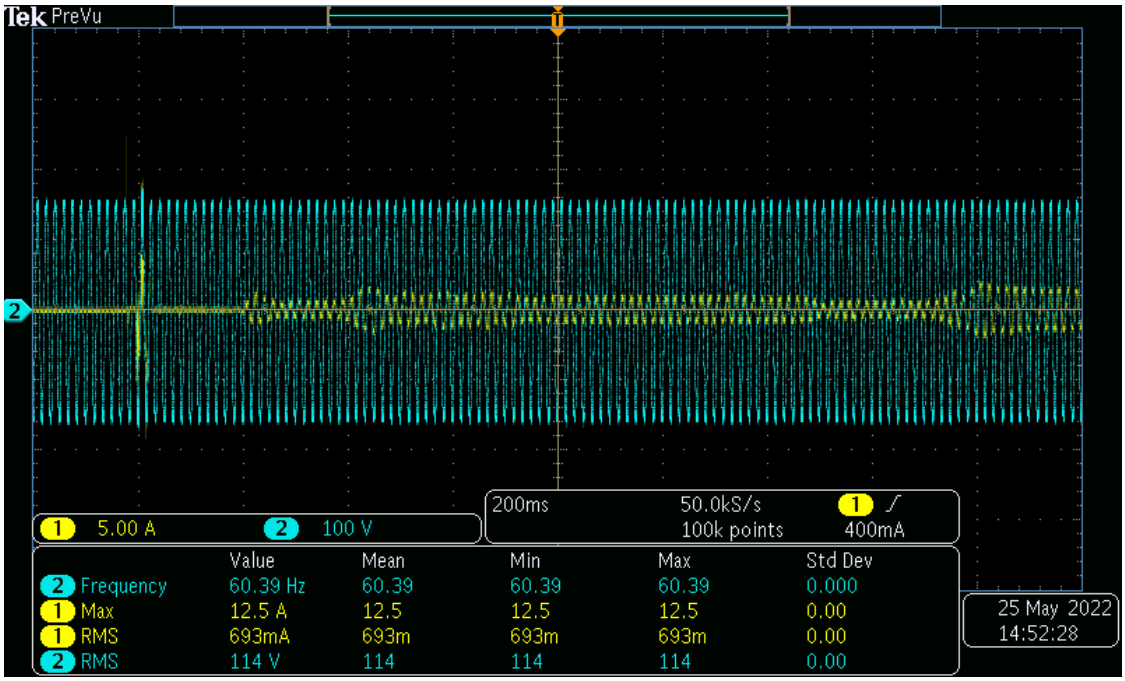

Figure 2-11: Measured laptop's current and voltage waveforms.

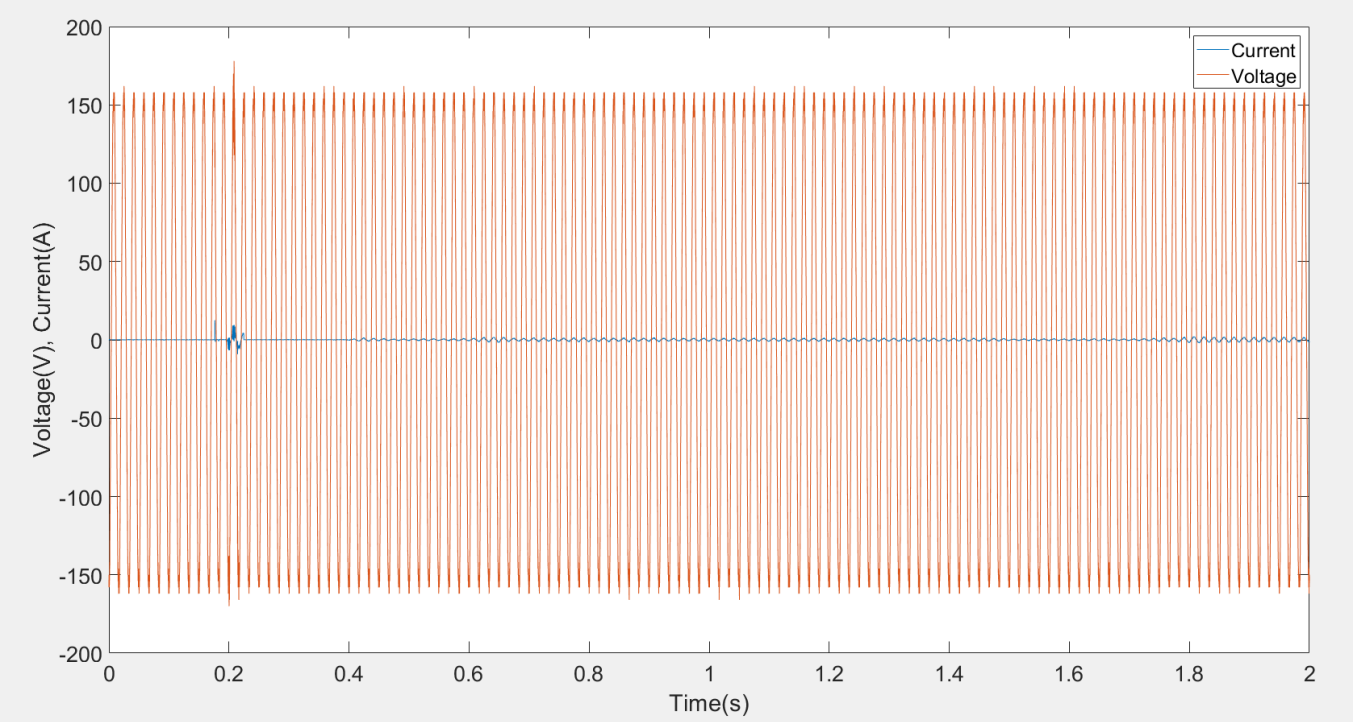

Figure 2-12: Laptop's current and voltage vs time.

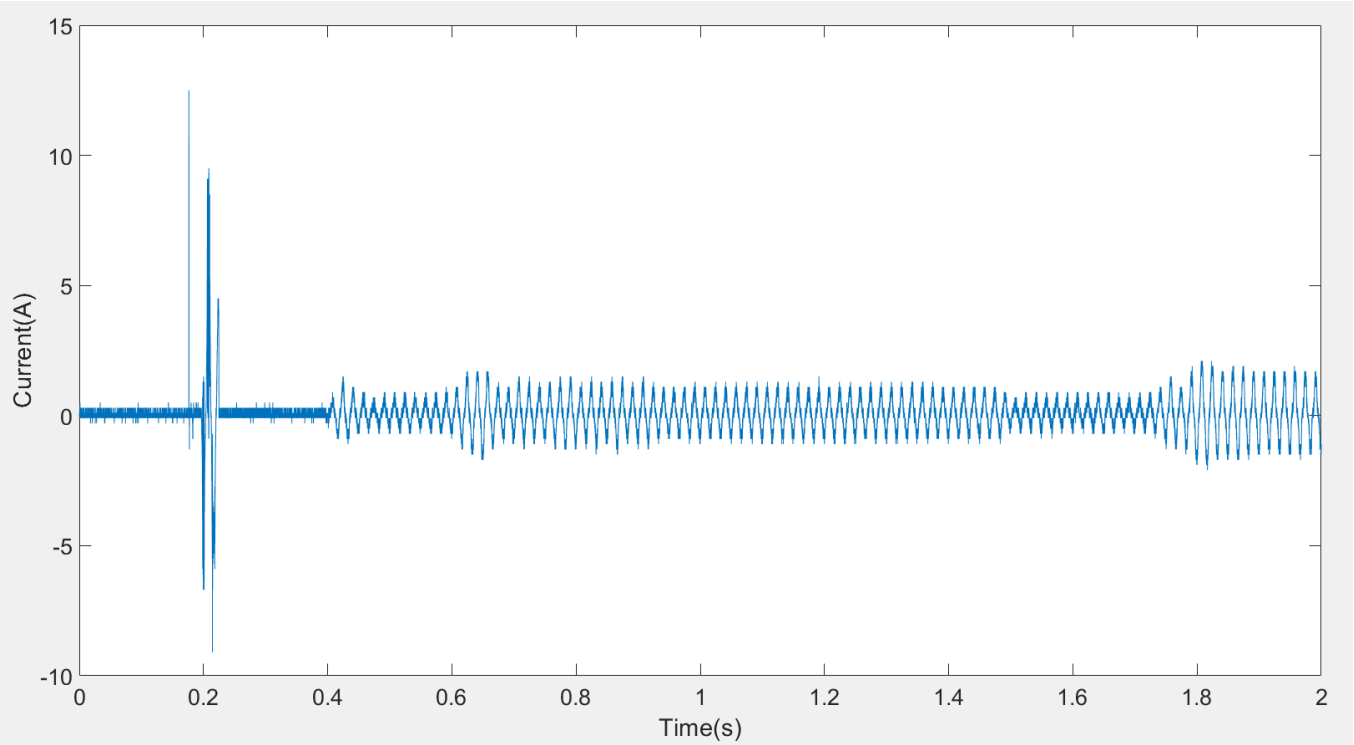

Figure 2-13: Laptop's current vs time.

2.5.4 Personal Computer

Transient and steady-state currents of a personal computer are observed. The values are similar to the laptop ones. The measured waveforms are shown in Figures 2-14, 2-15 and 2-16.

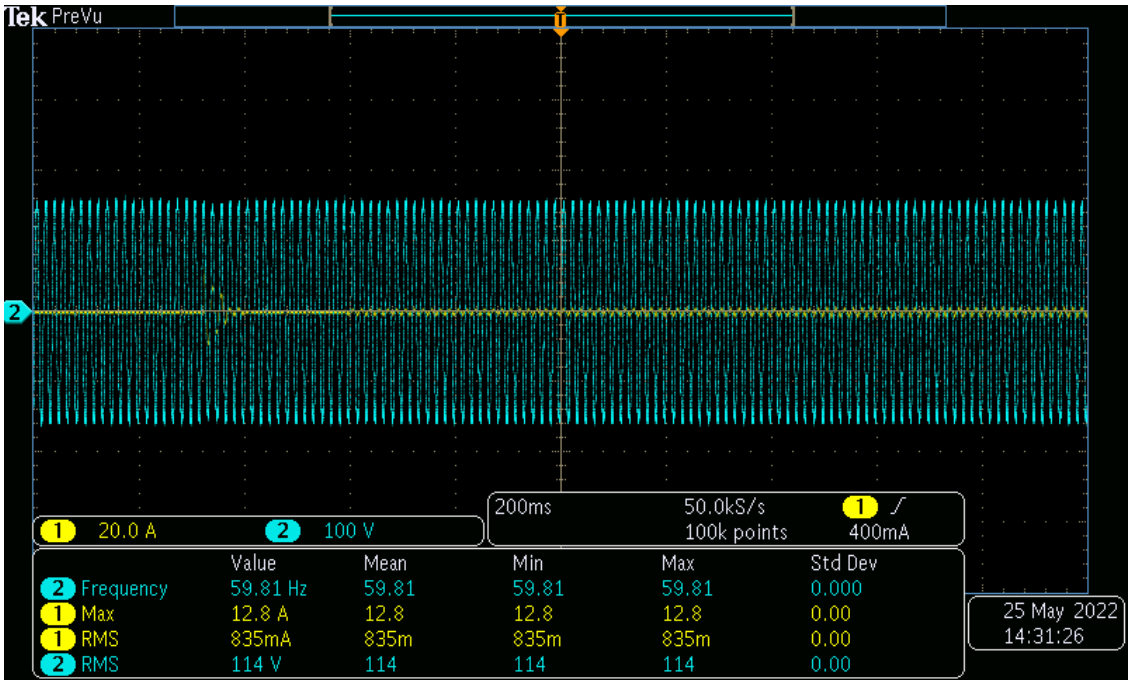

Figure 2-14: Measured PC's current and voltage waveforms.

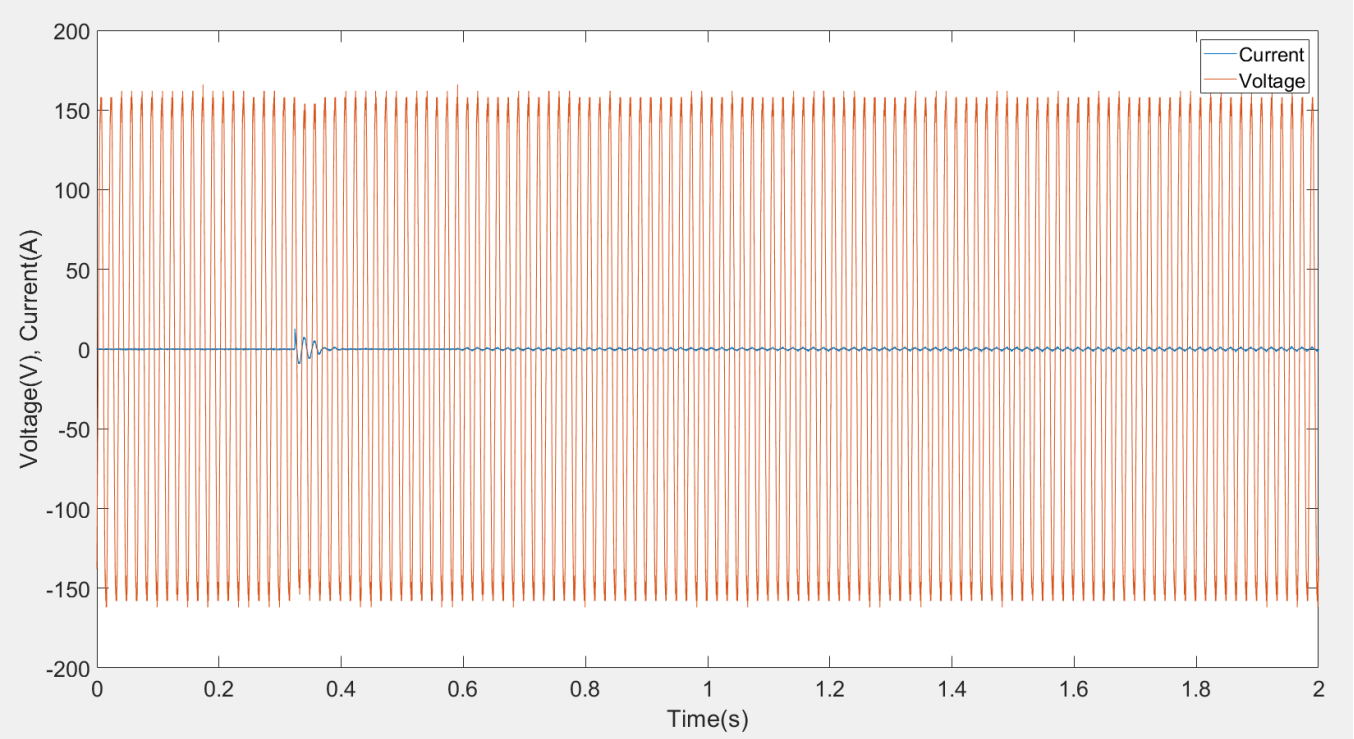

Figure 2-15: PC's current and voltage vs time.

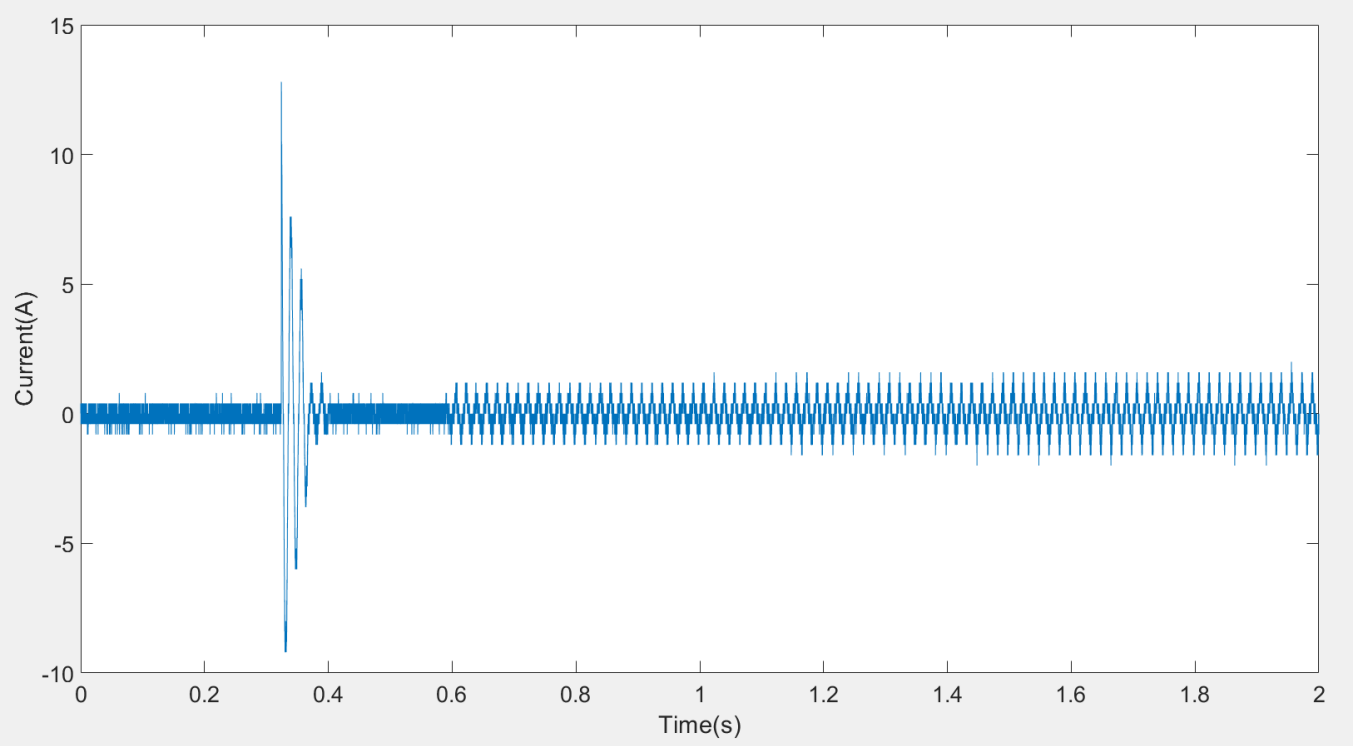

Figure 2-16: PC's current vs time.

2.5.5 Fridge

The transient and steady state currents of a refrigerator have been observed. Contrary to other household appliances, the duration of transient current was observed to be longer. The waveforms are shown in Figures 2-17, 2-18 and 2-19.

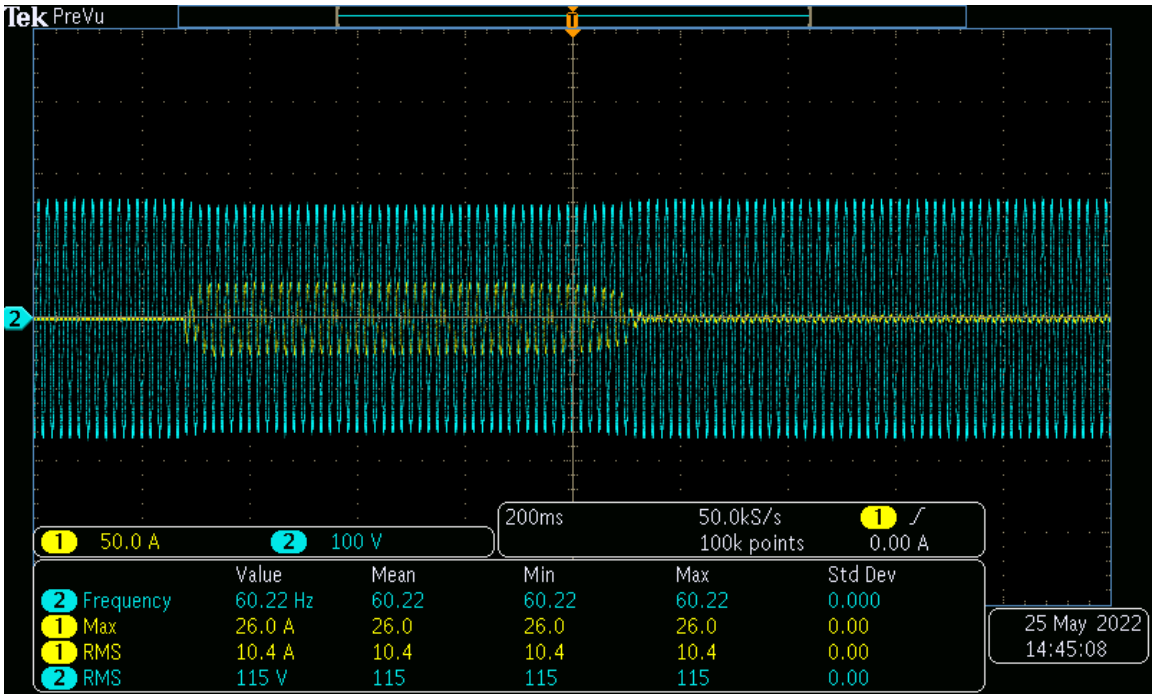

Figure 2-17: measured fridge's current and voltage waveforms.

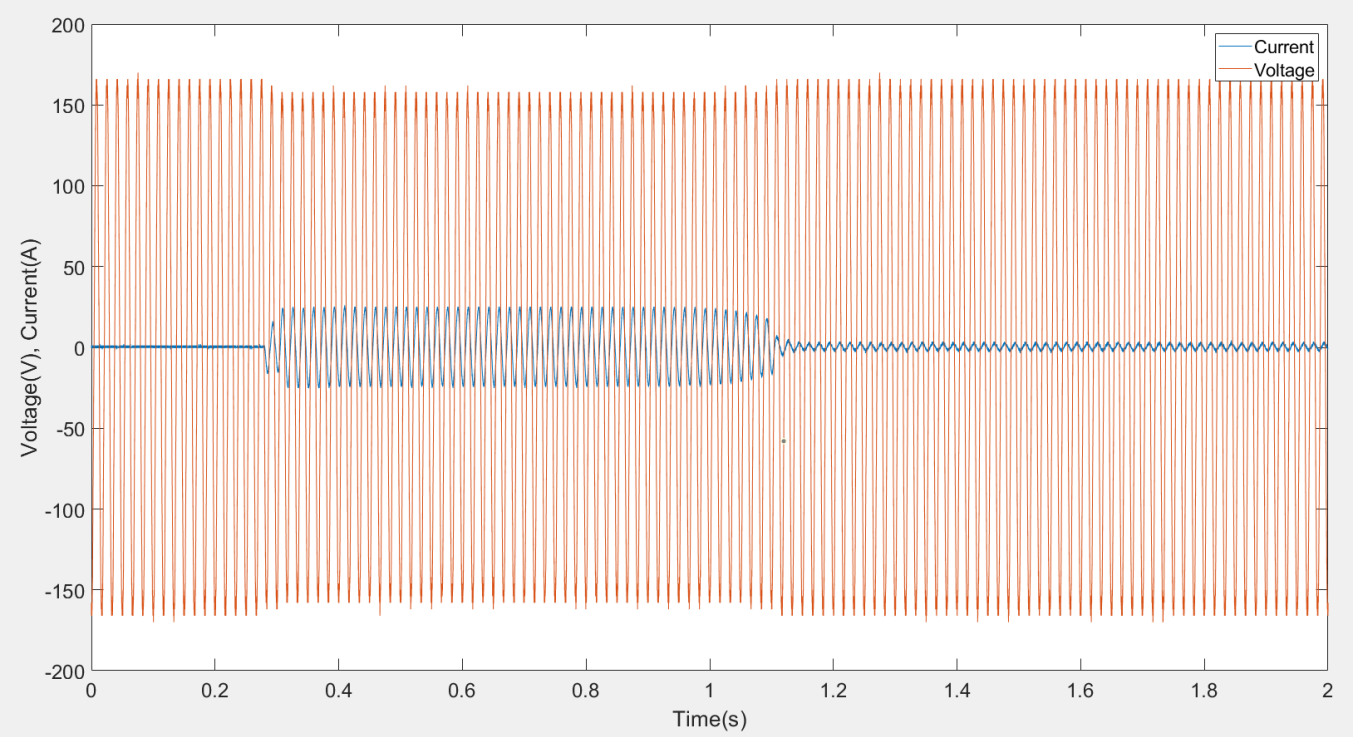

Figure 2-18: Fridge's current and voltage vs time.

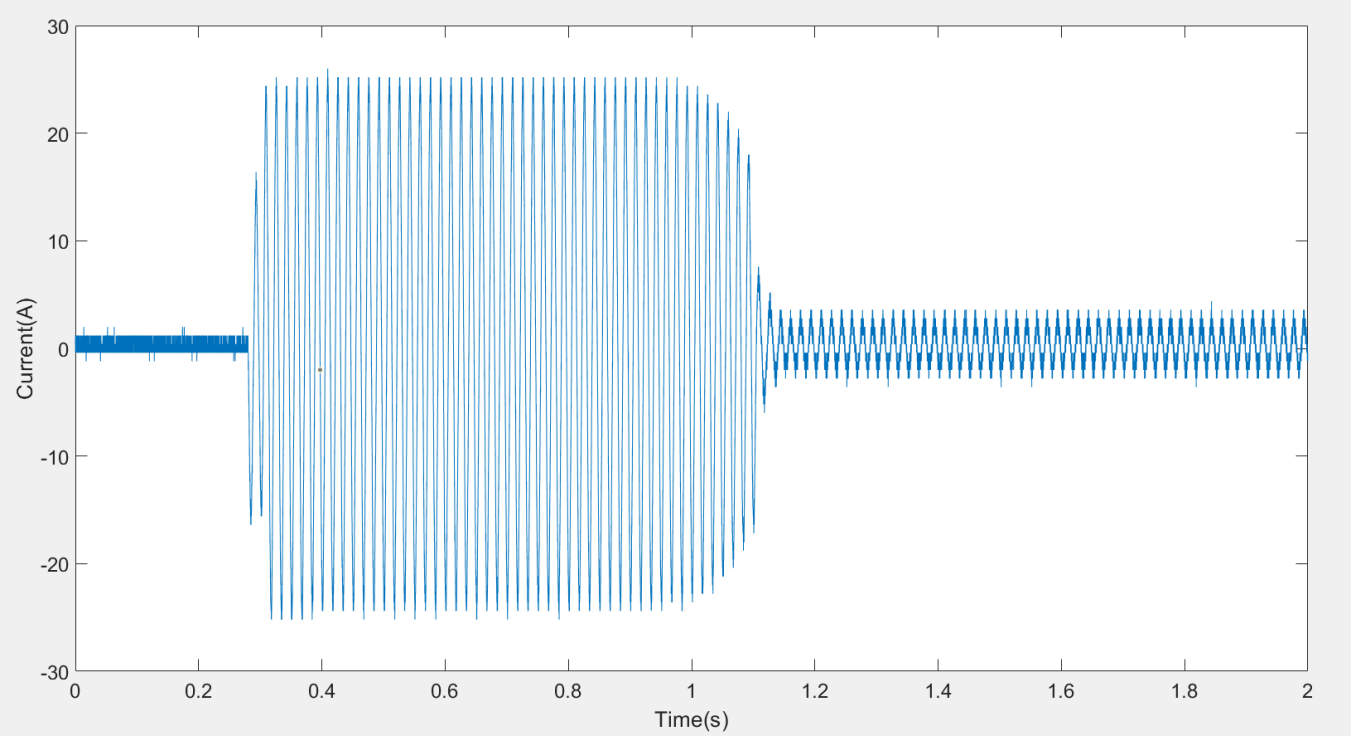

Figure 2-19: Fridge's current vs time.

The steady state and transient currents of household appliances, which will be powered by the battery of the electric vehicle, were examined. The maximum current of 30 A will be drawn from the battery has been found. As a result of the results obtained, it was observed that the system to be installed could meet the household load.

Table 2-2 Continuous and transient power consumption

Type of Load	Continuous power consumption	Transient consumption	
		Power	Duration
Kettle	1400 W	-	-
Microwave	1700 W	630 W	0.01 s
Fridge	400 W	3000 W	0.8 s
Laptop	72 W	1500 W	0.02 s
Personal Computer	102 W	1536 W	0.04 s

Continuous and transient power consumptions are shown in Table 2-2. When V2L system is activated, it will only provide power to the designated emergency loads; refrigerator, kettle, microwave, etc. Since house appliances will be turned on using V2L for a limited time in certain situations, it is anticipated that the system will be able to operate these loads.

3 Battery

3.1 Introduction

The heart of contemporary electric vehicles is the battery. By providing a sustainable and eco-friendly alternative to conventional internal combustion engines, electric car batteries have revolutionized the automobile industry. These cutting-edge energy storage systems are built on cutting-edge technology that effectively powers electric vehicles with a variety of rechargeable battery chemistries, including lithium-ion, solid-state, and nickel-metal hydride. [14]. Technology advancements in electric car batteries continue to increase performance, charge times, and overall vehicle range as the demand for electric vehicles rises. [14]. Widespread adoption of electric vehicles depends on overcoming current limitations and further developing the capacities of these key power sources, thus paving the way for a greener and more sustainable future in transportation [15].

3.2 Battery Types

3.2.1. Lithium-ion (Li-ion) batteries

Modern technology is no longer complete without lithium-ion (Li-ion) batteries, which power a variety of gadgets including smartphones, computers, and electric cars. Due to their appealing qualities, such as high energy efficiency, lack of memory effect, extended cycle life, high energy density, and high-power density, lithium-ion batteries are now the most suitable energy storage device for EVs. [15] When these batteries are being charged and discharged, lithium ions are transported between the anode and cathode through the electrolyte, which serves as a medium for ion transportation. [16]. Li-ion batteries have many advantages, but they also have several drawbacks, including susceptibility to high temperatures, the possibility of thermal runaway, and probable capacity deterioration over time. To address the rising need for effective energy storage solutions, manufacturers and researchers are always attempting to make Li-ion batteries safer, more effective, and more sustainable [16]. The energy densities of various commercial rechargeable batteries are compared in Figure 3-1, which amply demonstrates the superiority of Li-ion batteries over other batteries [17].

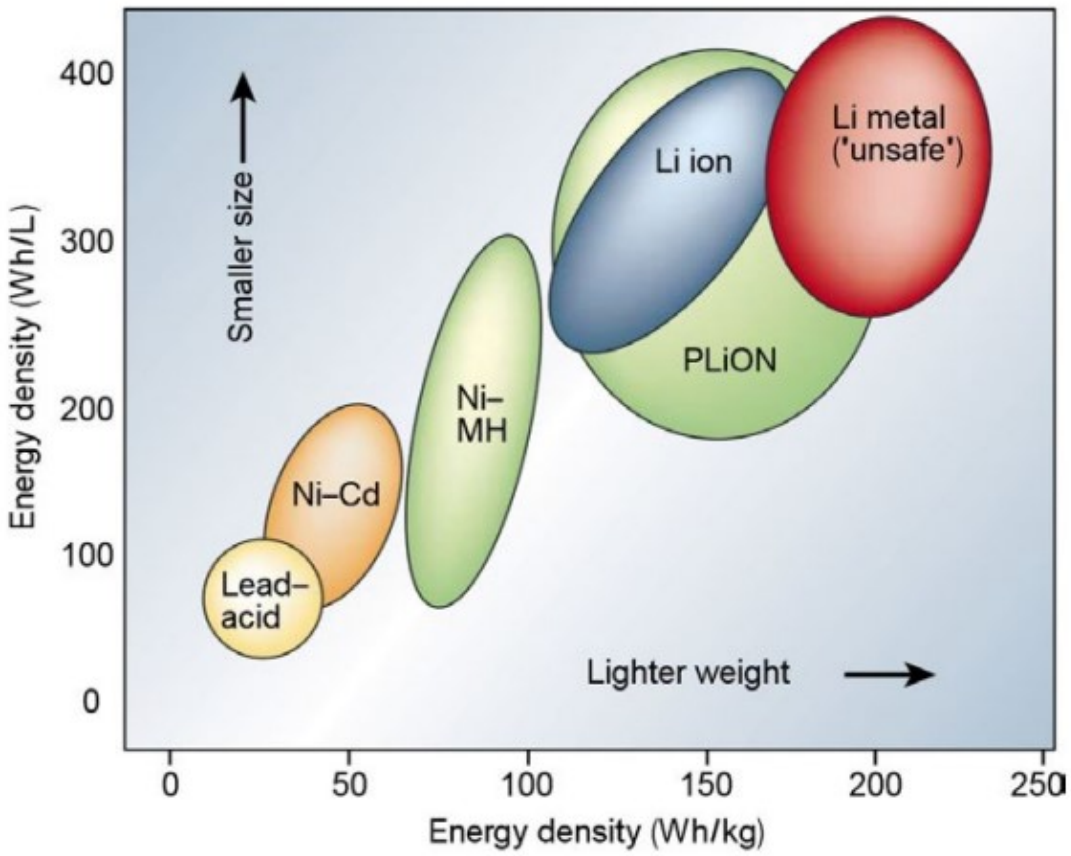

Figure 3-1: Comparison of energy densities and specific energy of different rechargeable batteries. Reproduced with permission [19].

3.2.2. Nickel-metal hydride batteries

Nickel-metal hydride batteries are more widely used in hybrid-electric vehicles, but are also used successfully in some all-electric vehicles [14]. Hybrid-electric vehicles do not derive power from an external plug-in source and instead rely on fuel to recharge the battery, which excludes them from the definition of an electric car [18].

Compared to lithium-ion or lead-acid batteries, nickel-metal hydride batteries have a longer lifespan. They are also secure and abuse-tolerant [14]. The main problems with nickel-metal hydride batteries are their high price, rapid rate of self-discharge, and the fact that they produce a lot of heat at high temperatures [14]. Due to these problems, these batteries are typically employed in hybrid electric vehicles rather than rechargeable electric vehicles [18].

3.2.3 Lead-acid batteries

In electric cars, lead-acid batteries are utilized to complement other battery loads [14]. Although these batteries are powerful, affordable, secure, and dependable, it is challenging to employ them in electric cars due to their short calendar life and subpar cold-temperature performance [14]. High-power lead-acid batteries are being developed, however they are currently exclusively employed as secondary storage in commercial vehicles [18].

3.2.4 Ultracapacitors

In the conventional sense, batteries are not what ultracapacitors are. As an alternative, they keep polarized liquid sandwiched between an electrode and an electrolyte. The liquid's ability to store energy grows together with its surface area [19]. Because they assist electrochemical batteries in balancing their load, ultracapacitors, like lead-acid batteries, are particularly valuable as secondary storage components in electric cars [19]. Ultracapacitors can also give extra power to electric vehicles during acceleration and regenerative braking [19].

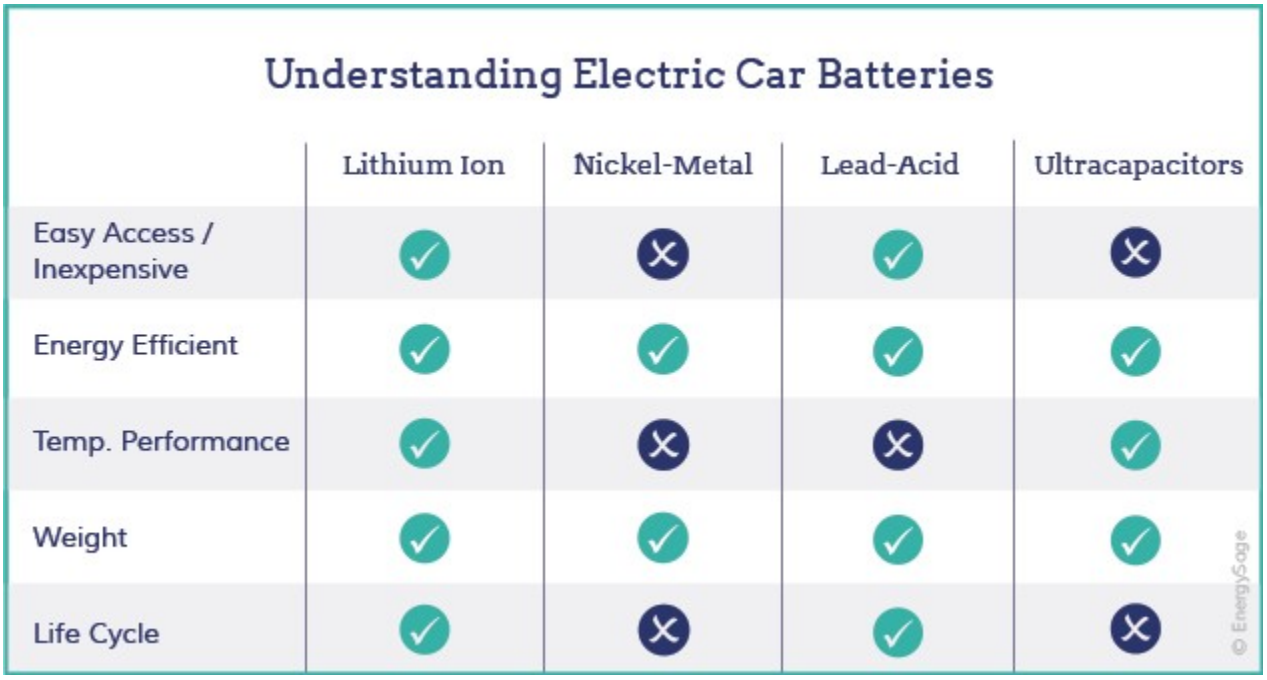

Figure 3-2: Comparison of electric car batteries [16].

3.2.5 Solid-State Battery

Solid-state batteries are currently in development, and they have not yet been used in electric vehicles [20]. According to Toyota, the first electric vehicles with solid-state batteries could be on the road by 2025 [20]. This could be a "game changer," considering that solid-state batteries are more energy-packed than lithium-ion batteries [20].

Another advantage of solid-state batteries is that they take up less space than lithium-ion batteries [21]. Solid-state batteries may quadruple the range of electric vehicles and boost performance due to their weight advantage. However, solid-state batteries are still in the research stage, and until they are mass-produced, it is unknown whether they are practically superior to lithium-ion batteries [18].

3.2.6 Lithium-Sulfur

Another option to lithium-ion batteries is lithium-sulfur batteries. Lithium-sulfur batteries, like solid-state batteries, have a greater range than lithium-ion batteries [22]. According to the European Commission, they are also less expensive to make and have a lower environmental impact than cobalt-based lithium-ion batteries [22]. Because lithium-sulfur batteries have a short lifespan, they are not used in EVs [25]. Nonetheless, researchers are developing studies to address this issue [23].

3.3 Nissan Leaf Battery

2018 Nissan Leaf model with a 40-kWh battery is one of the few cars in the market with V2G technology. It has a 110-kW electric motor with 320 Nm of torque. The model can be charged with either 6.6 kW onboard charger, or with a 50 kW CHAdeMO charger [24]. In this section, a 40-kWh battery model is highlighted with a brief description of the different dynamics [24].

3.3.1 Battery Characterization

The 40-kWh battery of the Nissan LEAF consists of 192 nickel manganese cobalt (NMC) cells distributed into 24 modules, where each module consists of 8 cells [25]. Of the 192 cells (N_c), 96 cells are connected in series (N_{cS}), and 2 in parallel (N_{cP}) [25]. The nominal voltage (V_{nc}) of a single cell is 3.65 V, and the nominal current capacity (I_{nc}) is 56.3 Ah [25]. Although 2018 Nissan Leaf is being marketed with a battery capacity of 40 kWh, the total usable battery capacity is 39.46 kWh calculated as follows.

$$Capacity = N_c \times V_{nc} \times I_{nc} \tag{3.1}$$

$$= 192 \text{ x } 3.65\text{V} \times 56.3 \text{ Ah} \tag{3.2}$$

$$= 39.46 \text{ kWh}$$

Moreover, the nominal voltage of the battery pack (V_{nb}) is calculated using nominal voltage of the single cell followed by the total number of cells as seen in.

$$V_{nb} = V_{nc} \times N_{cS} \tag{3.3}$$

$$= 3.65\,V \times 96 \text{ cells} \tag{3.4}$$

$$= 350\,V$$

The initial current capacity (Cbin) is obtained through the use of nominal current capacity and the total number of cells in parallel as shown below.

$$C_{bin} = I_{nc} \times N_{cP} \tag{3.5}$$

$$= 56.3 \text{ Ah} \times 2 \text{ cells} \tag{3.6}$$

$$= 112.6 \text{ Ah}$$

This capacity will decrease over time due to the degradation process of the battery. The current and voltage of the DC electrical equivalent circuit are obtained using Ohm's law. The battery is modeled as the Thevenin equivalent with an ideal voltage source. V_{oc} and a resistor R_{batt}. The resulting battery voltage therefore depends on the charge/discharge current and is given by the following equation;

$$V_{batt} = V_{oc} - I_{batt} \times R_{batt} \tag{3.7}$$

V_{oc} represents open-circuit voltage, whereas R_{batt} stands for the resistive part of the battery. From the following equation, it is important to mention when I_{batt} is positive, battery is discharging and vice versa, when I_{batt} is negative, battery is charging.

Power flowing into the battery (P_{batt}) is given.

$$P_{batt} = V_{batt} \times I_{batt} \tag{3.8}$$

Furthermore, open-circuit voltage could be obtained by the sum of open-circuit voltage of all cells (V_{oc_cell}) which is taken as a function of the SOC of the cell in series using;

$$V_{oc} = V_{oc\_cell} \times N_{cS} \tag{3.9}$$

Figure 3-3 shows the OCV versus SOC of a Li-ion battery cell.

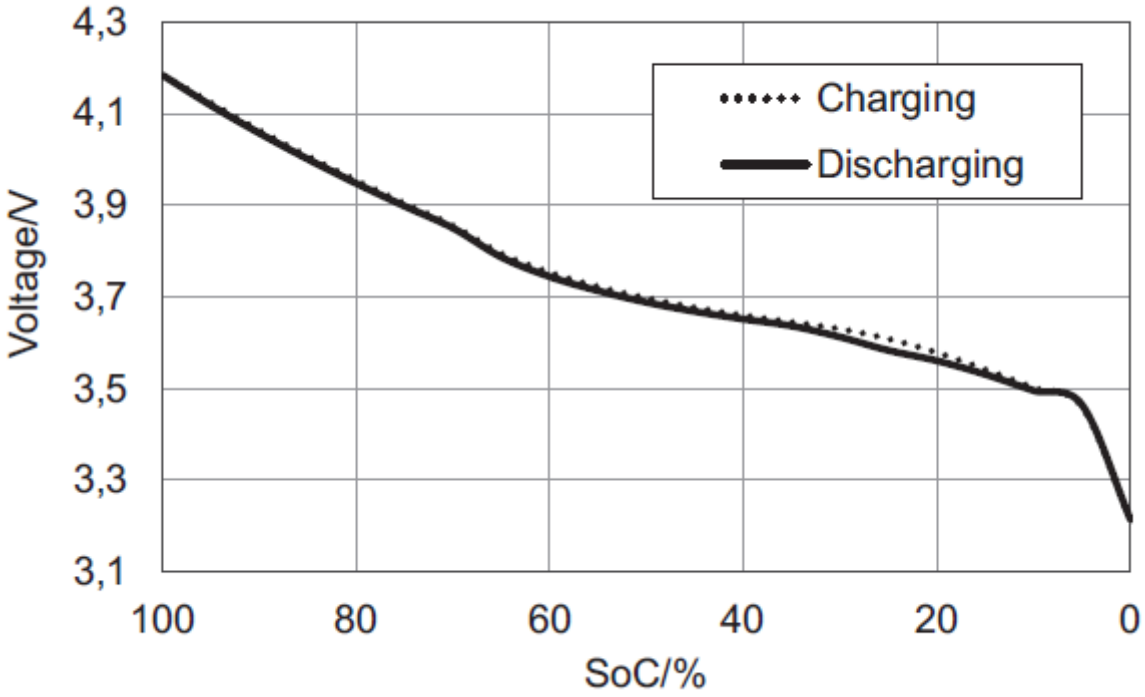

Figure 3-3: Experimental OCV-SOC curve of Li-ion cell [26].

3.4 Battery Modelling

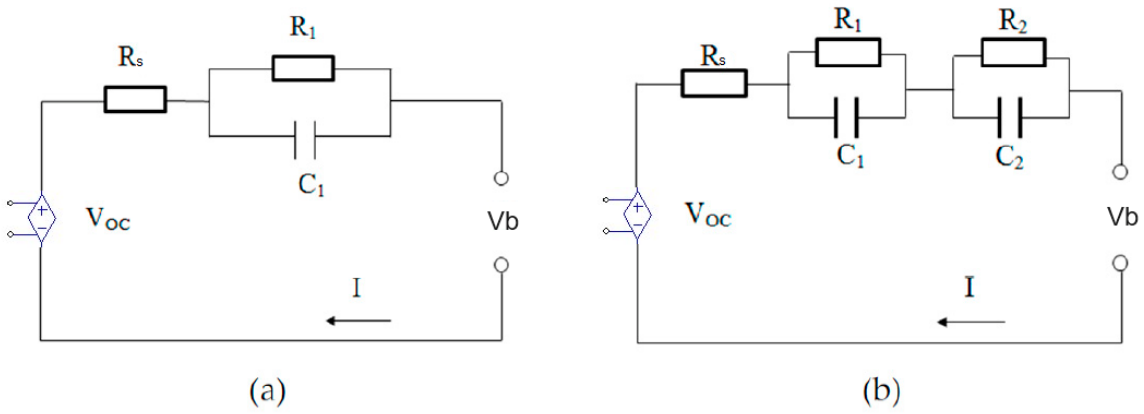

Figure 3-4: (a) The first order resistor-capacitor (RC), and (b) the second order RC equivalent circuit models [27].

- Batteries and other electrochemical cells can be modeled at various levels depending on the use of the model [27].
- Battery models are useful for battery design, performance evaluation and system simulation at the application level [27].
- At the most complex level, the fundamental physics and chemistry-based theories are used to develop theoretical models of electrochemical cells. These models reflect material properties and design factors on the device performance [27].

Electric circuit models of the battery, that emphasize the macroscopic behavior, are more useful for the performance evaluation at a system level, such as EVs and for the design of these systems.

3.5 Parameters Calculation

In this investigation, an equivalent electrical circuit model is suggested for simulation purposes and to model the transient behavior of a battery cell. The model was comprised of different parts, such as a series DC internal resistance or ohmic resistance, a DC voltage source, and two RC parallel circuit networks.

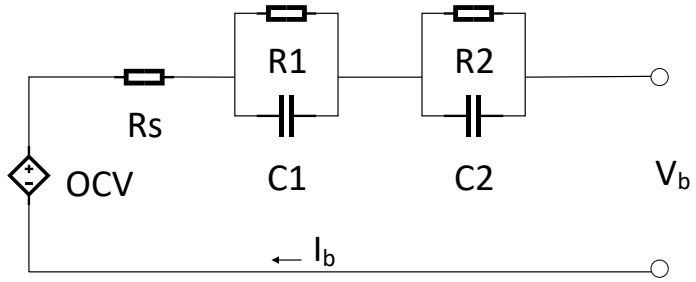

Figure 3-5: Second order RC battery equivalent model [28].

Series resistance shows internal DC resistance. This resistance is responsible for the immediate voltage decrease when a current is applied to the battery cell. A DC voltage source or controlled voltage source demonstrates the model open circuit voltage (OCV) of a battery cell. Note that this voltage is dependent on the state of charge (SOC) [28].

To determine the transient response of the terminal voltage, two RC parallel networks were employed. The prime RC network (R1 and C1) demonstrated the small-time constant of the battery cell feedback and was employed to model double-layer capacitance and the charge transfer procedures. The secondary RC network (R2 and C2), demonstrated the lengthy-time constant of the battery cell feedback and was employed to model the diffusion procedures. In the investigated model, the parameters were dependent on the current, SOC [28].

To obtain the parameters, real Nissan Leaf battery model is used as an experimental battery and tested according to test method in Table 3-1.

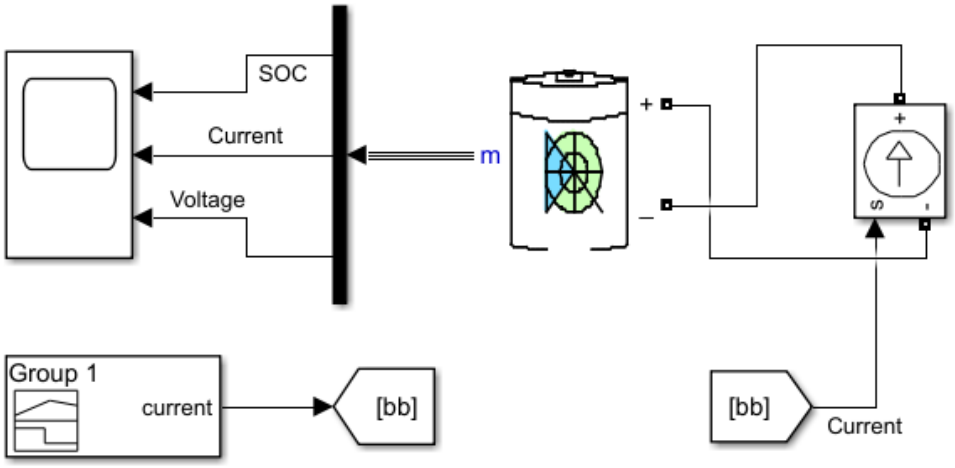

Figure 3-6: MATLAB SIMULINK simulation for testing battery cell.

Table 3-1 Test method for the battery cell.

Step	Description
1	Full charging of the battery with 0.25C current rate
2	Discharging the battery with 0.25C current rate to 95% *SOC*
3	Rest period: 180 min.
4	Discharging the battery with 0.25C current rate to 90% *SOC*
5	Rest period: 180 min.
6	Discharging the battery with 0.25C current rate to 85% *SOC*
7	Rest period: 180 min.
8	Discharging the battery with 0.25C current rate to 80% *SOC*
9	Rest period: 180 min.
10	Discharging the battery with 0.25C current rate to 75% *SOC*
11	Rest period: 180 min.
12	Discharging the battery with 0.25C current rate to 70% *SOC*
13	Rest period: 180 min.
14	Discharging the battery with 0.25C current rate to 65% *SOC*
15	Rest period: 180 min.
16	Discharging the battery with 0.25C current rate to 60% *SOC*
17	Rest period: 180 min.
18	Discharging the battery with 0.25C current rate to 55% *SOC*
19	Rest period: 180 min.
20	Discharging the battery with 0.25C current rate to 50% *SOC*

21	Rest period: 180 min.
22	Discharging the battery with 0.25C current rate to 45% *SOC*
23	Rest period: 180 min.
24	Discharging the battery with 0.25C current rate to 40% *SOC*
25	Rest period: 180 min.
26	Discharging the battery with 0.25C current rate to 35% *SOC*
27	Rest period: 180 min.
28	Discharging the battery with 0.25C current rate to 30% *SOC*
29	Rest period: 180 min.
30	Discharging the battery with 0.25C current rate to 25% *SOC*
31	Rest period: 180 min.
32	Discharging the battery with 0.25C current rate to 20% *SOC*
33	Rest period: 180 min.
34	Discharging the battery with 0.25C current rate to 15% *SOC*
35	Rest period: 180 min.
36	Discharging the battery with 0.25C current rate to 10% *SOC*
37	Rest period: 180 min.
38	Discharging the battery with 0.25C current rate to 5% *SOC*
39	Rest period: 180 min.

After simulating the battery with this test method, the OCV is obtained and used to determine battery parameters.

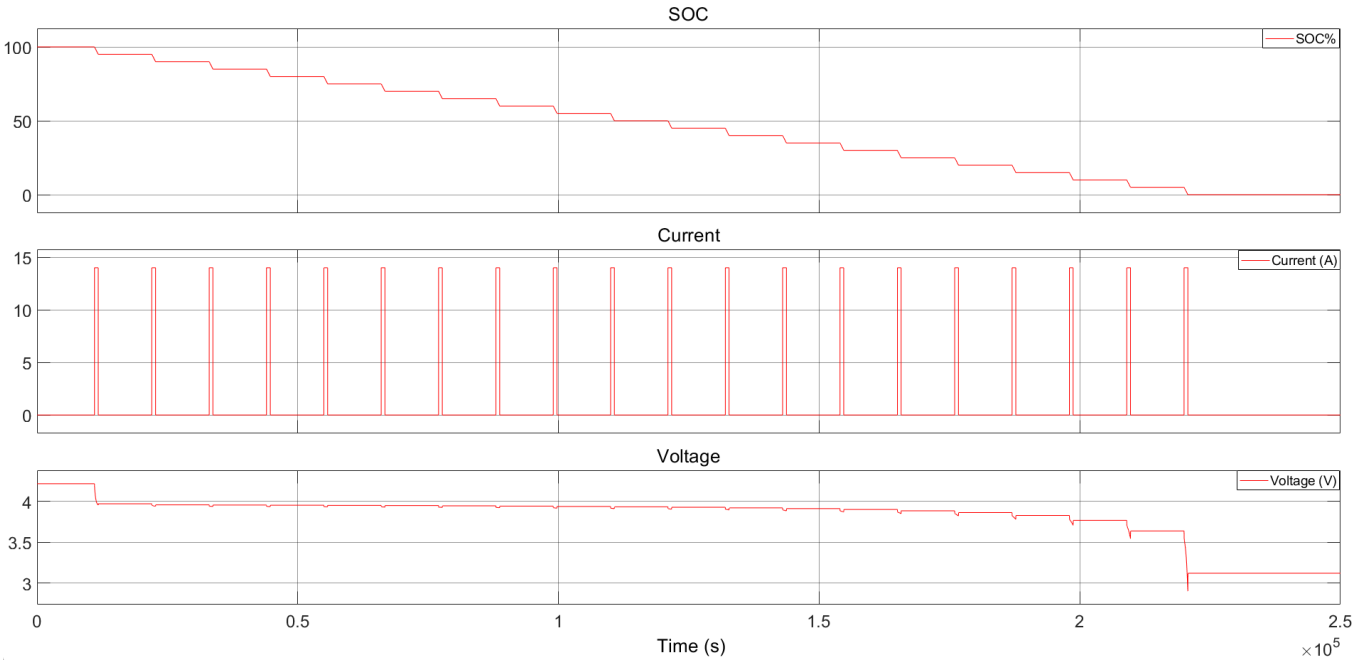

Figure 3-7: Waveforms of battery cell testing simulation.

Table 3-2 SOC-OCV results of battery cell testing simulation.

SOC	1	0.95	0.9	0.85	0.8	0.75	0.7	0.65	0.6	0.55
OCV	4.2158	3.9711	3.9580	3.9557	3.9537	3.9514	3.9489	3.9459	3.9425	3.9385
SOC	0.5	0.45	0.4	0.35	0.3	0.25	0.20	0.15	0.10	0.05
OCV	3.9338	3.9281	3.9211	3.9122	3.9007	3.8852	3.8630	3.8287	3.7689	3.6378

3.5.1 Calculation of Ohmic Resistance

The ohmic resistance (R_s) could be determined from the immediate voltage decline after the current pulse was applied. The voltage response of a Li-ion battery cell to a discharging current pulse (I) of 15 A is illustrated in Figure 3-8.

$$R_s = (V_0 - V_1)/ I \tag{3.10}$$

where V_0 is the cell OCV at the time of applying the current pulse, and V_1 is the cell OCV after 1 s from the current pulse excitation instant.

Table 3-3 SOC-R_s results of battery cell testing simulation.

SOC	1	0.95	0.9	0.85	0.8	0.75	0.7	0.65	0.6	0.55
***R_s* (Ω)**	7.78e-4	7.27E-4	7.26E-4	7.30E-4	7.35E-4	7.40E-4	7.46E-4	7.53E-4	6.96E-4	7.71E-4
SOC	0.5	0.45	0.4	0.35	0.3	0.25	0.20	0.15	0.10	0.05
***R_s* (Ω)**	7.82E-04	7.95E-04	8.12E-04	8.33E-04	8.60E-04	8.97E-04	9.51E-04	1.03E-03	1.18E-03	1.50E-03

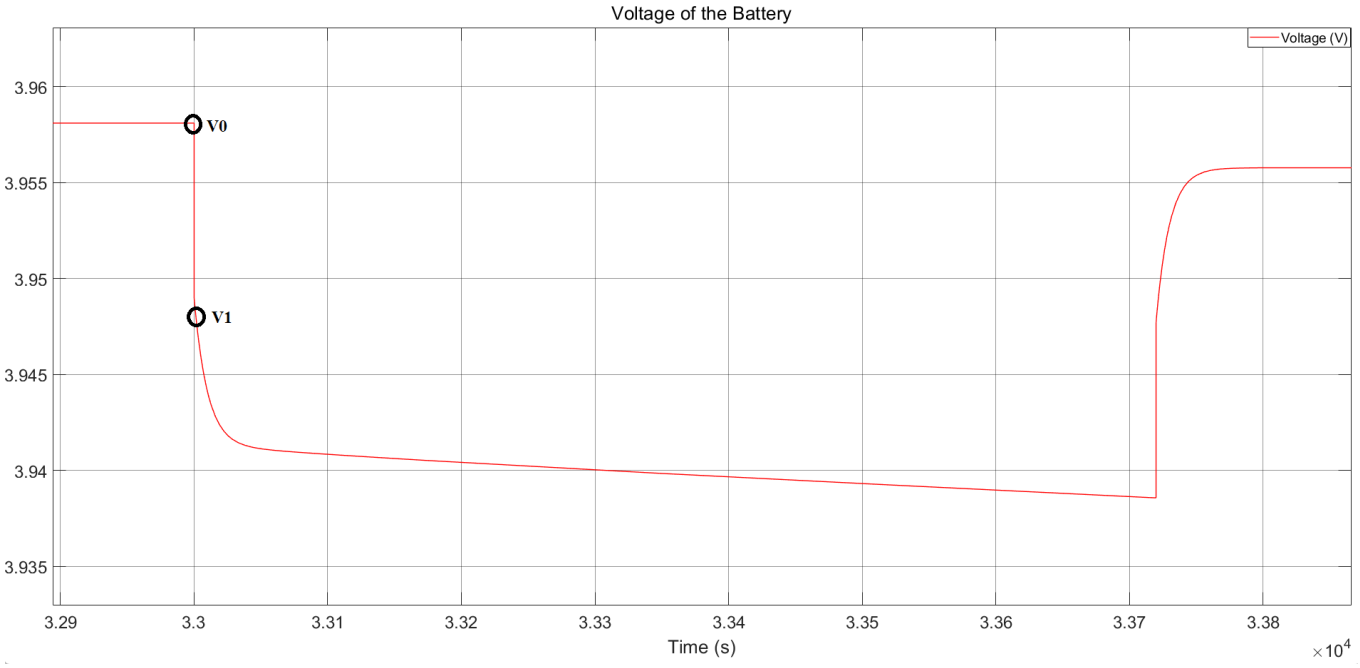

Figure 3-8: OCV during a discharging current pulse.

3.5.2 RC Values Determination

The amount of RC parallel networks (R_1, C_1, R_2, and C_2) were considered as a function of current and SOC.

3.5.2.1 R1 Calculation;

The voltage response of a battery cell to a discharging current pulse is illustrated in Figure 3-9. The following equation was used to calculate the value of the resistance R_1.

$$R_1 = (V_1 - V_2)/ I, \tag{3.11}$$

where, V_2 is the cell OCV after 50 s from the discharging current excitation instant.

Table 3-4 SOC-R_1 results of battery cell testing simulation.

SOC	1	0.95	0.9	0.85	0.8	0.75	0.7	0.65	0.6	0.55
R_1 **(Ω)**	3.86E-03	6.13E-04	4.86E-04	5.06E-04	5.37E-04	5.72E-04	6.12E-04	6.58E-04	7.77E-04	7.75E-04
SOC	0.5	0.45	0.4	0.35	0.3	0.25	0.20	0.15	0.10	0.05
R_1 **(Ω)**	8.50E-04	9.41E-04	1.05E-03	1.20E-03	1.39E-03	1.65E-03	2.03E-03	2.64E-03	3.77E-03	6.52E-03

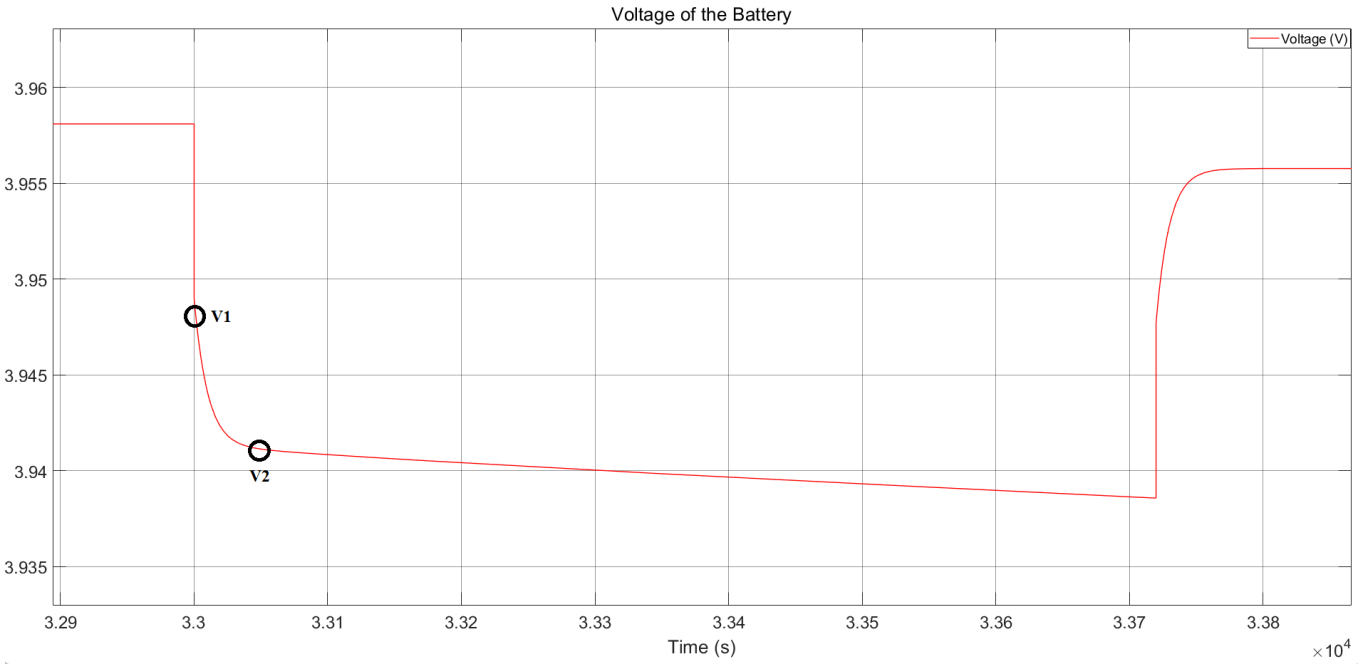

Figure 3-9: OCV during a discharging current pulse.

3.5.2.2 R2 Calculation

The voltage response of a battery cell to a discharging current pulse is illustrated in Figure 3-10. The value of the resistance R_2 was calculated by the following equation.

$$R_2 = (V_2 - V_3)/I \tag{3.12}$$

where, V_3 is the cell OCV after 700 s from the discharging current pulse excitation instant.

Table 3-5 SOC-R_2 results of battery cell testing simulation.

SOC	1	0.95	0.9	0.85	0.8	0.75	0.7	0.65	0.6	0.55
***R₂* (Ω)**	1.40E-02	7.92E-04	1.82E-04	1.71E-04	1.91E-04	2.17E-04	2.48E-04	2.87E-04	3.36E-04	3.98E-04
SOC	0.5	0.45	0.4	0.35	0.3	0.25	0.20	0.15	0.10	0.05
***R₂* (Ω)**	4.80E-04	5.91E-04	7.44E-04	9.67E-04	1.31E-03	1.21E-03	2.88E-03	5.05E-03	1.11E-02	4.45E-02

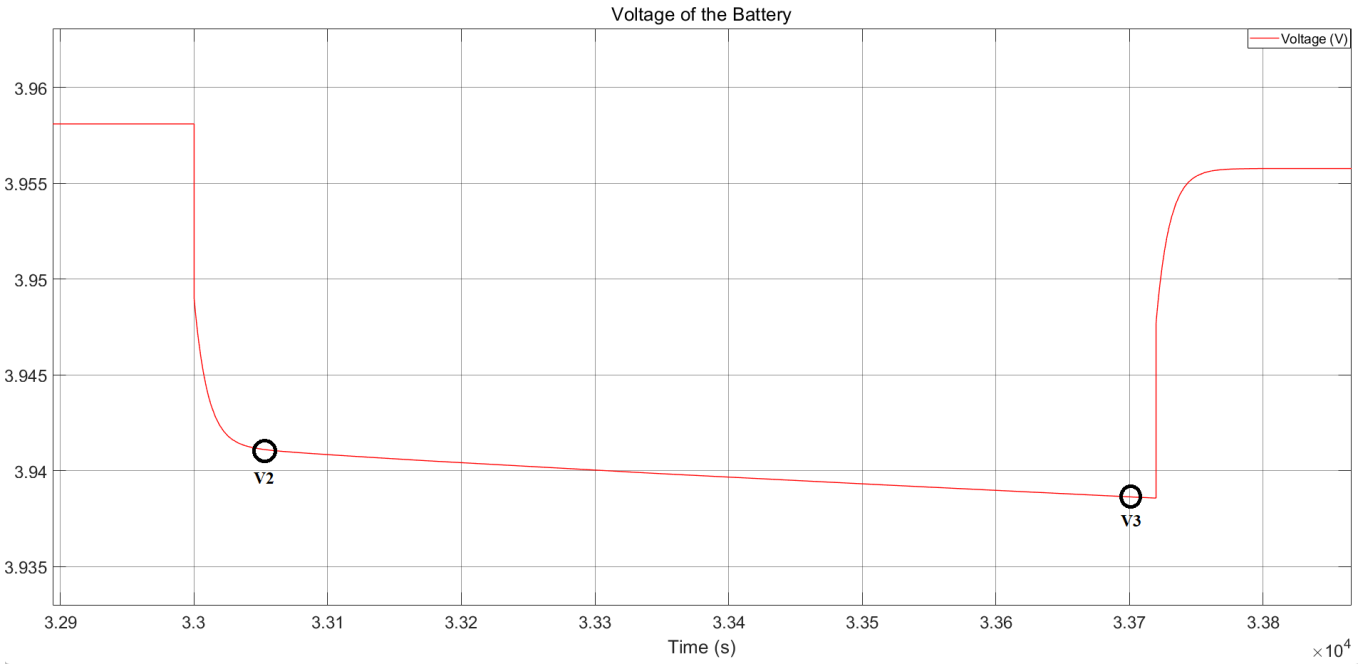

Figure 3-10: OCV during a discharging current pulse.

3.5.2.2 C1 and C2 Calculation

The values of the capacitances C_1 and C_2 are determined by using the following equations [28].

$$C_1 = 8I / ((V_2 - V_1) * \ln(\frac{V_2}{V_1})) \quad (3.13)$$

$$C_2 = 9I / ((V_3 - V_2) * \ln(\frac{V_3}{V_2})) \quad (3.14)$$

Table 3-6 SOC-C_1 results of battery cell testing simulation.

SOC	1	0.95	0.9	0.85	0.8	0.75	0.7	0.65	0.6	0.55
C1	1.80E+5	6.77E+6	1.07E+7	9.88E+6	8.78E+6	7.73E+6	6.74E+6	5.83E+6	4.18E+6	4.20E+6
SOC	0.5	0.45	0.4	0.35	0.3	0.25	0.20	0.15	0.10	0.05
C1	3.48E+6	2.83E+6	2.25E+6	1.74E+6	1.29E+6	9.10E+5	5.96E+5	3.49E+5	1.68E+5	5.40E+4

Table 3-7 SOC-C_2 results of battery cell testing simulation.

SOC	1	0.95	0.9	0.85	0.8	0.75	0.7	0.65	0.6	0.55
C₂	1.18E+4	3.59E+6	6.76E+7	7.70E+7	6.16E+7	4.78E+7	3.65E+7	2.72E+7	1.99E+7	1.41E+7
SOC	0.5	0.45	0.4	0.35	0.3	0.25	0.20	0.15	0.10	0.05
C₂	9.68E+6	6.39E+6	4.01E+6	2.37E+6	1.29E+6	1.51E+6	2.61E+5	8.38E+4	1.67E+4	9.24E+2

Table 3-8 Average values of battery parameters

Battery Parameter	**Average Value**
R_s	0.00085 Ω
R_1	0.00157 Ω
R_2	0.00429 Ω
C_1	3.9E+6 *u*F
C_2	1.9 E+7 *u*F

3.6 Simulation of the Battery Model

After obtaining the required model parameters, the simulation model of the lithium-ion battery can be established in MATLAB SIMULINK. The simulation of the established second-order RC model is shown in Figures 3.11. It can be seen that the simulation model is mainly composed of two parts. The SOC input, and the circuit parameter module. The SOC input module is based on Ah capacity of li-ion battery cell turned to ampere second. The SOC value can be obtained by multiplying 56 A into 3600 second. The battery cell parameters, which are calculated in the section 3.5, are used in this model. The simulation model has two inputs: the load current profile and the initial SOC of the battery in ampere-second. The load current is set to 15 A. The maximum value of SOC is set to 1, and the minimum value is 0, so as to prevent the battery from overcharge and over-discharge. In this simulation, the influence of temperature

change on the output voltage of a lithium-ion battery is ignored. Finally, the actual voltage curve is compared with the simulation curves of the models to verify the accuracy of the models.

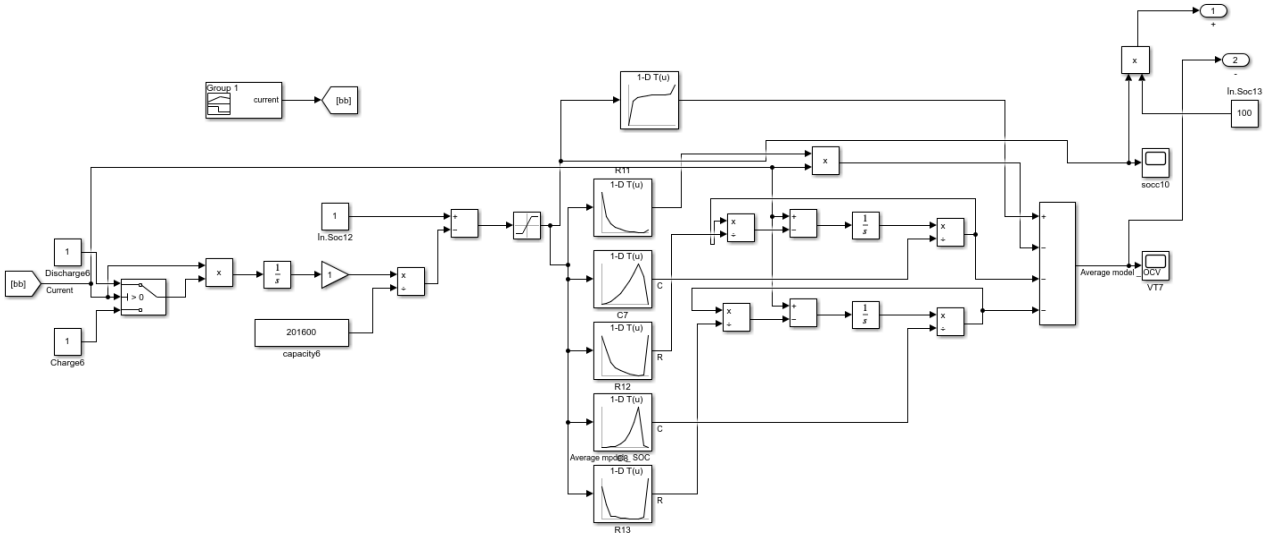

Figure 3-11: MATLAB SIMULINK simulation of designed battery.

The battery parameters, which are calculated in section 3.5, vary according to the SOC. Thus, a look-up table for each parameter is created. Four simulations are performed. Two with the lookup tables, and the other two uses the average values of the parameters. The simulation circuit for comparison is shown in Figure 3-12. The results of the 4 models are compared with the results of the car battery. All model has been tested with a discharging current of 15 A. The battery to be used in the experiment was compared with first order and second order RC batteries. SOC and OCV graphs are shown in Figures 3-13, 3-14 and 3-15.

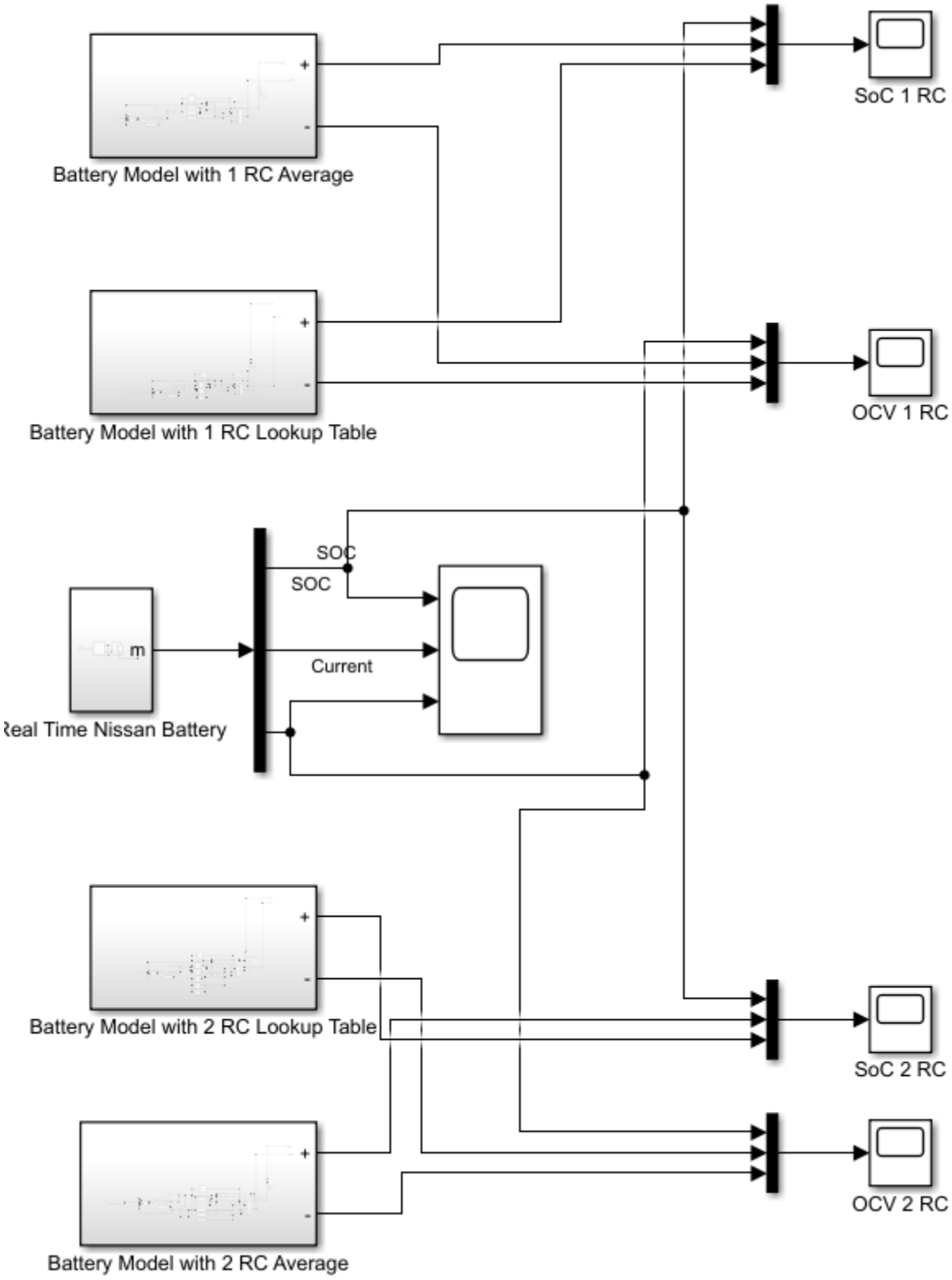

Figure 3-12 MATLAB SIMULINK simulation of battery comparison.

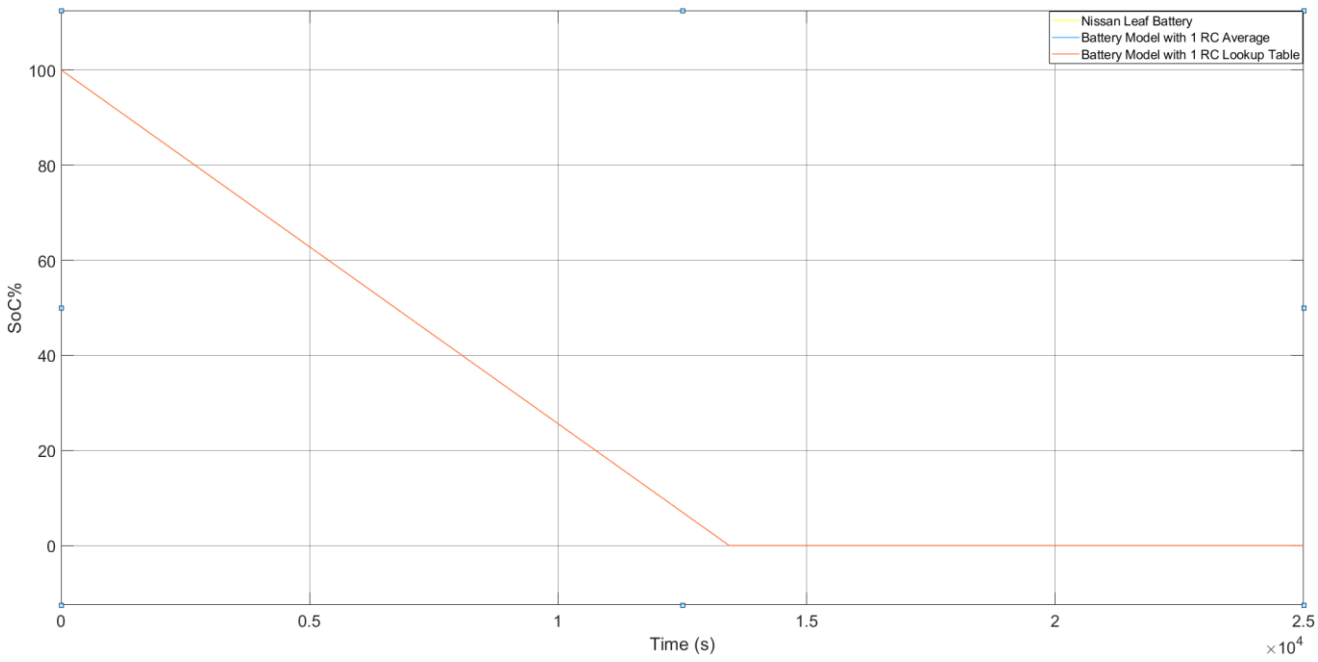

Figure 3-13: SOC results of comparison simulation.

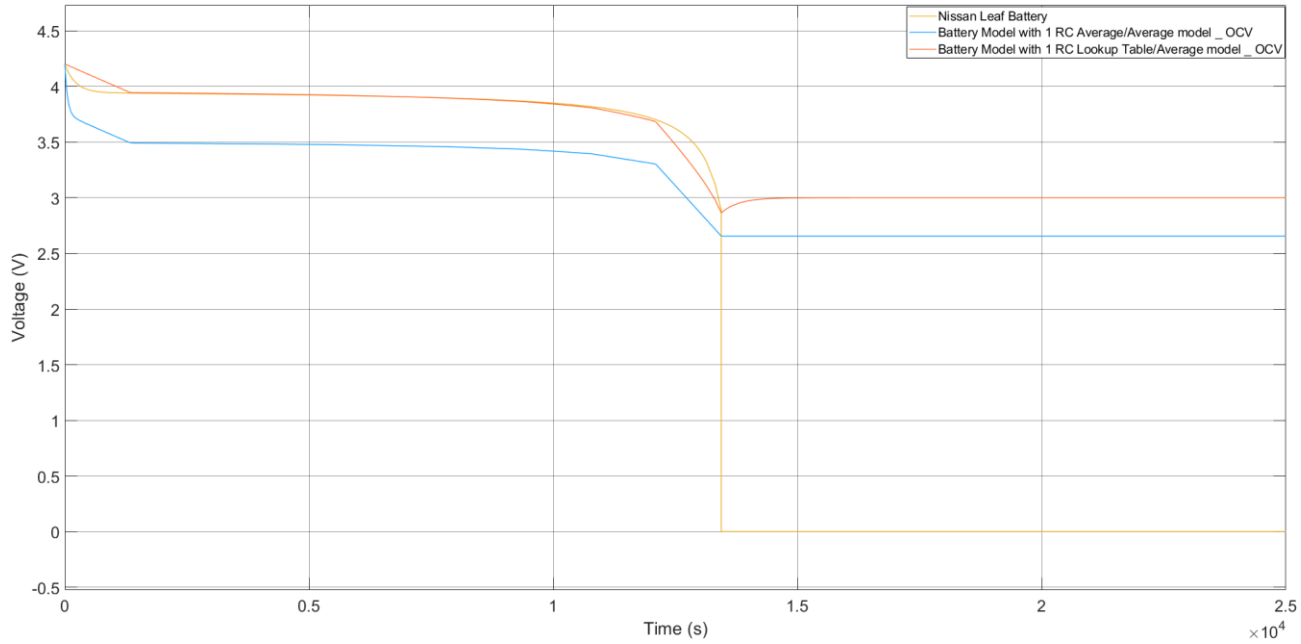

Figure 3-14: OCV results of first order RC batteries comparison.

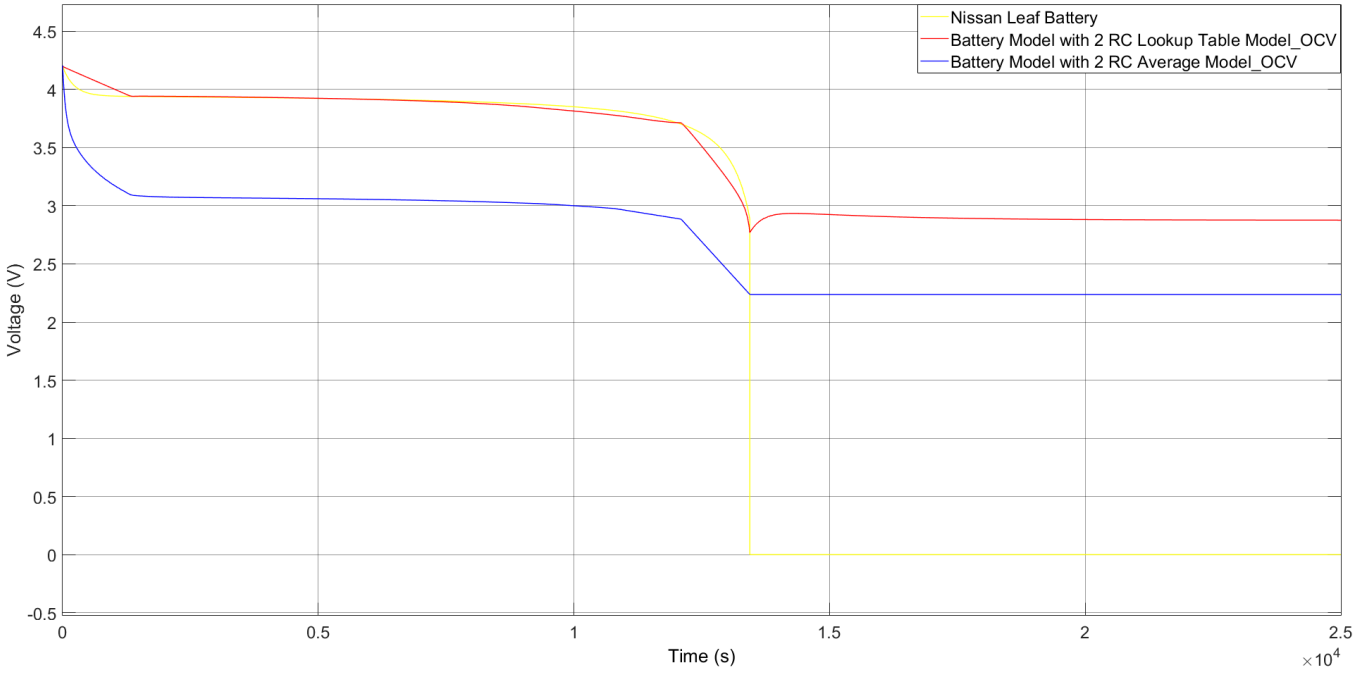

Figure 3-15: OCV results of second order RC batteries comparison.

3.7 Results

In this study, battery cell models were tested as first-order RC branch and second-order RC branch and their results were compared with the real battery result. At the same time, this comparison was made using both the lookup tables of the circuit parameters and the average values. This is to observe which battery model was closer to the actual operation of the real battery. As a result of the simulation, second order RC branch with look up tables and first order RC branch with look up tables gave the best results. However, Results of second order branch is slightly better. Therefore, it is decided to use second order RC battery cell model with look up tables.

4 System Design and simulation

4.1 Introduction

As mentioned in chapter 2, V2L system provides transmission of energy from the battery of the electric vehicle to the house. It is the conversion of the DC voltage of the car battery to a grid-like AC voltage through the inverter and a low-pass filter. In this chapter, the inverter and the low-pass filter are to be designed and examined, and then the simulation are carried on and results are examined.

4.2 Inverter

Bidirectional DC-AC converters are critical in applications such as continuous power supply, electric vehicles, renewable energy grid integration, energy storage systems, and micro-grids. In real-world applications, such as charging and discharging batteries for electric vehicles and energy storage systems, the DC voltage of the storage battery can be lower or higher than the peak amplitude of the AC line voltage. [29]. A bidirectional DC-AC inverter is used to convert DC voltage to AC voltage.

A full-bridge configuration for the employed single-phase inverter is shown in Fig. 4.1. The full-bridge inverter is a critical component in modern power electronics; it converts direct current (DC) from sources such as lithium-ion batteries or solar panels to alternating current (AC), which is a common supply for residential, commercial, and industrial loads. To generate AC output voltage from a DC input, this inverter uses a full bridge architecture composed of four switches arranged in an "H" shape. Its advanced control methods, such as Pulse Width Modulation (PWM), allow for precise regulation of the output voltage and frequency, ensuring compatibility with a wide range of electrical loads [30]. As the demand for renewable energy and energy-efficient systems continues to grow, the full bridge DC-AC inverter plays a huge role in the seamless integration of these technologies into the existing power grid.

The bipolar Pulse-Width Modulation (PWM) switching technique is a common way for managing the output voltage in power electronic converters, particularly in motor control, audio amplifiers, and uninterruptable power supply [31]. In this technique, the width of the generated pulses is modulated in proportion to the magnitude of the analogue input signal. The bipolar PWM minimizes ripple content and harmonic distortion in the output waveform by switching the polarity of the output voltage, resulting in enhanced power quality and efficiency [32]. Furthermore, the bipolar PWM technology reduces the possibility of transformer saturation and electromagnetic interference (EMI), making it a popular choice

for many power conversion systems. Thus, bipolar PWM switching has become a vital tool in current power electronics and control systems due to its excellent voltage management [33].

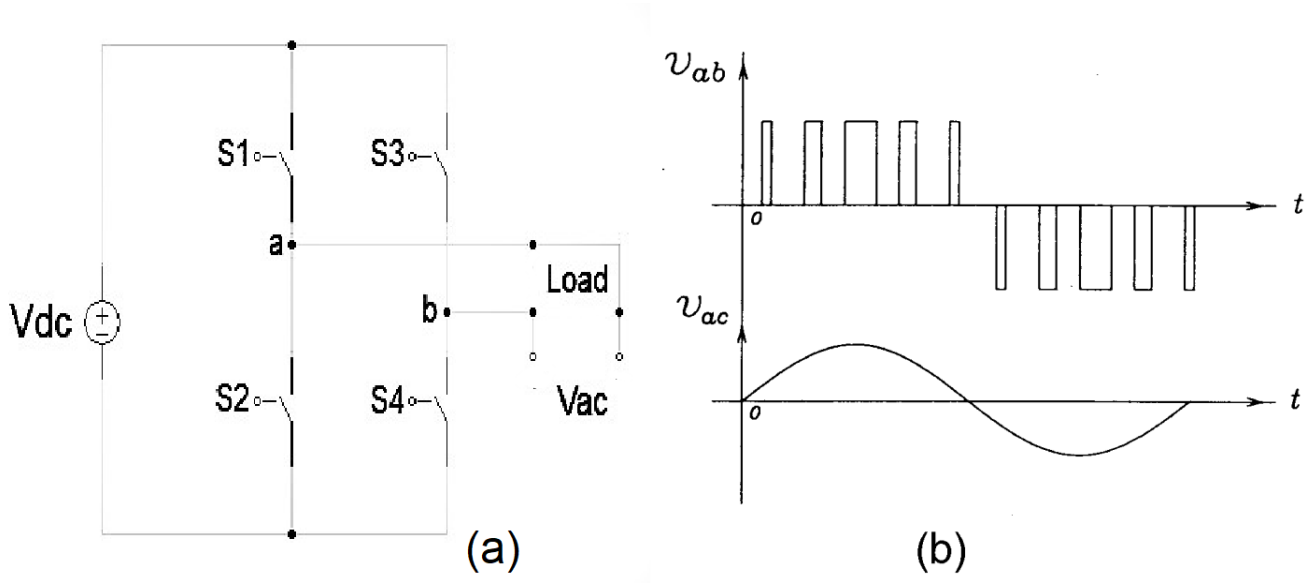

Figure 4-1 Traditional bridge-type PWM inverter. (a) Topology. (b) Waveforms [30].

A full-bridge inverter, as depicted in Fig. 4-1, is an inverter with four switches and one input DC voltage. The load is connected in the mid of the two legs. When S1 and S4 are turned on and S3 and S2 are turned off, current flows through S1 to the load and back to the DC bus via S4. When S3 and S2 are turned on and S1 and S4 are turned off, current flows in the opposite direction to the load through S3 and back to the DC bus through S2. Bipolar pulse width modulation is used to drive the current through the load in an alternating direction. This is the main concept for generating an AC waveform [34].

The grid current has a frequency of 60 Hz. This means that the switches must be activated and deactivated 120 times every second. This can't be done mechanically or manually. As a result, MOSFETs or IGBTs are used instead of manual switches for ON/OFF applications. MOSFETs or IGBTs can easily turn ON and OFF 10000 times per second when heat sinks are used [35].

4.3 LC Filter

LC Filters are important components in electronic circuits because they filter and shape signals [36]. These passive filters, which are made up of inductors (L) and capacitors (C), are meant to selectively allow some frequency ranges to pass through while attenuating others [36].

When the output AC current is the primary control objective, first-order passive L-type filters are typically utilized on the AC side of PWM inverters. The primary function of an L-type filter is to reduce current ripples caused by inverter switching [37] [38]. Because of the unavoidable huge filter size, this type of filter is limited in low- switching-frequency applications of high-power PWM inverters. The third-order LCL-type filter is an alternative filter construction that can achieve a lower degree of current harmonics with less total filter inductance at lower switching frequencies. LCL-type filters, on the other hand, can generate steady-state and transient difficulties with output current due to resonance. When the output voltages are the primary control goals, second-order passive LC-type filters have been commonly utilized on the AC terminals of PWM inverters [36]. The main purpose of the LC filters is to attenuate the voltage ripple that stems from inverter switching [36].

The output voltage on the LC filter capacitor is controlled by switching the PWM inverter, where the LC filters introduce a time delay and produce resonance in the output AC voltage. Various techniques to controlling the output voltage across the LC filter capacitor have so been examined [36]. A second-order LC filter is used in this simulation. The equivalent circuit of the LC filter is shown in Figure 4-2.

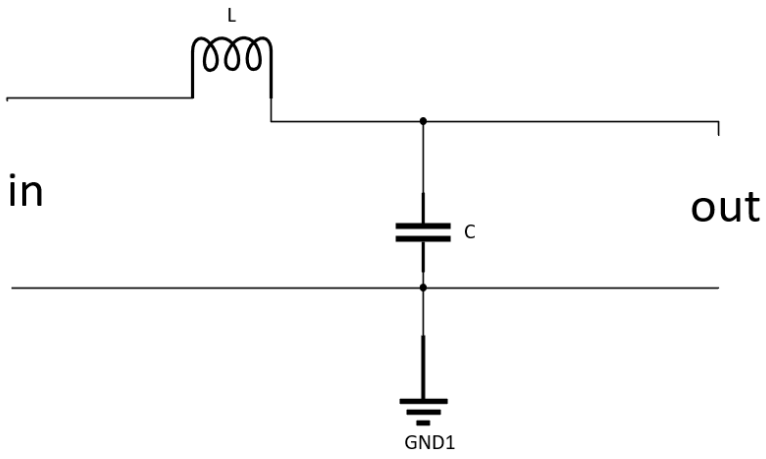

Figure 4-2 LC Filter equivalent circuit.

The cut-off frequency of the low-pass filter has to be at least 10 times higher than the frequency of the fundamental component, which is 60 Hz. This is to ensure no attenuation is taking place for the fundamental component at 60 Hz. Also, the value of the cut-off frequency of the low-pass filter has to be 10% to 20% of the switching frequency, which is 10 kHz. This is to ensure excellent filtering dynamics for the switching harmonics [35].

As for the filter inductance, its value is chosen so that the harmonics of the inductance current must be limited below 2% of the fundamental current.

$$L_f = \frac{V_{h-pk}}{2\pi f_h \sqrt{2} \Delta I_h} \tag{4.1}$$

$$L_f = \frac{170}{2\pi 10 x 10^3 \sqrt{2} x 16} \cong 0.1\ mH, \tag{4.2}$$

where V_{h-pk} is the peak voltage and f_h is the cut-off frequency. Hence, the minimum inductance value is 0.1 mH. The chosen inductance is 0.5 mH.

With the cut-off frequency and filter inductance in hand, it is easy to find of the filter capacitance from the following equation,

$$f_c = \frac{1}{2\pi\sqrt{L_f C_f}} \tag{4.3}$$

$$1000 = \frac{1}{2\pi\sqrt{0.5 x 10^{-3} C_f}}, \tag{4.4}$$

which found to be 50.66 μF. The chosen value of the filter capacitance is 50 μF. This makes the exact cut-off frequency of the filter is 1.006 kHz, which is acceptable.

The system devices are ordered accordingly. All the modeling procedures are done based on the specifications of the house and the devices. The specifications of the commercial device are brought in Table 4-1.

Table 4-1 System Devices

Device Name and Brand	Characteristics	
Inverter APS	Input	DC: 850 V
	Output	AC: 120 V/60 Hz
Filter Inductor	0.5 mH	
Filter Capacitor	50 μF	

4.4 Control

The electrical circuit along with the equivalent circuit of the inverter are shown in Fig. 4-3 and Fig. 4-4. The system circuit consists of four stages. The DC bus, the H-bridge, the low pass filter, and the load. The equivalent circuit of the inverter is shown in Fig.4-4, where M is the modulation index, which is the ratio between modulating (control) signal v_{ctr} and the peak value of the switching (triangle) signal $\hat{v}_{tri}$ [35]. The simulation testing parameters are as given in Table 4-2.

Table 4-2 System parameters

System parameters	
V_{dc}	400 V
L_f	0.5 mH 200 A
C_f	50 μF 400 V
R_l	7.5 Ω
L_l	980 μH

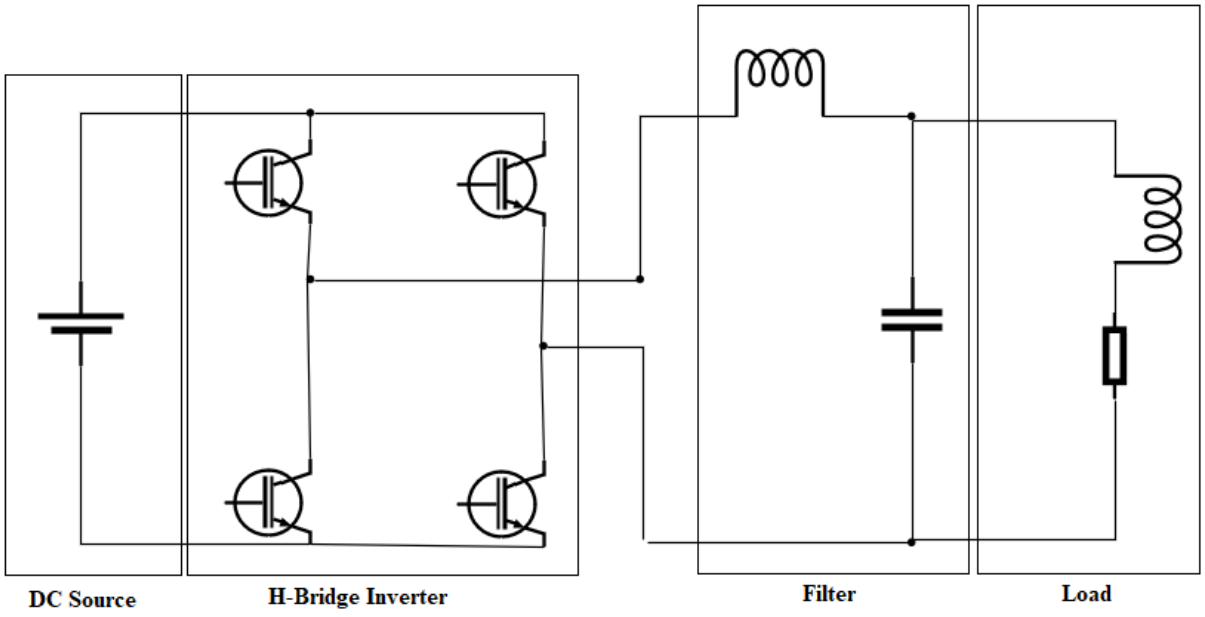

Figure 4-3: The V2L electrical circuit.

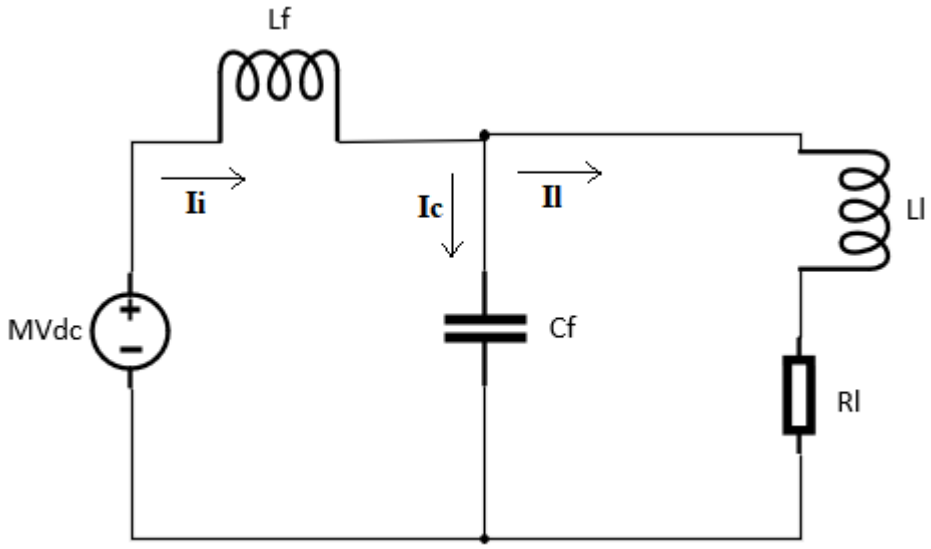

Figure 4-4: The equivalent circuit of the V2L system.

By applying Kirchhoff current law on the equivalent circuit, one can obtain the following.

$$i_i(t) = i_c(t) + i_l(t) = \ i_c(t) + \frac{v_c(t)}{R_l + jX_l} \tag{4.5}$$

$$i_i(s) = i_c(s) + \frac{v_c(t)}{R_l + SL_l}\,. \tag{4.6}$$

From Kirchhoff voltage law, the following equations are obtained.

$$M(t)V_{dc} = L_f \frac{di_t}{d_t} + v_c(t)\,, \tag{4.7}$$

$$M(s)V_{dc} = sL_f i_i(s) + v_c(s)\,, \tag{4.8}$$

$$i_c(t) = C_f(\frac{dv_c(t)}{dv})\,, \tag{4.9}$$

$$i_c(t) = C_f s v_c(s)\,. \tag{4.10}$$

By substituting (4.6) and (4.10) in (4.8), the following is obtained.

$$M(s)V_{dc} = sL_f \left[i_c(s) + \frac{v_c(s)}{R_l + sL_l}\right] + v_c(s) \tag{4.11}$$

$$= sL_f \left[C_f s v_c(s) + \frac{v_c(s)}{R_l + sL_l}\right] + v_c(s) \tag{4.12}$$

$$= [s^2 L_f C_f + s\frac{L_f}{(R_l L_l s)} + 1]v_c(s)\ \ . \tag{4.13}$$

Therefore, the transfer function of the capacitor voltage to modulation index (voltage plant) can be obtained as follows.

$$\frac{v_s(s)}{m(s)} = \frac{V_{dc}}{L_f} \frac{\frac{1}{C_f}\left(\frac{R_l}{L_l}+s\right)}{s^3+s^2\left(\frac{R_l}{L_l}\right)+s\frac{1}{C_f}\left(\frac{1}{L_f}+\frac{1}{L_l}\right)+\frac{R_l}{L_l L_f C_f}}. \tag{4.14}$$

Knowing that $i_{c\,=\,C_s s v_c(s)}$, thus, the transfer function of the capacitor voltage to the modulation index (voltage plant) can be obtained as follows.

$$\frac{v_s(s)}{m(s)} = \frac{V_{dc}}{L_f} \frac{\frac{1}{C_f}\left(\frac{R_l}{L_l}+s\right)}{s^3+s^2\left(\frac{R_l}{L_l}\right)+s\frac{1}{C_f}\left(\frac{1}{L_f}+\frac{1}{L_l}\right)+\frac{R_l}{L_l L_f C_f}}. \tag{4.15}$$

By substituting equation (4.10) into (4.12), the following is obtained.

$$\frac{v_c(s)}{i_i(s)} = \frac{\left(\frac{R_l}{L_l}+s\right)}{C_f\left(s^2+\frac{R_l}{L_l}s+\frac{1}{L_l C_f}\right)}. \tag{4.16}$$

By substituting equation (4.16) into (4.14), the transfer function of the inductance current to the modulation index (current plant) can be obtained as follows.

$$\frac{i_i(s)}{m(s)} = \frac{\frac{V_{dc}}{L_f}\left(s^2+\frac{R_l}{L_l}s+\frac{1}{C_f L_l}\right)}{s^3+s^2\left(\frac{R_l}{L_l}\right)+s\frac{1}{C_f}\left(\frac{1}{L_f}+\frac{1}{L_l}\right)+\frac{R_l}{L_l L_f C_f}}. \tag{4.17}$$

By plugging the values of the LC filter and the load into equations (4.15) and (4.17), the voltage and current plants are obtained as follows.

$$G_v(s) = \frac{v_s(s)}{m(s)} = \frac{1.6e10\ s + 7.18e14}{s^3 + 44898\ s^2 + 6.041e07\ s + 1.79e12} \tag{4.18}$$

$$G_i(s) = \frac{i_i(s)}{m(s)} = \frac{40s^2 + 1.796e06\, s + 8.163e08}{5e{-}05s^3 + 2.245\, s^2 + 3020\, s + 8.98e7} \tag{4.19}$$

Having one closed control loop to control the output voltage is feasible. However, this results in having a high order controller (complex design). Thus, adding a current inner control loop along with voltage outer control loop simplifies the controller design and enhances the shape of the waveforms. The bode plots of the voltage and current plants are shown in Fig.4-5 and 4-6.

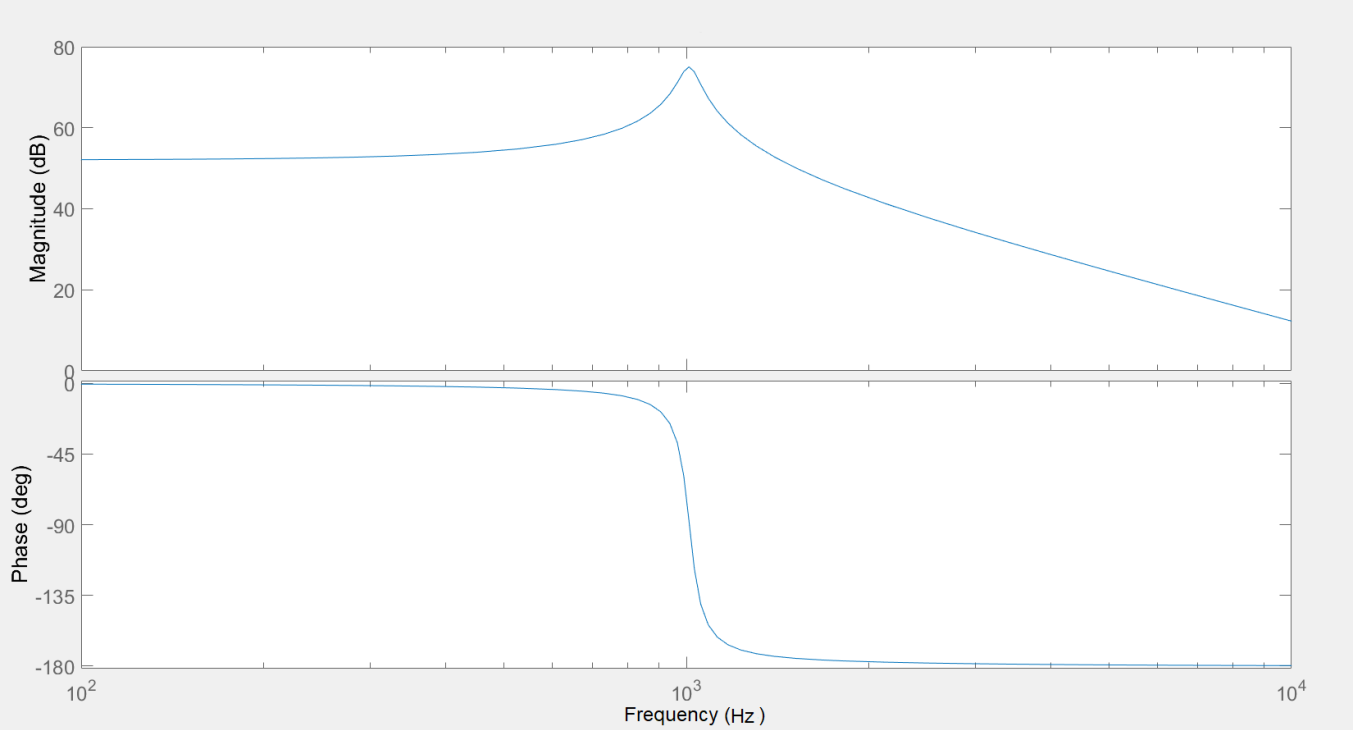

Figure 4-5 Bode Plot of the voltage plant.

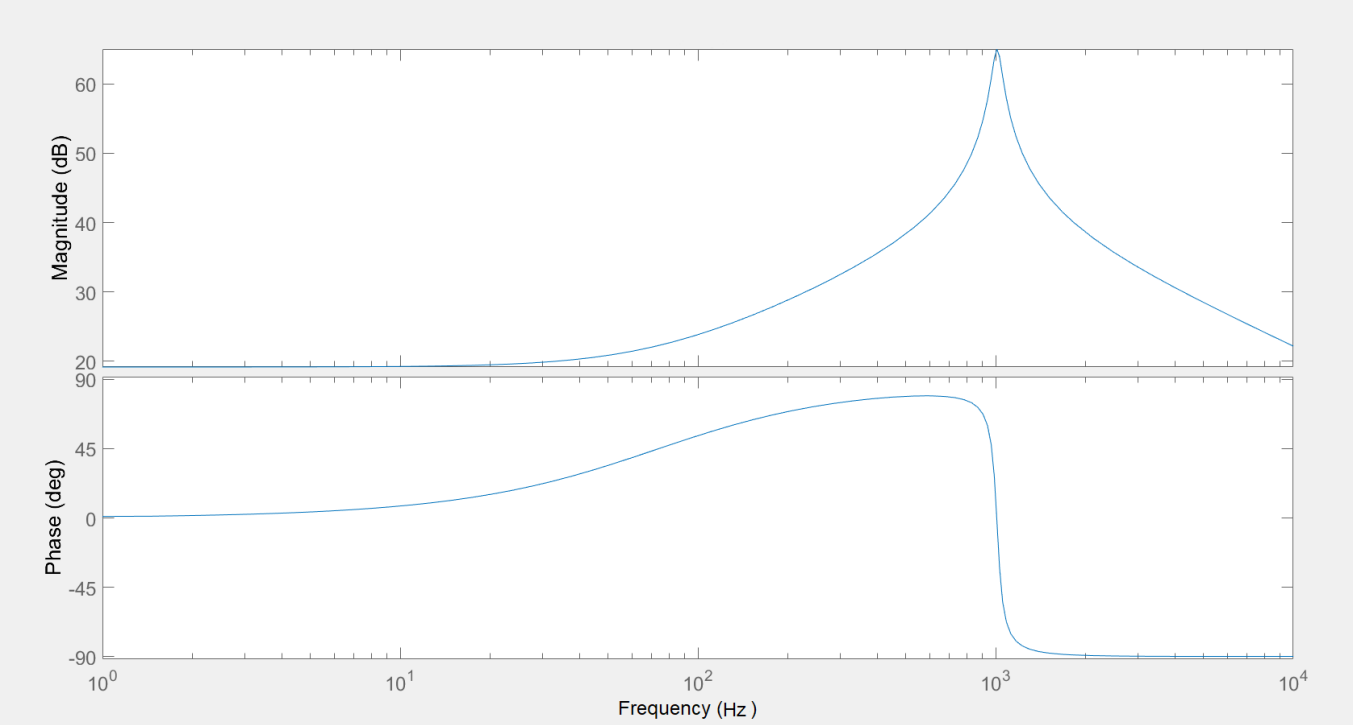

Figure 4-6: Bode Plot of the current plant.

As can be seen from the obtained transfer functions, the system is third order. This means that if one controller is chosen to control the output voltage of the whole system, the controller has to be a 3-pole PI controller or PI type 3. However, to reduce the controller order to a simple first order PI controller, two cascaded closed loop controllers are used. One for the inner current control loop, and the other one for the outer control loop. The design of PI controller can be done using several methods. It can be designed using Ziegler Nicholas, Pole placement method and Frequency response [42]. For simplicity, SISO tool from MATLAB SIMULINK is used to tune the controller and evaluate the suitability of bandwidth and stability.

The PI controller transfer function is represented as follows.

$$K_p + \frac{K_i}{s} = K_p \frac{s+K_i/K_p}{s} \quad . \tag{4.20}$$

For obtaining accurate values of K_p and K_i, the SISO tool in MATLAB SIMULINK is used. Since the voltage loop and current loop are decoupled, each PI controller can be designed separately. The PI

controller for the current loop is designed for the plant given by equation (4.19). Therefore, the open loop transfer function of the inner current loop $G_{i\_OL}(s)$ is as follows.

$$G_{i\_OL}(s) = K_p \frac{s+K_i/K_p}{s} \times G_i(s) \tag{4.21}$$

The PI controller for the outer voltage loop is designed for the following plant.

$$\frac{G_{i\_OL}(s)}{1+G_{i\_OL}(s)} \times \frac{v_c(s)}{i_i(s)} \tag{4.21}$$

It is, basically, the transfer function of the closed inner current loop multiplied by equation (4.16). Figure 4-7 shown the block diagram of the outer voltage control loop with the inner current loop.

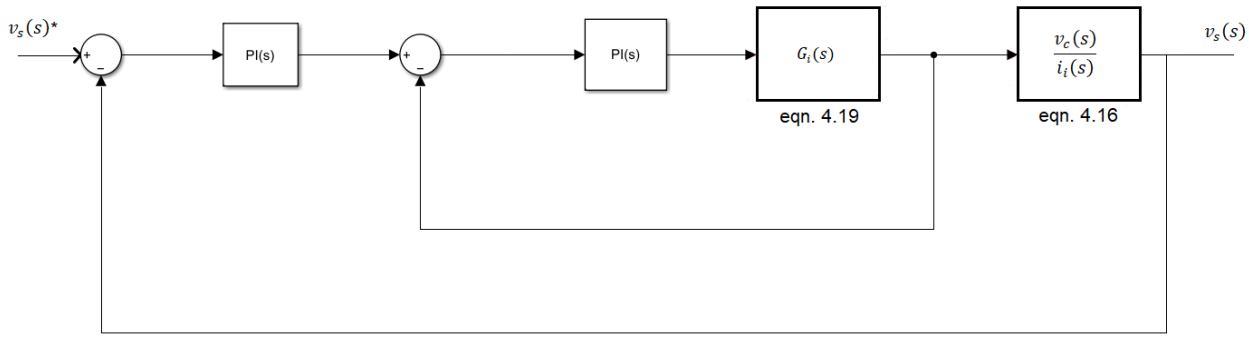

Figure 4-7 the block diagram of the outer voltage control loop with the inner current loop.

The obtained PI controller parameters by MATLAB SIMULINK SISO tool are brought in Table 4-3. K_{pi} is the proportional gain of the current controller, K_{ii} is the integral gain of the current controller, K_{pv} is the proportional gain of the voltage controller, and K_{iv} is the integral gain of the voltage controller.

Table 4-3 Control Parameters

Current loop	K_{pi}	3.97
	K_{ii}	1170
Voltage loop	K_{pv}	0.38115
	K_{iv}	400

4.5 Simulation

MATLAB SIMULINK program is used to realize the simulation. The battery, which is designed in chapter 3, is connected to the Full bridge IGBT single-phase inverter. The designed LC filter is connected at the output of the inverter to have a sinusoidal voltage signal at the load side. The simulation circuit is shown Figure 4-8.

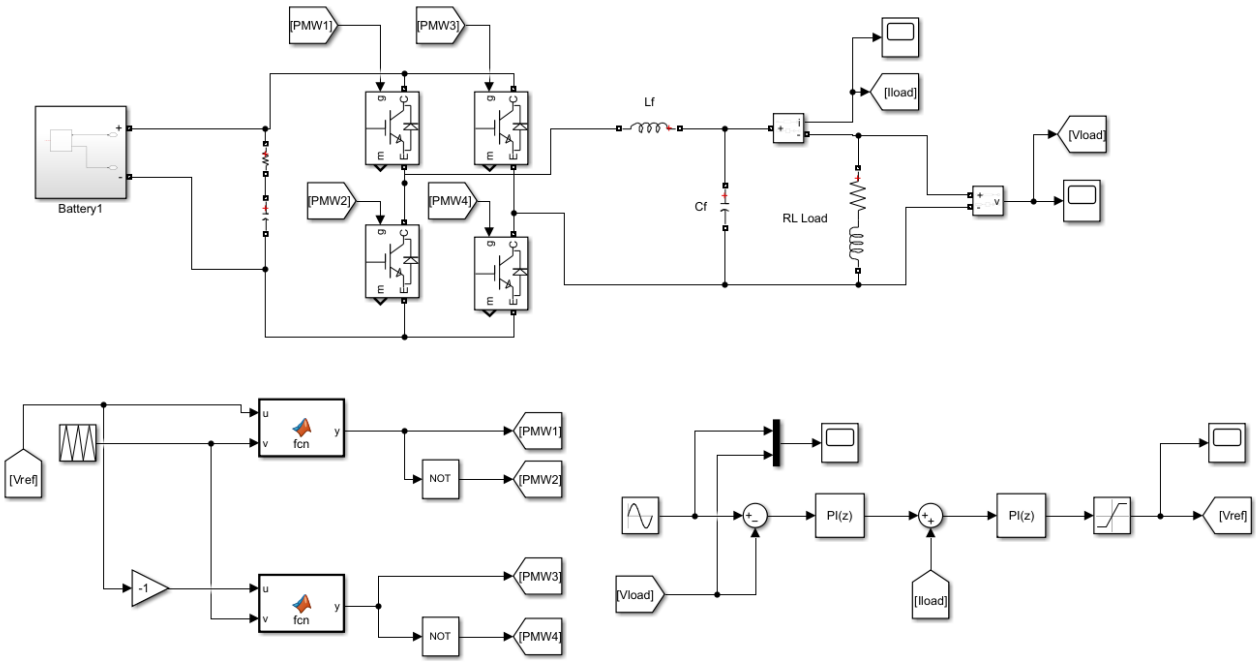

Figure 4-8: MATLAB SIMULINK simulation of complete system.

A designed car battery of 400 V is connected to the inverter input. The unfiltered output voltage of the inverter is passed through an LC filter of 0.5 mH and 50 μF. Finally, it is applied to the load that is similar to the household load. For control, the filter inductance current and the filter capacitor voltage are sensed and sent to the control circuit. The sensed output voltage is compared with the desired reference AC voltage of 120 V, 60 Hz. As a result of this simulation, a 120 V, 60 Hz voltage waveform is obtained. The output voltage and current results and PWM waveforms are shown in Figures 4-9 to 4-12.

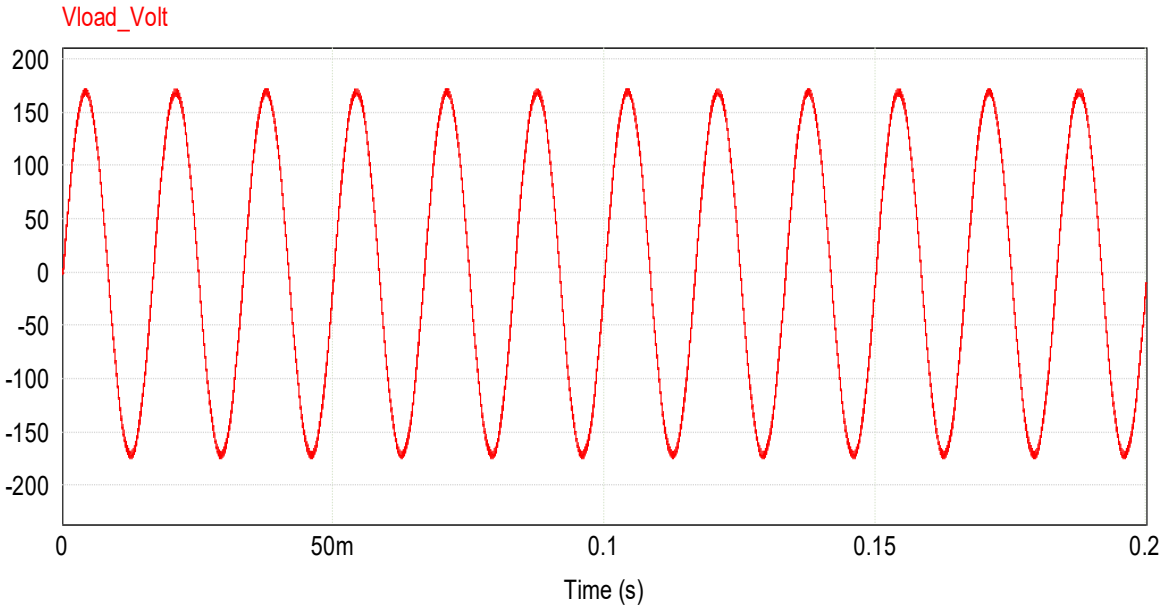

Figure 4-9: Output voltage result of the system.

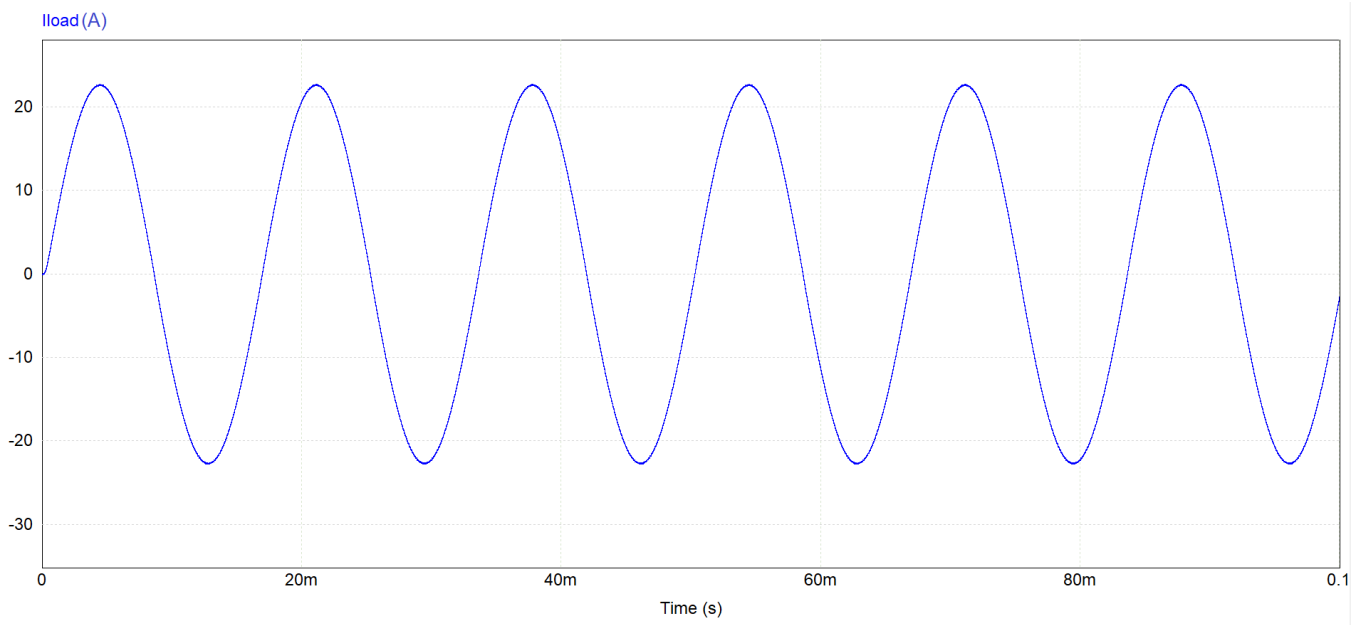

Figure 4-10: Output current result of the system.

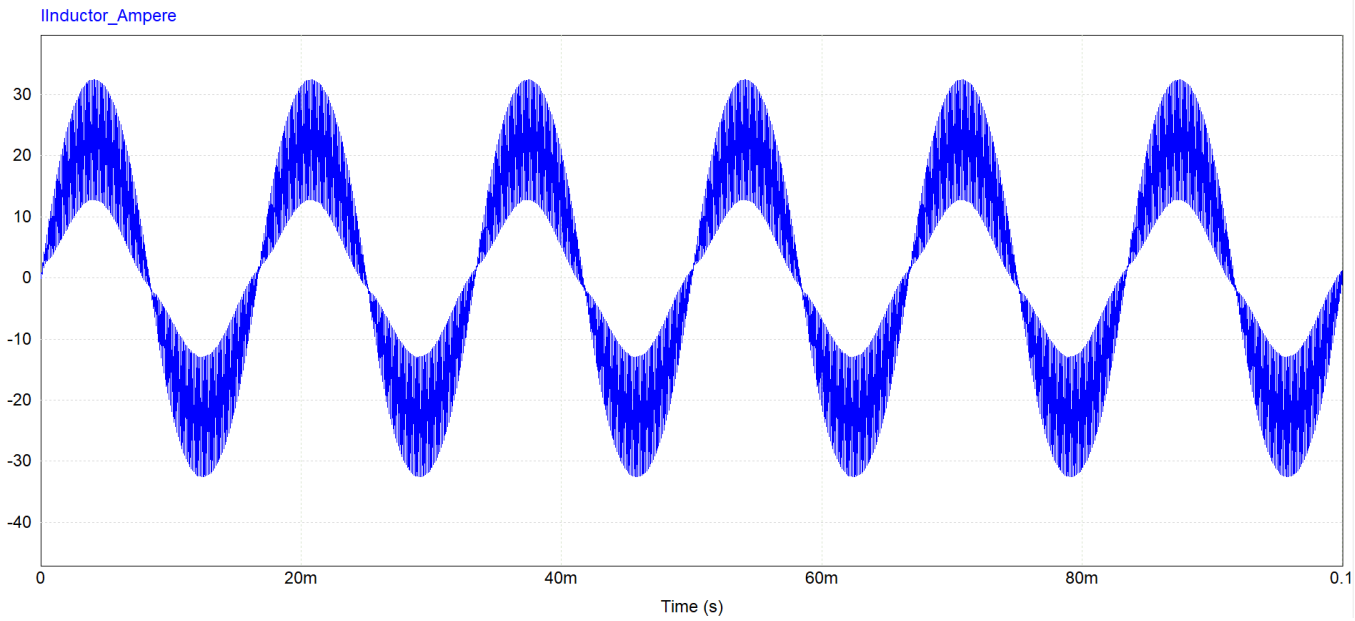

Figure 4-11 Inductor current result of the system.

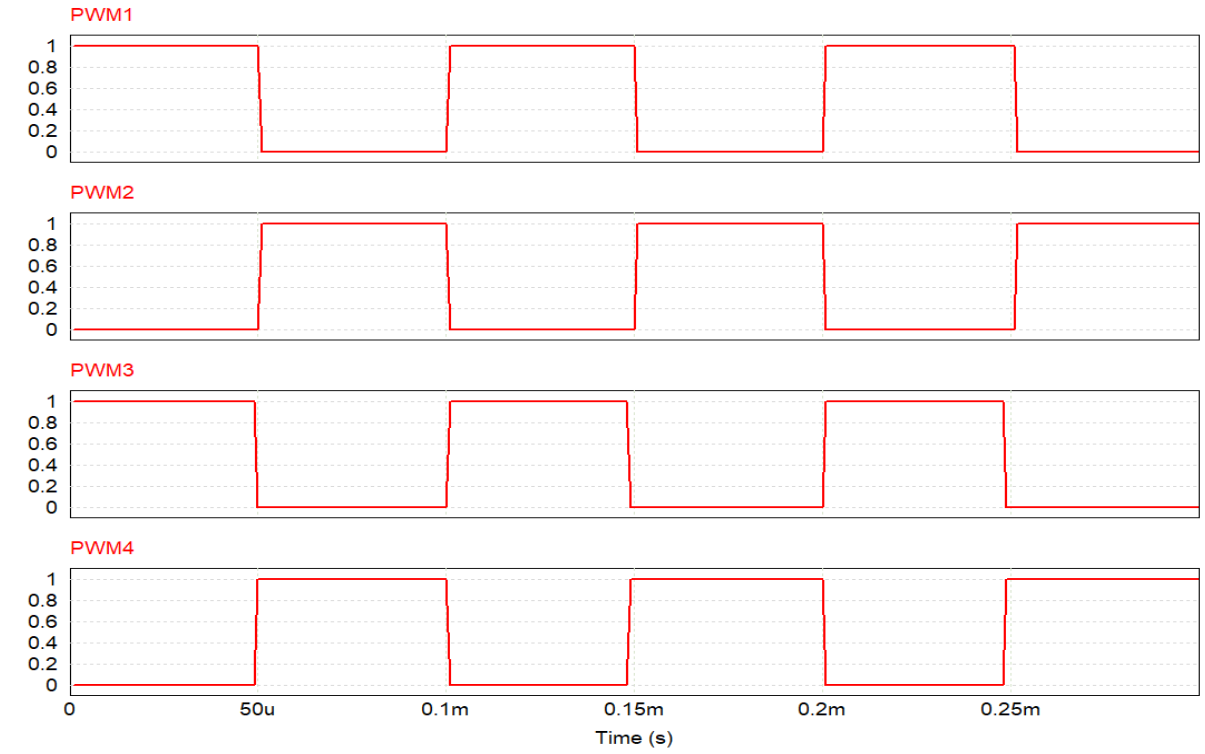

Figure 4-12: PWM Waveforms of the system.

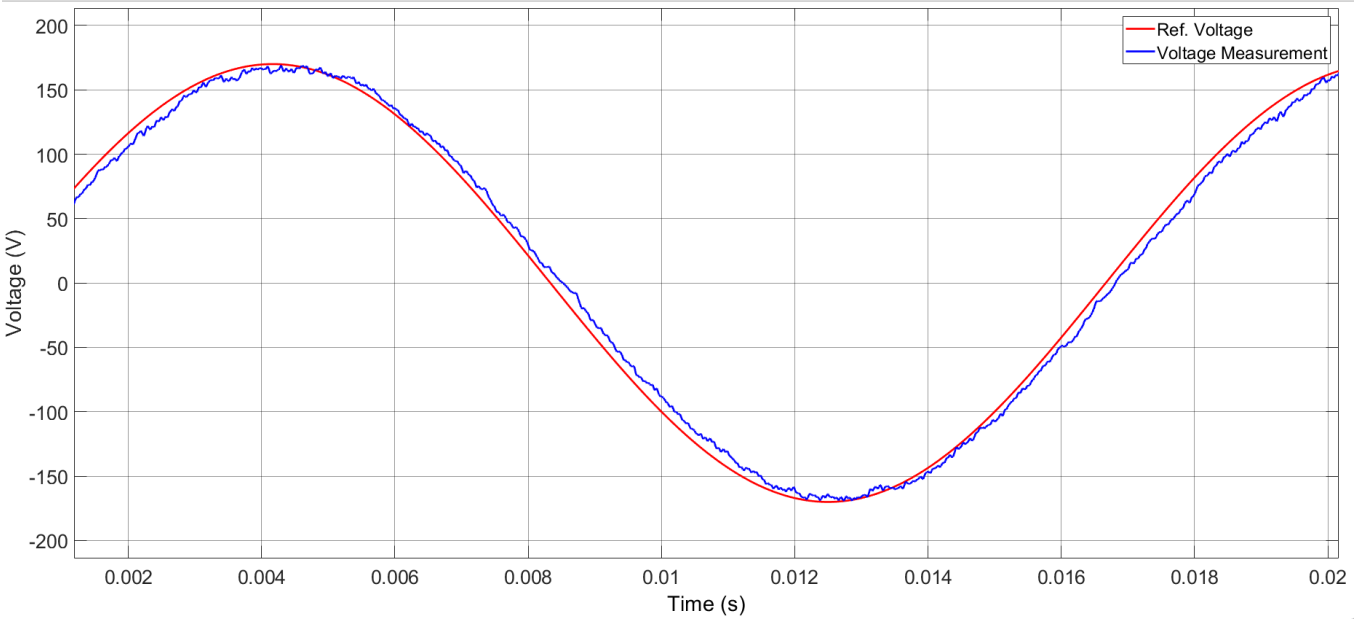

Figure 4-13 Comparison of Output and Reference Voltage

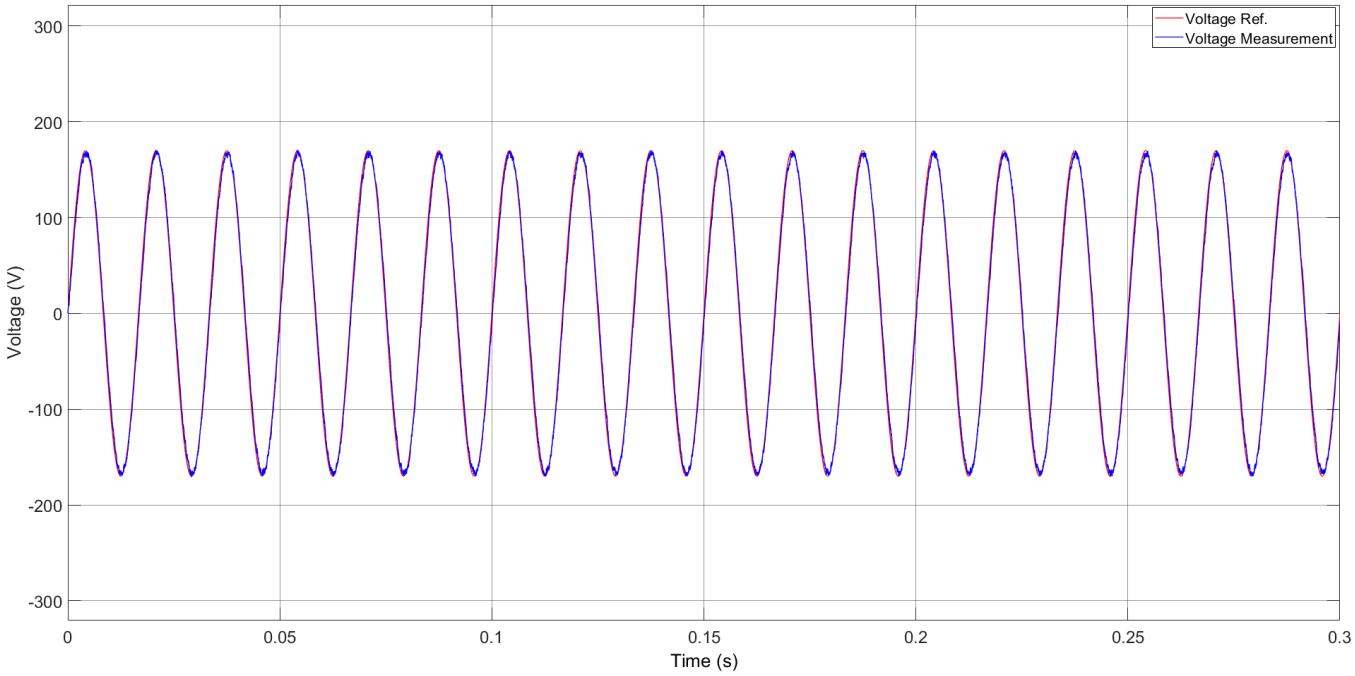

Figure 4-14 Output and Reference Voltage

As can be seen from Figure 4-13 and 4-14, the output voltage is not following exactly the reference voltage. There is a small phase shift delay. This is expected since a proportional integral controller is used. Since the application is off grid, this is not an issue. However, if the system is to be connected to the grid, then a different type of controller is need. A proportional resonance control is usually used for such an application.

5 Experimental Setup

5.1 Introduction

The system which is designed and simulated in Chapter 4 is built experimentally in this chapter.

5.2 Setup

This experimental setup is built step-by-step to make an AC grid-like voltage from the DC car battery voltage at the PEER group laboratory.

A Variac and a 3-phase rectifier are used to make a DC car battery-like voltage. The generated DC voltage acts as the battery voltage. Two legs of an APS three-phase inverter are used to form an H-bridge single-phase inverter. Then, the AC voltage created at the inverter output is filtered out using an LC filter, which was designed in Chapter 4. Finally, a resistive dummy load is used to test the circuit functionality. Then different types of loads such as kettle, microwave, and laptop are powered on using the built V2L circuit. The transient and steady-state results are captured via an oscilloscope. Figure 5.1 shows the schematic of the system.

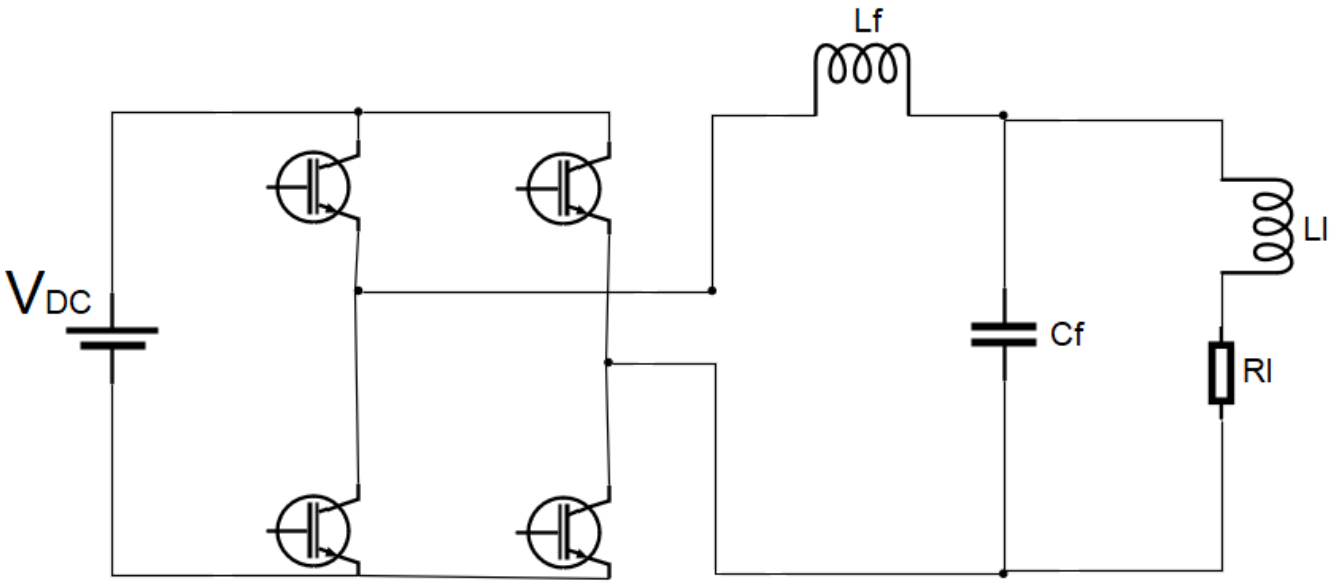

Figure 5-1: Schematic of the System.

Figure 5.2 shows the experimental setup of the circuit in Figure 5.1. The values of the elements used in the setup are in Table 5.1. Vdc is the input voltage of the inverter. The values of the inductor and capacitor are chosen to be close to the designed circuit of Chapter 4 according to the available elements in the laboratory.

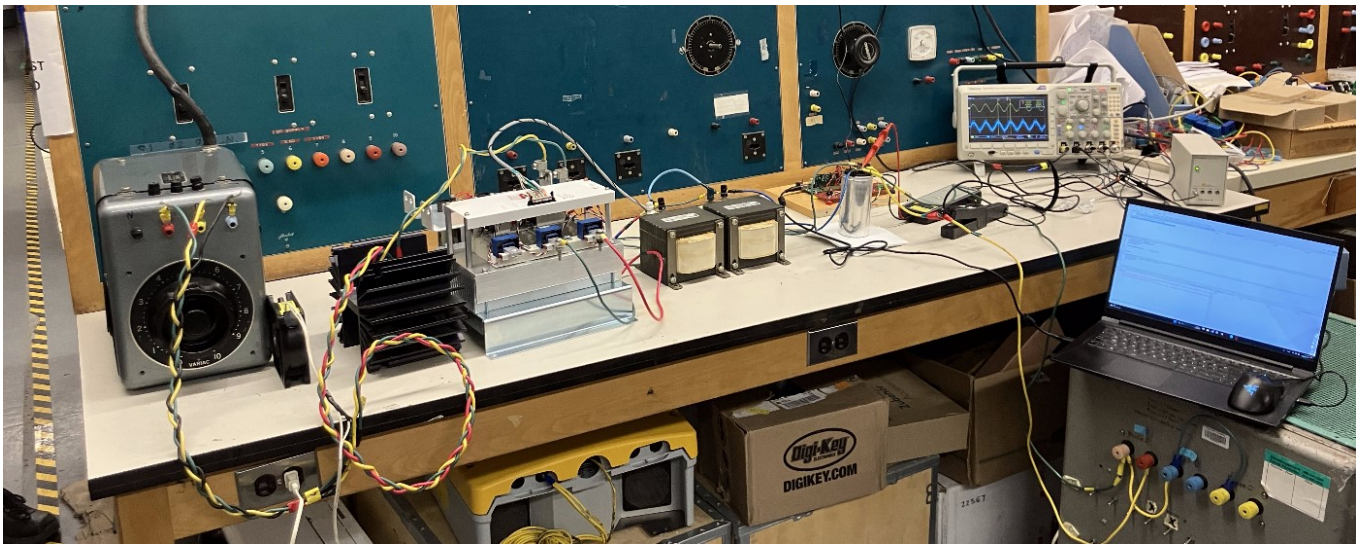

Figure 5-2: Experimental Setup.

Figure 5-3: Experimental setup; (1) Variac, (2) 3-φ rectifier, (3) Controller, (4) Resistive load, (5) Inverter, (6) DSP board and the level Shifter circuit, (7) Oscilloscope, (8) LC Filter.

Table 5-1 The values of the elements used in the setup

Vdc	300 V
C_f	50 μF
Lf	0.5 mH, 20A
Rl	7.5 Ω
M	0.75
Ll	980 μH

First, Opal-RT real-time simulator is used for the control part of the circuit. Then, it is decided to use a DSP microcontroller instead to make the circuit portable. The used DSP microcontroller model is F28335 from Texas Instrument. This microprocessor uses a 5 V DC for its input port. The output PWM digital signals are from 0 to 3.5 V. In order to transfer the simulation to this microcontroller, the simulation that is created in MATLAB program is first converted into code by MATLAB compiler. Then, this code is transferred to code composer studio (CCS), which is the program of Texas Instrument, making it ready to be written on the microcontroller processor. Finally, the code adjustments are made and transferred to the processor.

Since the PWM digital signal of the inverter has to be from 0 to 15 V, four of a HCPL2200 level shifter are used to convert the 0 to 3.5 V PWM digital signals of the F28335 microcontroller to 0 to 15V digital signals. The connection diagram of the F28335 microcontroller with the level shifter, and the experimental setup connection are shown in Figures 5-4 and 5-5.

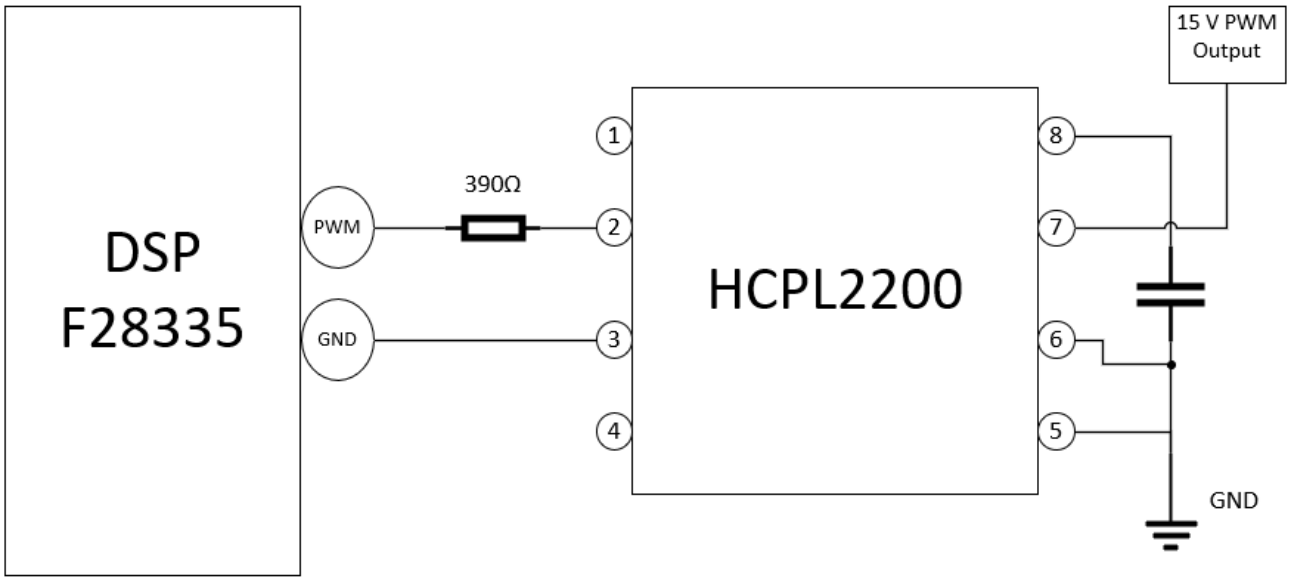

Figure 5-4: The connection diagram of the F28335 processor and the level shifter.

The HCPL-2200 is a low input current logic gate optocoupler. To connect the level shifter with the DSP board, a 390 Ohm resistor is selected for low current draw. In addition, as indicated in the datasheet of the level shifter, a 0.1 µF capacitor needed to be connected between the output legs 5,6 and 8.

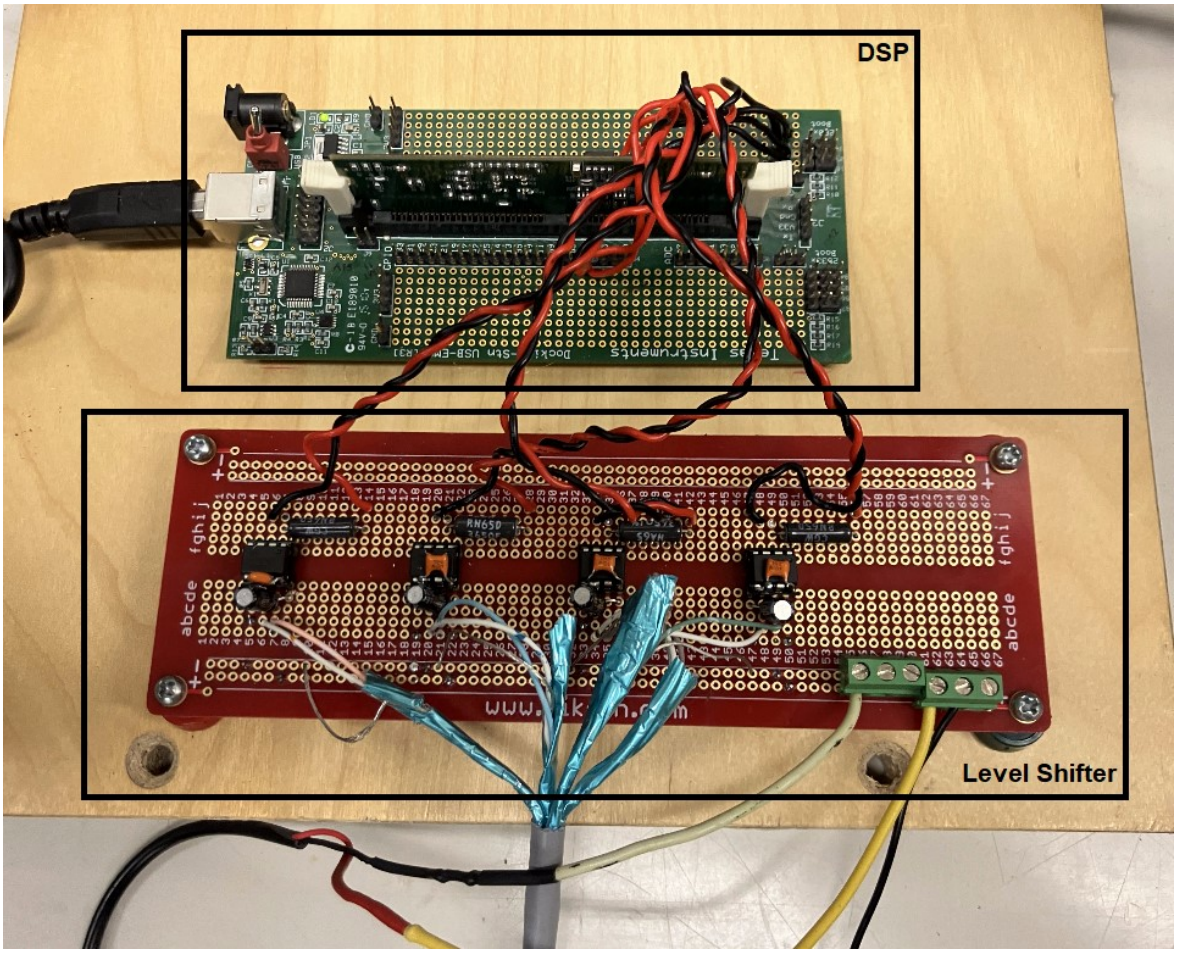

Figure 5-5: Experimental Setup Connection of DSP board and the Level Shifter.

5.3 Results

The system built in the laboratory is supplied from the Grid. The AC grid voltage is then rectified with a 3-phase diode bridge rectifier. As a result of this process, a battery-like voltage is created. Then, the obtained signal is sent to the inverter, and as a result, an AC voltage signal is obtained. The obtained voltage signal is passed through an LC filter. The system was completed by connecting to the load in the laboratory. Results from Experimental Setup are shown in Figures 5-6 to 5-12.

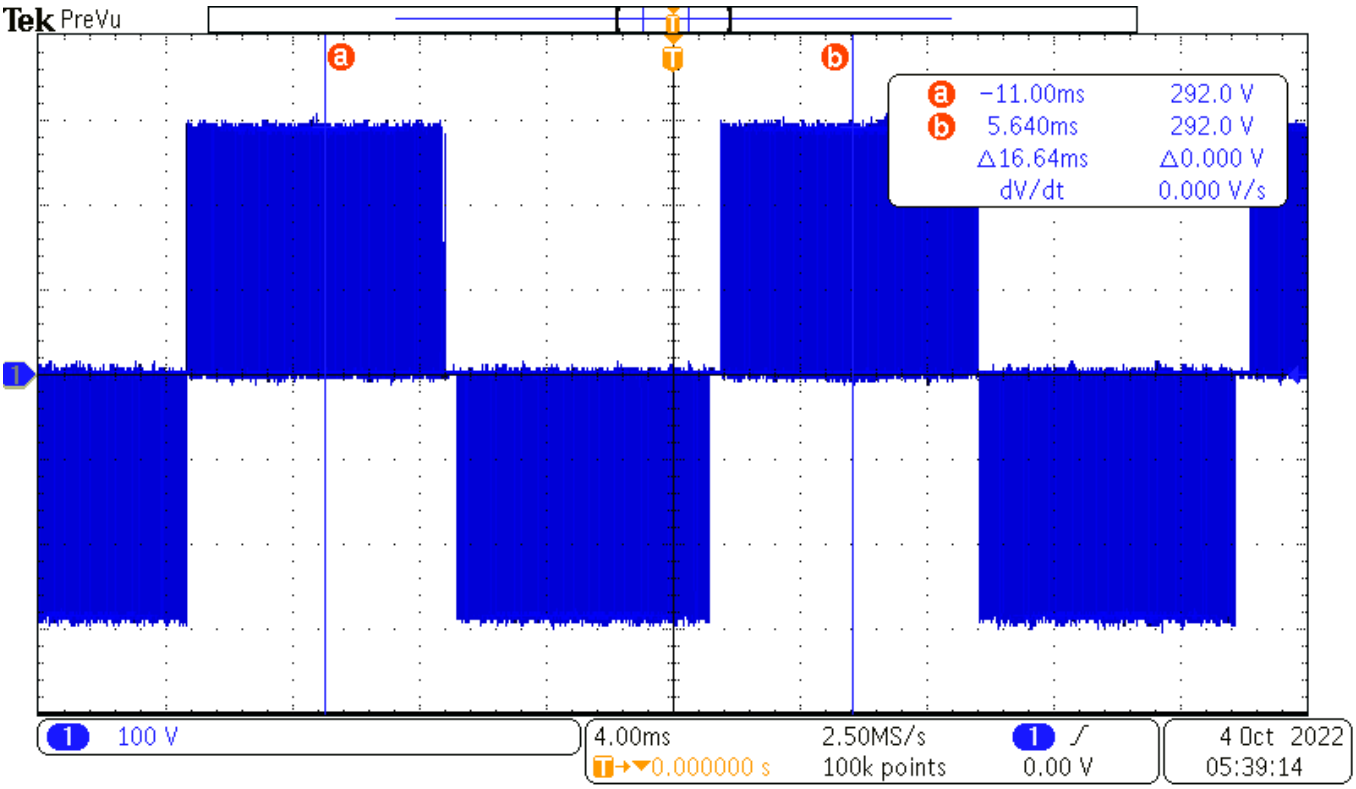

Figure 5-6: Output Voltage of the Inverter without Filter.

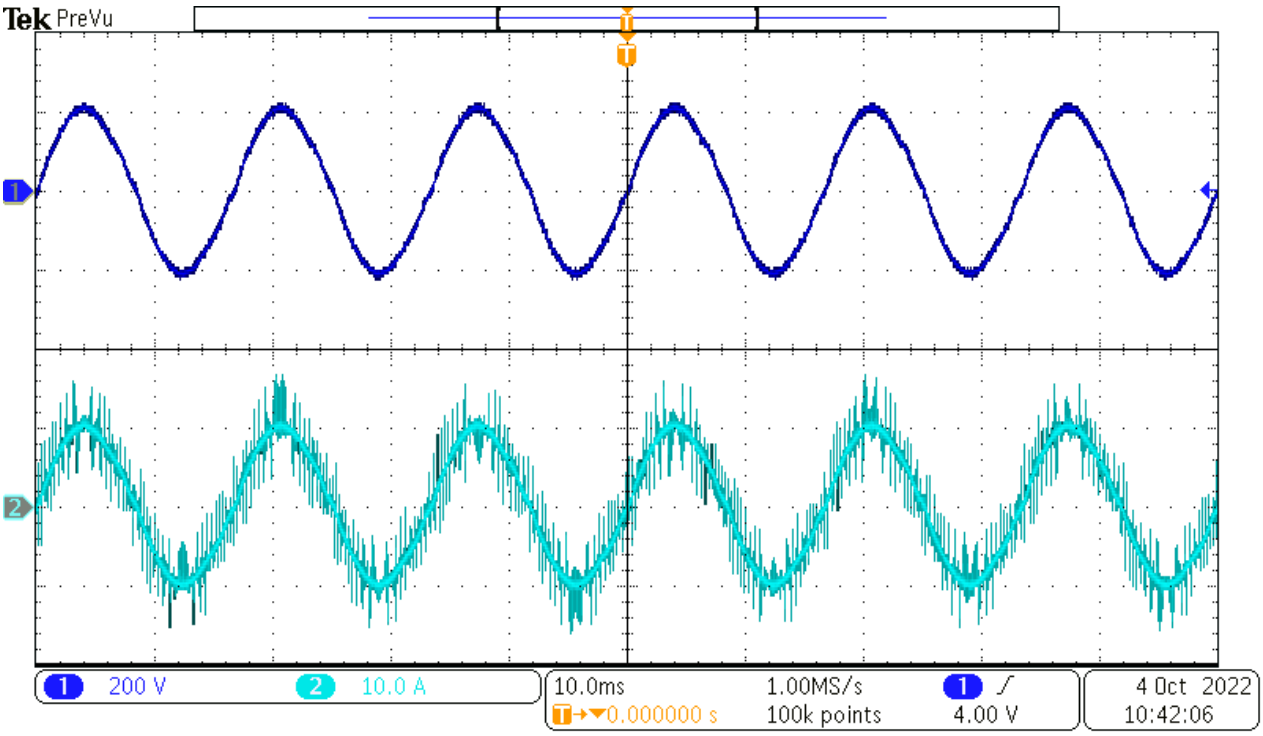

Figure 5-7: Load voltage and current.

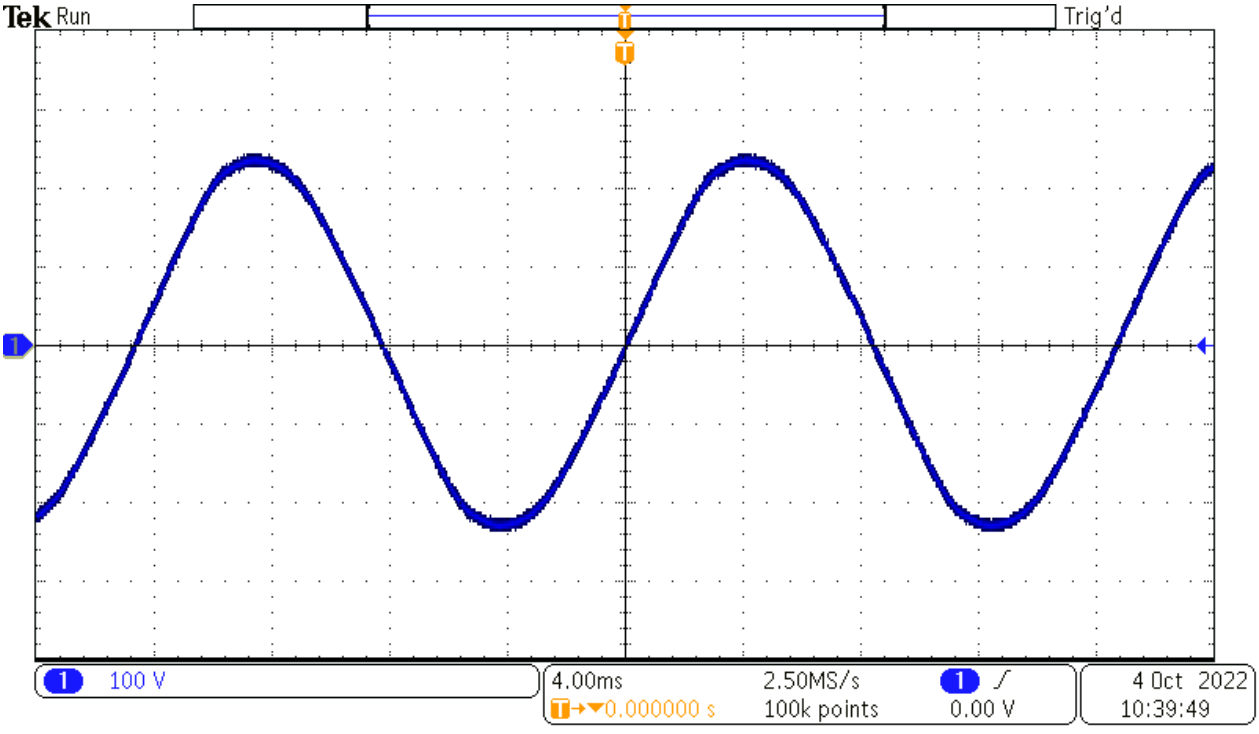

Figure 5-8: Load Voltage.

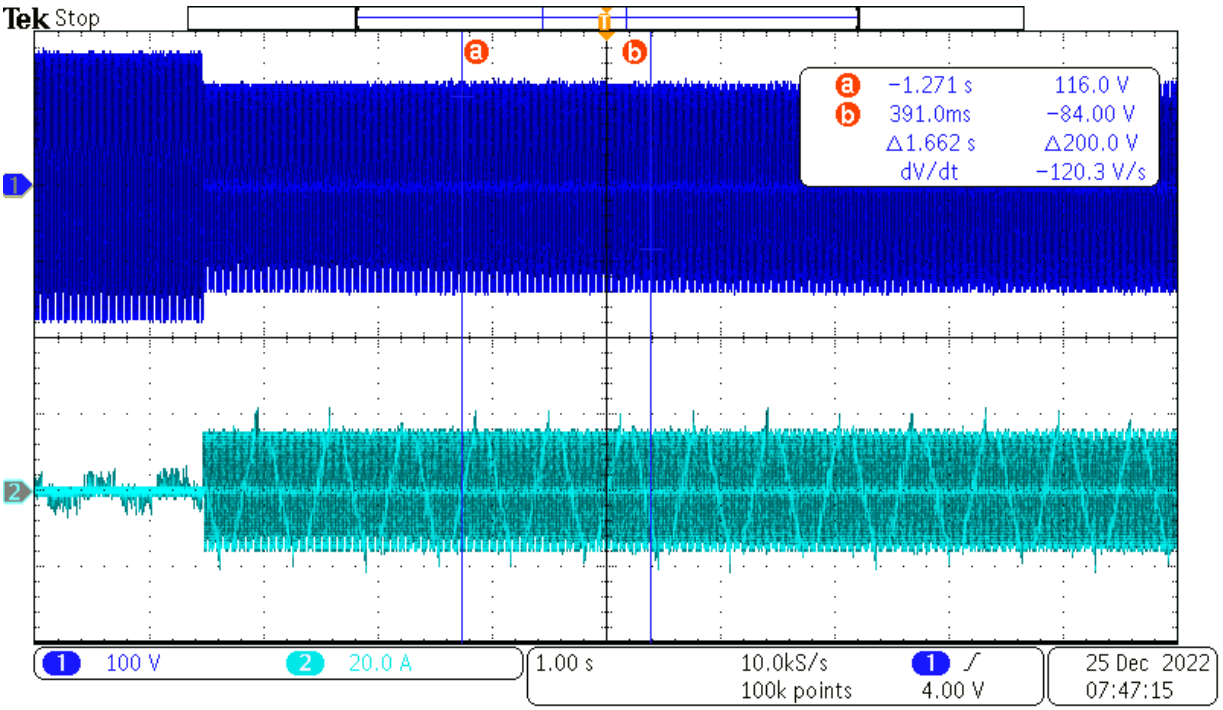

Figure 5-9 Transient Current and Voltage of Kettle

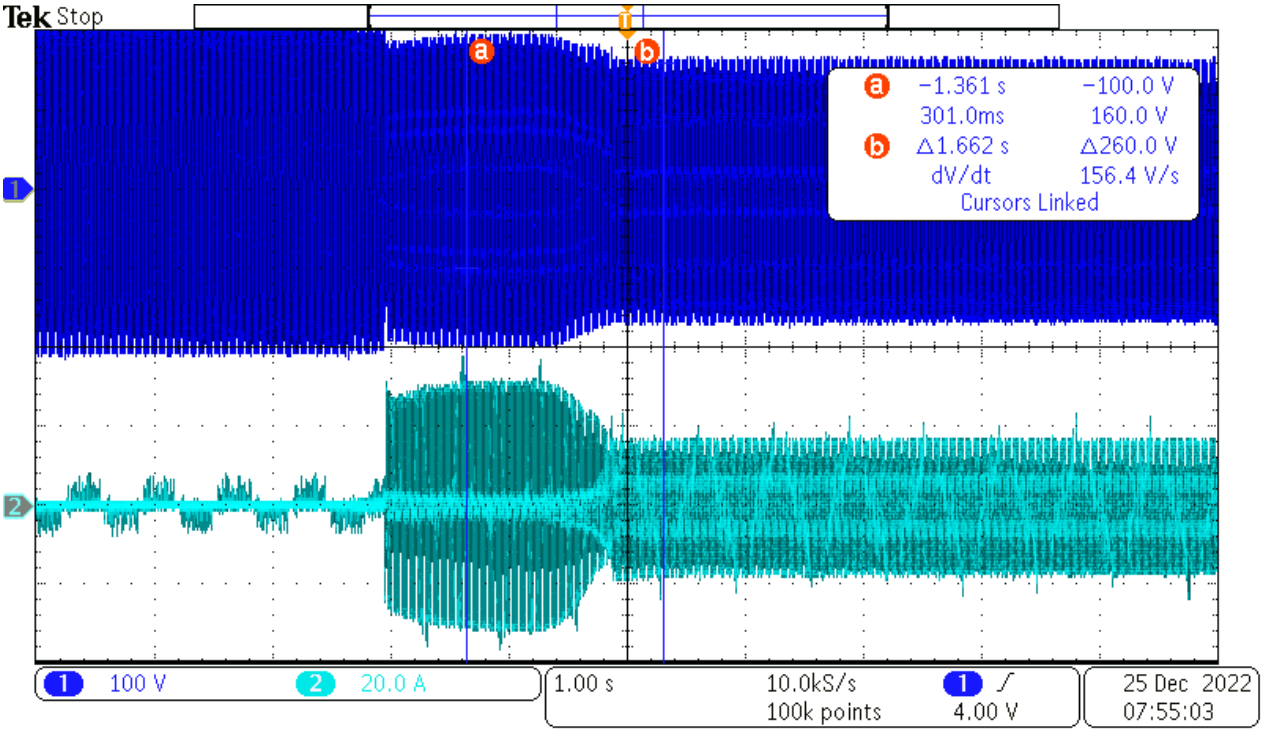

Figure 5-10 Transient Current and Voltage of Microwave

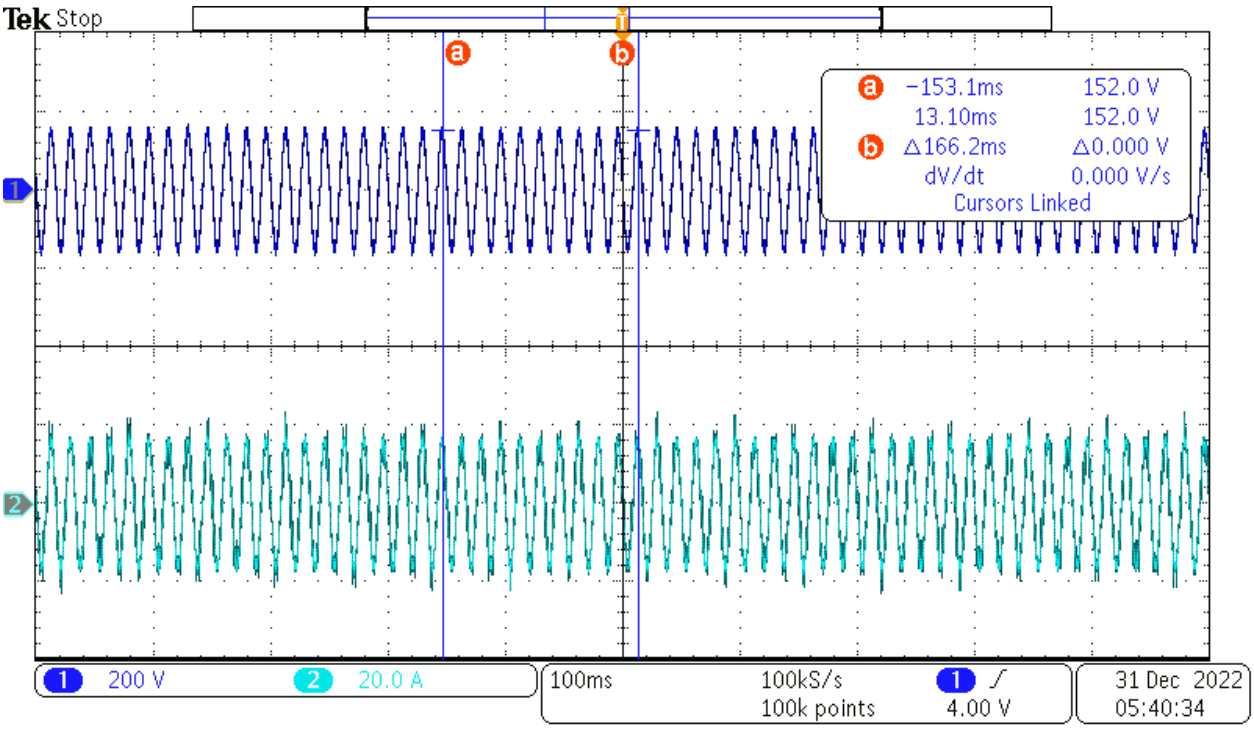

Figure 5-11 Steady-State Current and Voltage of Kettle

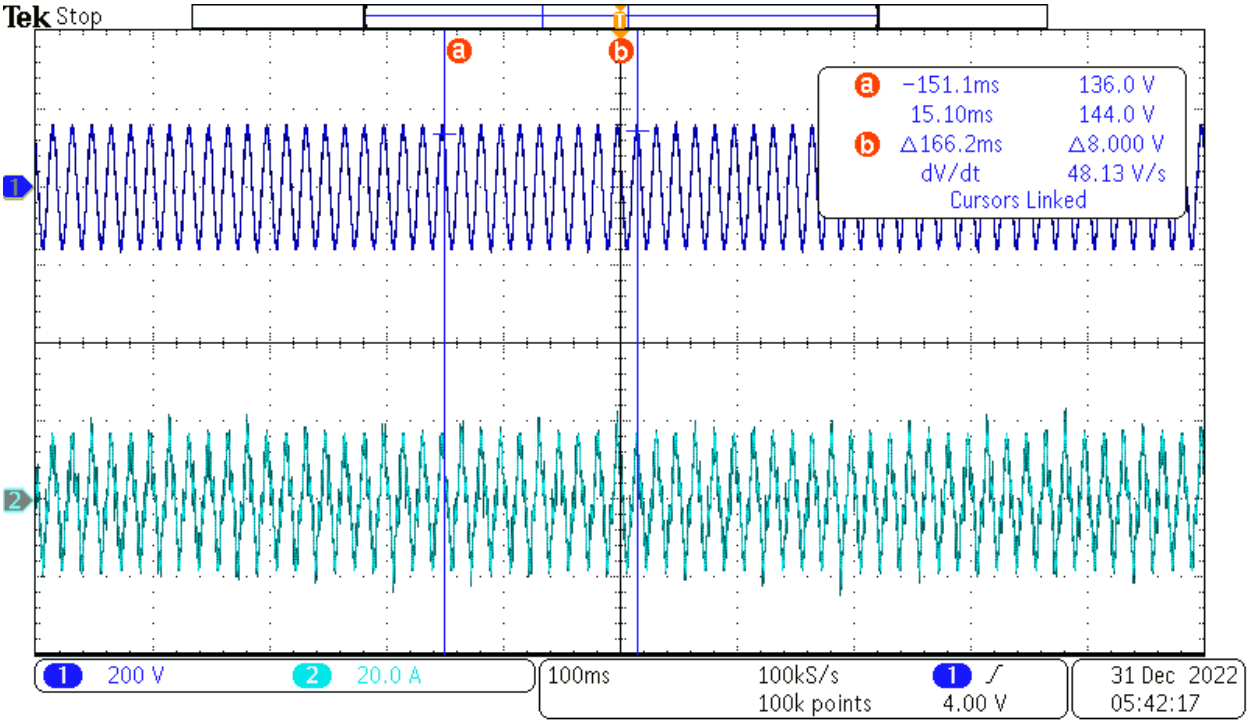

Figure 5-12 Steady-State Current and Voltage of Microwave

As can be seen, the results of the experimental setup are very similar to the ones obtained from the simulation. As a result of the experiment, 120 V RMS is obtained as desired. As observed, the result obtained is found to be strong enough to feed the household load.

5.4 Summary

In this chapter, an experimental setup was performed. The purpose of the experiments was to see if it is possible to make a grid-like voltage in real conditions with this topology. This goal is reached through this experiment. Moreover, The V2L/V2H system has been achieved in a portable and viable way.

6 V2L/H Integration with the FBL

6.1 Introduction

This chapter discusses the feasible methods of powering the loads of the Future Buildings Laboratory (FBL) from the EV battery. Method 1 is V2L. In this method, some of the house loads are independently fed by the EV battery via an inverter. This was simulated and tested in the preceding chapters. Method 2 is V2H. In this method, the EV battery is integrated with the electrical system of the FBL.

6.2 CHAdeMO Connector

With multiple standards, types, connectors, and words used to define chargers, the field of electric vehicle (EV) charging systems is fast growing. The phrase 'electric vehicle supply equipment' (EVSE) refers to the piece of equipment used to charge an electric car. EVSE are further classified into three tiers based on their output power capacities [43]. Level 1 and 2 EVSE provide alternating current (AC) to an electric vehicle's onboard charger, whereas level 3 systems provide direct current (DC) to the EV [43]. The word 'charger' is deceptive for levels 1 and 2, as they are not truly chargers. They provide AC power to the EV, where the onboard charger converts the AC to DC and charges the batteries [43].

The name CHAdeMO is a contraction of the French term "charge de move," or "let's charge and move," and is short for the Japanese term "let's have some tea," indicating that CHAdeMO intends to provide rapid charging infrastructure so that EV owners can recharge their vehicles in as little time as possible [44]. Rapid chargers often seek to charge batteries to 80% capacity because charging durations from 80% to 100% increase dramatically due. CHAdeMO's strength has been its emphasis on safety, with manufacturers obliged to have their chargers authorized and tested by CHAdeMO before they can be marketed as official chargers [44]. The CHAdeMO protocol makes use of a special connector built specifically for DC quick charging. The CHAdeMO protocol also supports bidirectional power flow, often called V2G [44]. CHAdeMO connector and pin layout can be seen in Fig 6-1. Pin layout explanations can be seen in Table 6-1.

Figure 6-1 CHAdeMO Connector and Pin Layout [45].

Table 6-1 Pin layout explanations [45].

Pin Layout	
1	Ground Wire
2	Charger start/stop 1
3	Idle/Empty
4	Charging Enable/Disable
5	Power Supply (-)
6	Power Supply (+)
7	Connection Check
8	Can Bus H
9	Can Bus L
10	Charger start/stop 2

6.2.1 Connector Interface and the Working Principal of CHAdeMO

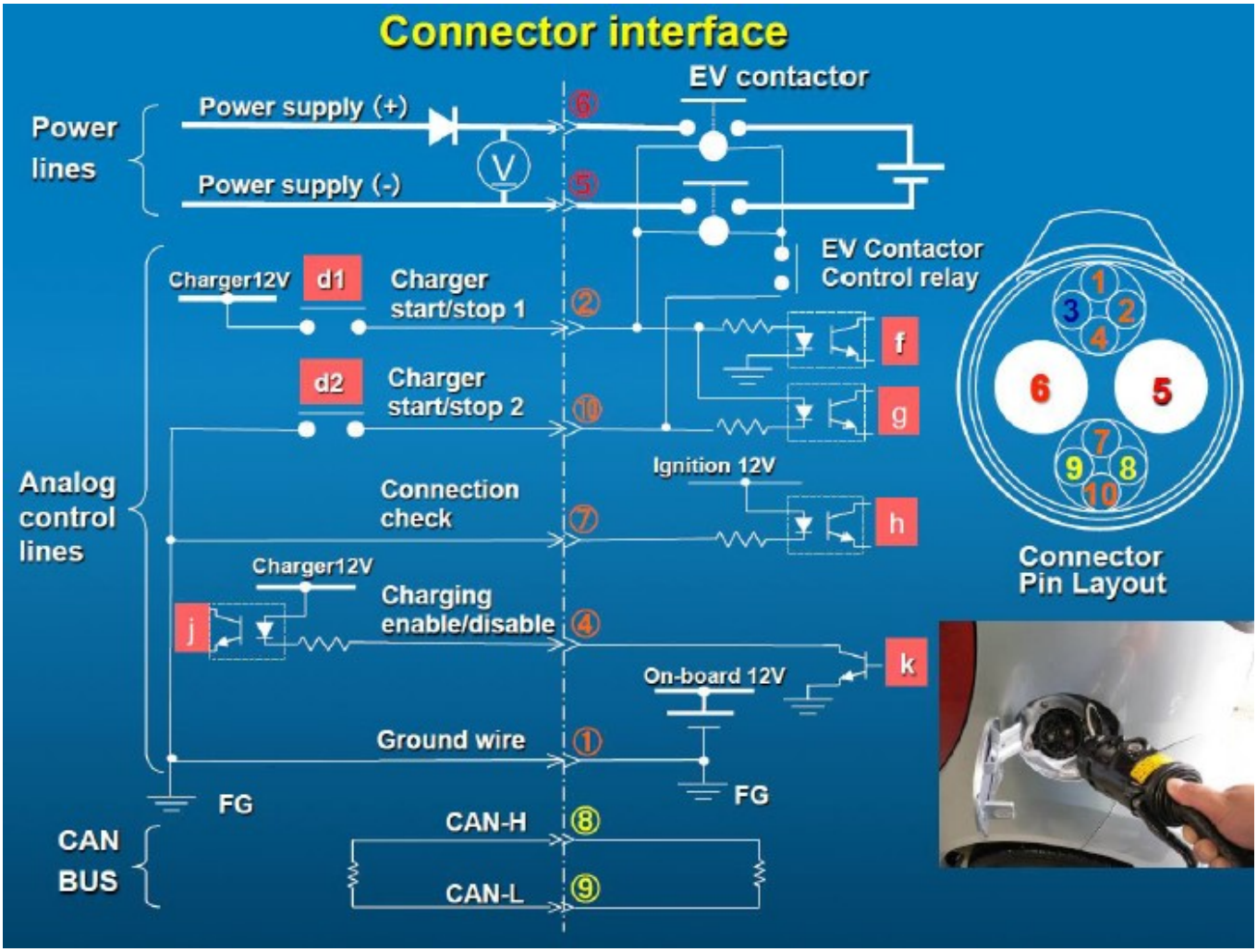

Figure 6-2 CHAdeMO connector interface [45]

The working principle of CHAdeMO is that when the user hits the start charge button, the charger sends a 12 V signal to the EV via the relay 'd1' and activates the photocoupler at 'f'. This is detected by the EV, which then transmits charging parameters (voltage and current restrictions, as well as battery capacity) through the CAN bus. The charger determines compatibility and broadcasts the maximum voltage and current to the EV through the CAN bus. When the EV is satisfied that the charger is compatible, it conducts

the transistor at 'k', which signals the charger that it has permission to enable charging [45]. The charger then secures the connector and tests the insulation and grounding. This verifies that the charger's connector and cable are in good working order and that charging may commence. The charger closes relay 'd2', which conducts the photocoupler at 'g', signalling to the EV that the preparation operations have been completed and charging can begin [45]. The EV may now close its main battery contactor because both 'd1' and 'd2' are now closed. This enables charging by direct connection between the charger and the EV battery pack. The EV broadcasts the required current through the CAN bus every 0.1 seconds, and the charger supplies it via constant current control. If a problem arises, the EV continuously monitors the battery pack characteristics (voltage, current, temperature, and so on) and can halt the current [45]. The connector interface can be seen in Fig. 6-2. The charging sequence can be seen in Fig. 6-3.

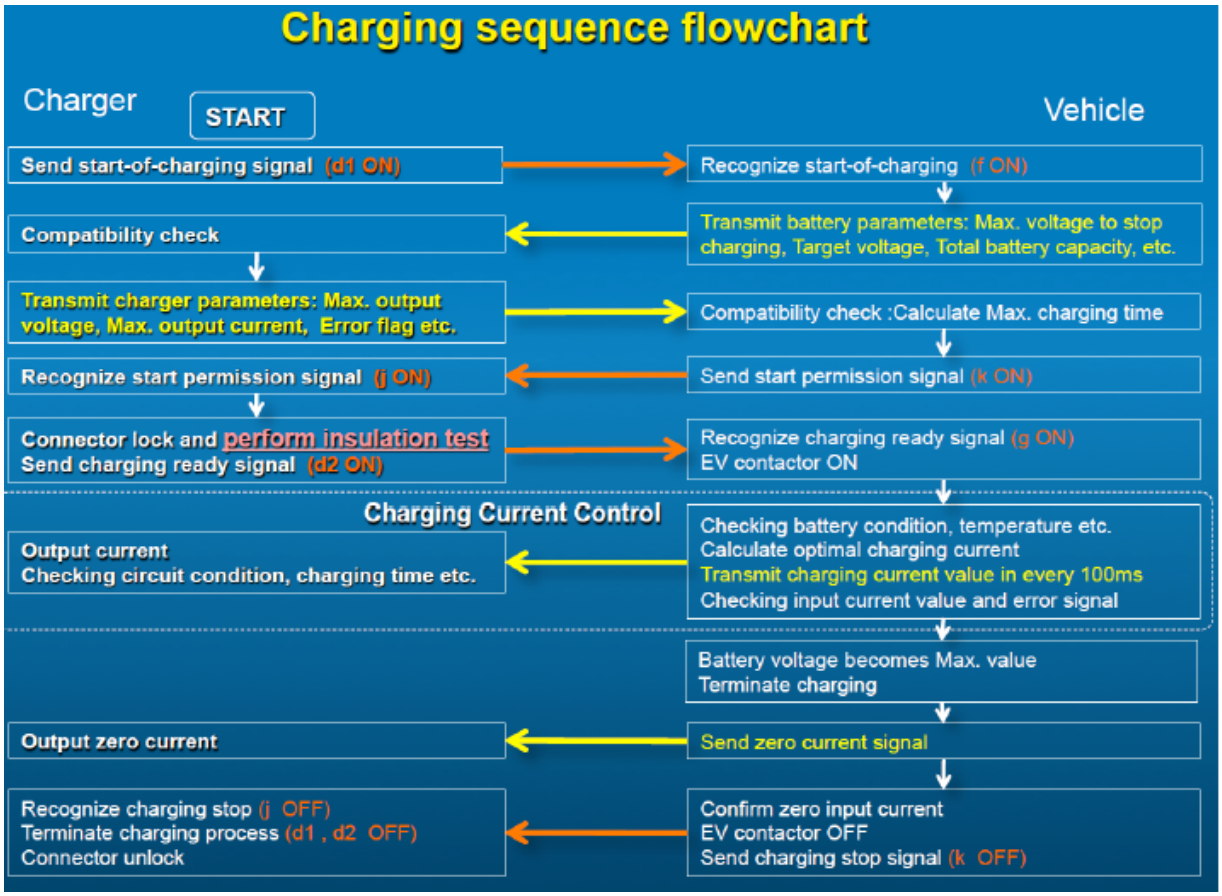

Figure 6-3 CHAdeMO charging sequence flowchart [45]

6.3 Methods of Connection

In this section, the previously mentioned connection methods will be explained. The house' solar system consists of solar panels, batteries, three grid-forming inverters (Sunny Island), and three grid-following inverters (Sunny Boy) working together. Figure 6-4 shows the electrical wiring diagram of the solar system at the FBL.

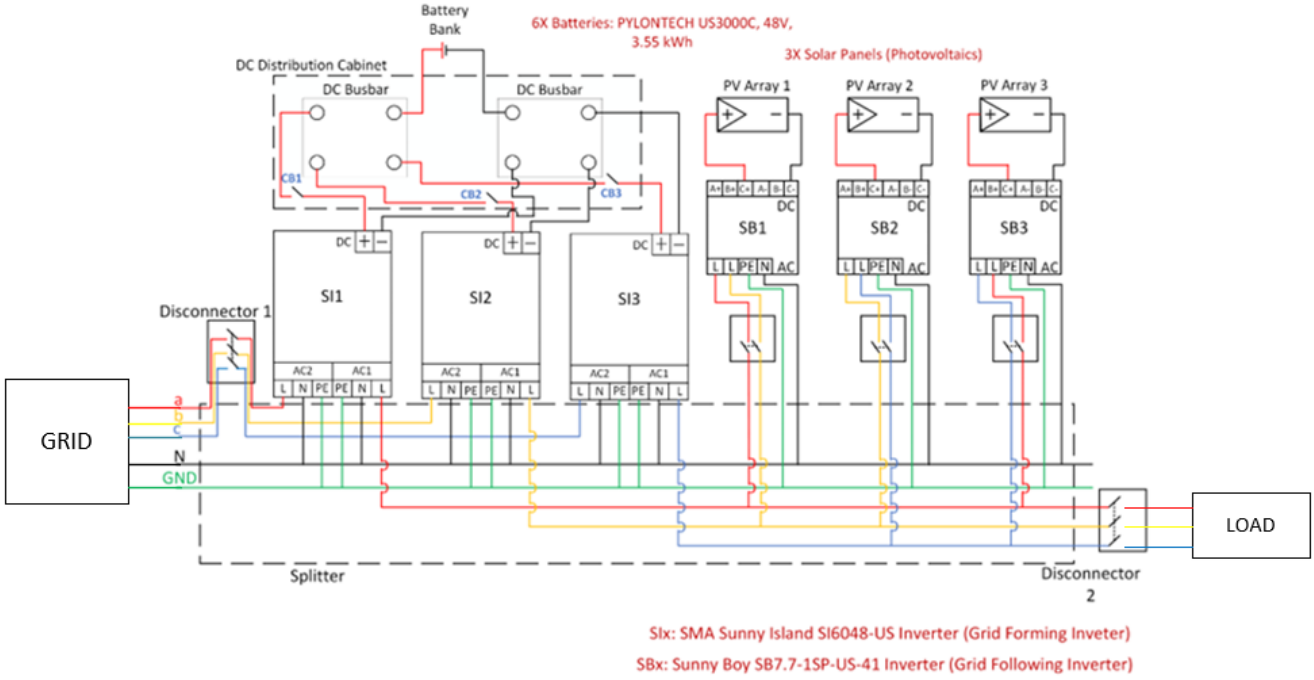

Figure 6-4 House Connection System.

6.3.1 Vehicle-to-Load (V2L)

In this method, the designed and simulated system in the previous chapters is used. This system is a V2L system and provides energy to one or more loads from the EV battery with the help of a single-

phase inverter and a low-pass filter. Figure 6-5 shows the V2L connection. The power from the EV battery is made available through an emergency socket to power independent house loads.

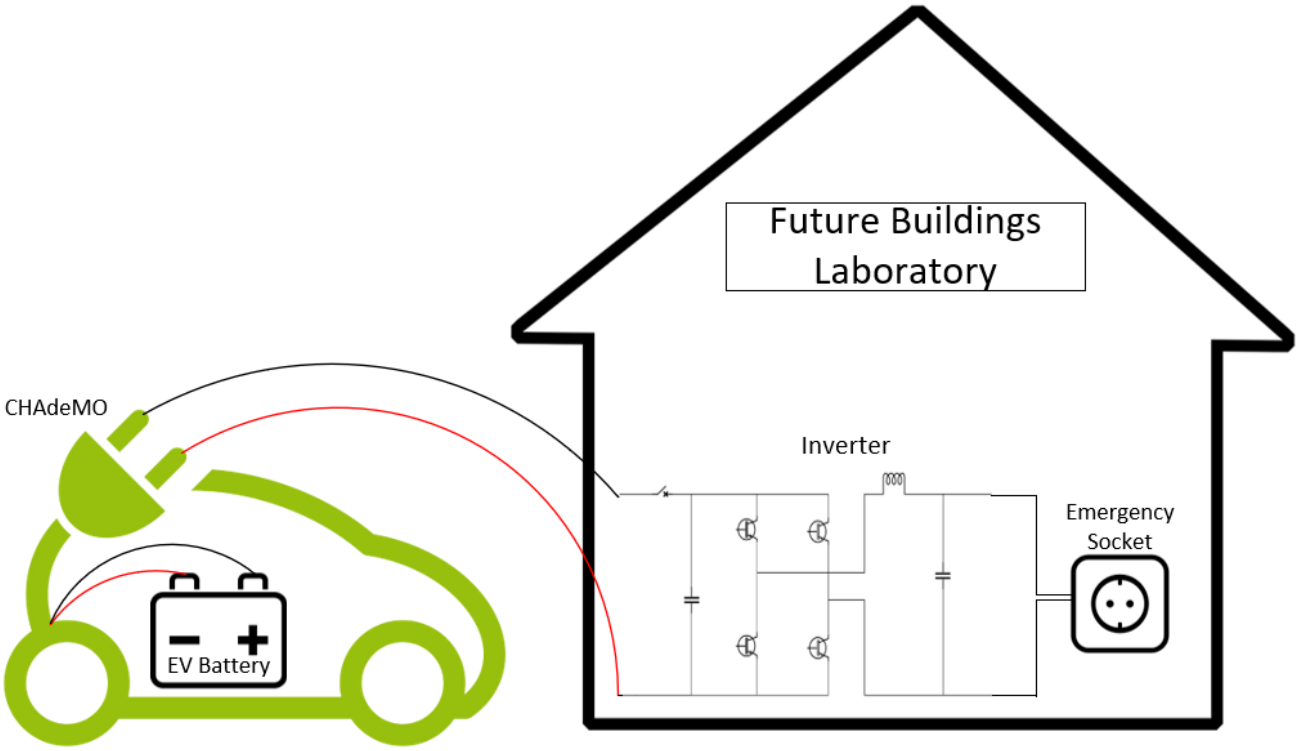

Figure 6-5 V2L connection (Method 1).

6.3.2 Vehicle-to-Home (V2H)

In this method, the EV battery is integrated with the electrical system of the FBL. There are two feasible ways of connection. The first is off-grid. The second is grid connected.

6.3.2.1 Off-Grid V2H

In this method, the EV battery will be connected to the off-grid EV system through a sub panel via the designed single-phase inverter. In order to avoid any possible issues with the existing electrical system of the solar house, the grid mains will be completely disconnected via a three-phase single pole three throw

(SP3T) changeover/transfer switch, which is planned to be installed. In addition, a single-phase single pole double throw (SP2T) changeover/transfer switch is to be installed on one of the three phases feeding the sub panel. The electrician has to ensure that the single-phase highly emergency loads, such as lightening and fire alarms, are fed by that phase which the SP2T is installed on. In this way, the user can manually control the operation of the emergency loads, need to be powered by the EV battery, via the sub panel circuit breakers. Figure 6-6 shows the diagram of the V2H off-grid connection.

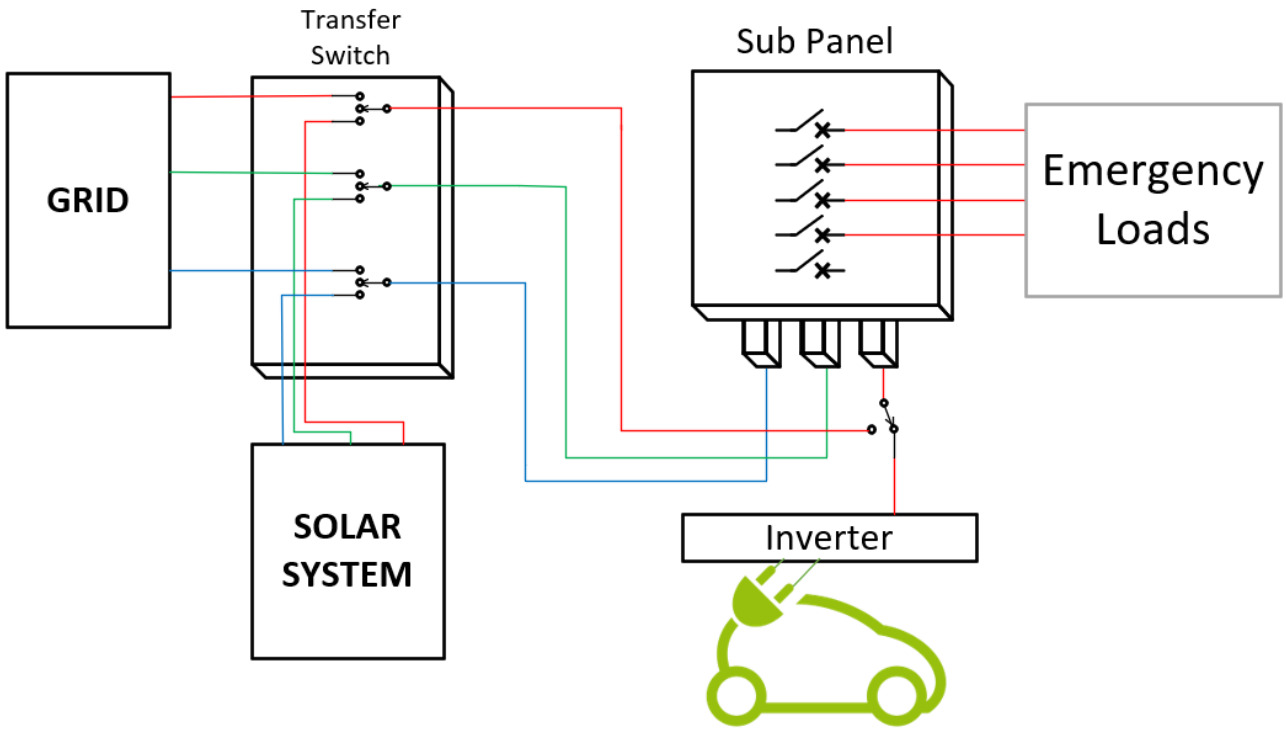

Figure 6-6 Off-grid V2H connection (Method 2)

Table 6-2 shows the single-phase emergency loads.

Table 6-2 Single Phase Emergency Loads

Single Phase Emergency Loads	
Exterior Lighting	105 VA
Mezzanine Lighting and Light Pit	826 VA
Ground Floor Lighting	891 VA
Dsc Intrusion Alarm Box	500 VA
Communication Panel With System	500 VA
Electrified Door	100 VA
Fire Alarm Control Panel	500 VA

6.3.2.2 On-Grid V2H

This method requires a grid-tie inverter. Therefore, in this method of connection, the EV battery is connected directly to the grid-following inverters (Sunny Boy inverters). For this reason, the specifications and the wiring of the Sunny Boy inverter are examined. Figure 6-7 shows the Sunny Boy Inverter.

Figure 6-7 Sunny Boy Inverter.

The Sunny Boy is a transformer-less PV inverter that converts the direct current of the PV array to grid-compliant alternating current and feeds it into the utility grid. The battery of the EV is connected to the Sunny Boy inverters together with the PVs. The characteristics of the Sunny Boy inverter are shown in Table 6-2. Figure 6-8 shows the connection of the EV battery to the Sunny Boy inverter.

Table 6-3 Sunny Boy Inverter Specifications

Sunny Boy SB7.7 US	
Input	
Max Power	10905 Wp
Max DC Voltage	600 V
MPPT Operating Voltage Range	100-550 V
Max Operating Current per MPPT	10 A
Output	
AC Nominal Power	6660/7680 W
Nominal Voltage	208/240 V
AC Grid Frequency	60/50 Hz
Max Output Current	32 A

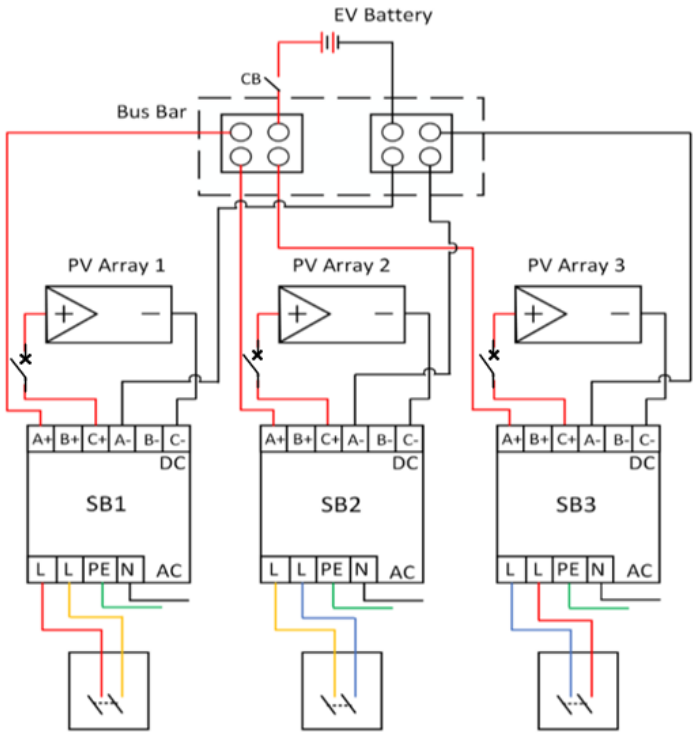

Figure 6-8 Grid connected V2H system (Method 2).

6.4 Enabling the Discharging Feature of EVs

Enabling the discharging feature of EVs is essential to establish any V2X connection. Most EVs are equipped with hardware and software features that protect the battery from being discharged unless instructed to perform so. In addition, in any EV, the discharging is made possible through the DC fast charging port, which comes with two configurations: ChAdeMO and CCS. Some of EVs which adopt CHAdeMO are Nissan Leaf, Mitsubish i-Miev, Mitsubishi Outlander PHEV, Kia Soul EV Mk1, and Citroen C-Zero. Nissan is leading the V2X technology with their Leaf since 2014. Also, the Mitsubishi i-

Miev was widely used for V2L especially during the Great East Japan earthquake in 2011. This section focuses on how to enable the discharging feature of a Nissan Leaf or a Mitsubishi i-Miev.

6.4.1 Manual Configuration for EV Battery Discharging

EV discharging is made possible via CAN Bus communication protocol between the bidirectional charger and the EV. Right now, there are few bidirectional chargers in the market. These are Quasar2 from Wallbox and FE-15/FE-20 from Fermata Energy. Both are mainly made to work with Nissan Leaf. While Quasar2 is legally marketed in China and Europe, its emerging in North America is yet to come. Probably by the end of 2023 or early 2024. However, Fermata Energy started the legal installation/integration of their EV bidirectional charger in the USA in 2021 with Nissan Leaf. It is being used for vehicle-to-grid (V2G) in public spaces, however, its functionality for homes as V2H is not published [46]. Therefore, at this moment, no commercial EV bidirectional chargers, which perform V2H/V2G, are available in Canada. Moreover, the CAN Bus protocol is monopolised by the CHAdeMO company. This leaves Canadian EV users, who would like to experience the V2H technology with no choice but to manually configure their vehicles to enable the discharging feature. Not all EVs could be manually configured for discharging. While the following configuration can be done for the Mitsubishi i-MiEV, it does not apply to the Nissan Leaf, even though both vehicles use CHAdeMO for DC fast charging. This is because some EV manufacturers equip their vehicles with discharging protection features that prevent any manual trials to discharge the battery.

To start manual discharging, the pins of the CHAdeMO connector to be connected to 12 V and ground are shown in Figure 6-9.

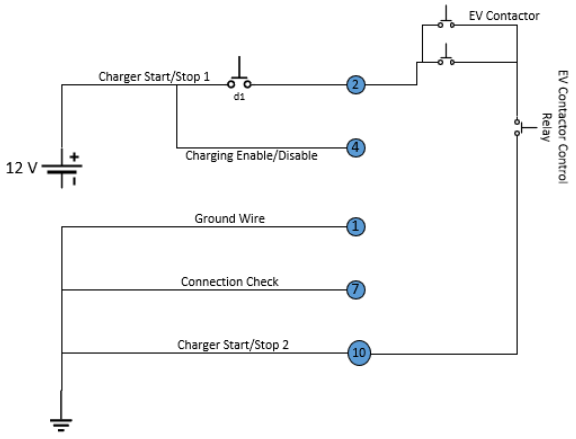

Figure 6-9 Discharging Interface.

Figure 6-10 shows the EV contactor control relay. This relay is responsible of opening/closing the EV contactor from the car side.

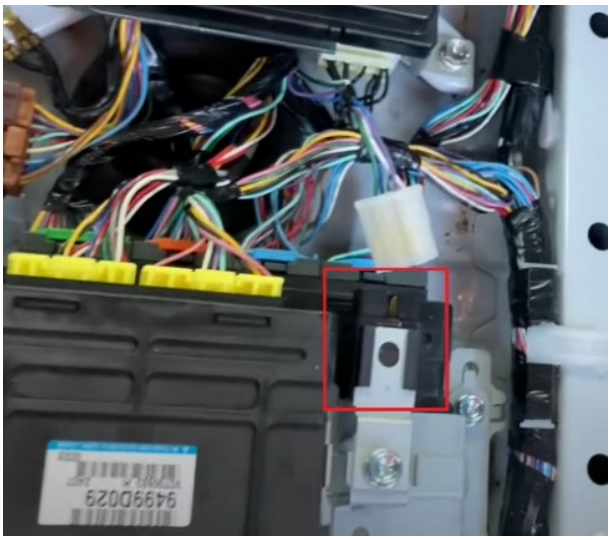

Figure 6-10 EV contactor control relay.

Figure 6-11 shows a connector that provides the connection number 2 in Figure 6-2. This connection connects the EV contactor control relay and charger start/stop 'd1'. By jumpering the top two terminals with each other, the internal connection of the EV for discharging can be manually activated. In addition, instead of creating an internal connection, two conductor wires can be connected to blue and white wires (top two terminals) to implement a switch button for activating charger start/stop 1. Figure 6-12 shows the connection of the EV contactor control relay's connector with conductor wires and switch.

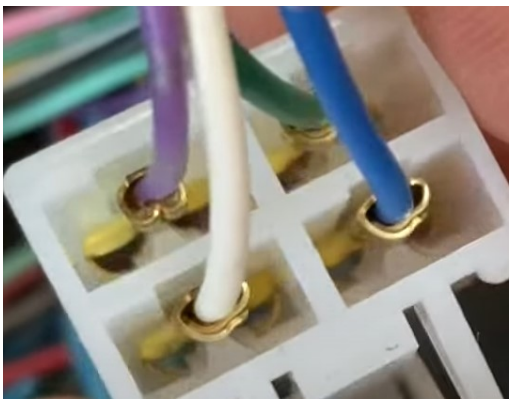

Figure 6-11 CHAdeMO connector of EV Car.

After the switch is implemented, the CHAdeMO connector can be plugged into the DC fast charging port. By turning on the switch, which manually closes the EV contactor, the EV battery voltage appears on terminals 5 and 6 of the CHAdeMO connector. Now the EV is ready for V2X operations.

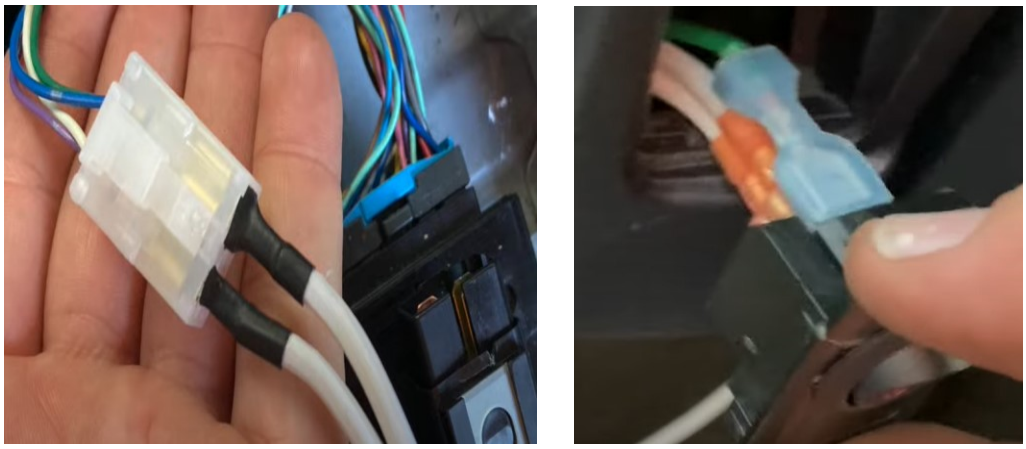

Figure 6-12 Switch and conductor wires.

Accidentally, if someone tries to turn on the EV while the discharging operation is established, the EV won’t turn on. Instead, a charger connected sign will be seen on the dashboard of the EV.

6.4.2 Enabling Nissan Leaf Battery Discharging Using Setec-Power V2H Inverter

Figure 6-13 Setec Power V2L Charger [48]

Due to the high protection features of the Nissan Leaf, the manual configuration option performed in the previous section cannot be used for the Nissan Leaf. The reason for this is that the controller area network (CAN) bus system which handles the charging and discharging operations. The controller area network (CAN) is a message-based serial field bus technology, which is used to decrease wiring harnesses and control the vehicle's electronics system [47]. Since this system is a control system that cannot be modified due to copyright reasons and cannot be used without a license, the Setec-Power V2H inverter can be used to obtain power from the Nissan Leaf Battery. Setec-Power has manufactured a single-phase inverter equipped with CAN bus protocol specifically for Nissan Leaf to enable its discharging feature. This can provide an alternative solution for V2L and V2H with Nissan Leaf in Canada. The Setec-Power V2H converter's specifications are shown in Table 6 4, and Figure 6-14 shows the converter in use with a Nissan Leaf in V2L configuration.

Table 6-4 Setec Power V2L Inverter specifications [48]

Rated input voltage	450 V
Rated capacity	6 kVA
Rated output power	4.2 kW
Rated output current	Max 38A/21A
Output frequency	50/60 Hz

Figure 6-14 the car and Setec power charger connection [48].

6.5 Experimental Results

Unfortunately, the purchased 2018 Nissan Leaf for the solar house project got an accident and went total loss. For this reason, the experimental results couldn't be performed with an electric vehicle. However, the EV replacement purchase has been done, and the new Nissan Leaf is expected to arrive in mid or end November 2023. Also, the Setec-Power converter for Nissan Leaf has been ordered and expected to arrive in early or mid December 2023. This will allow testing the designed inverter with the Nissan Leaf at the solar house for V2L and V2H, with the CAN bus protocol is being taking care of by the Setec-Power converter.

7 Conclusion and Future Work

7.1 Conclusion

This research is done to explain the V2L system with the Nissan Leaf electric car. The simulation results have shown that the topologies and the control circuits used in this research are adequate resemblance of the real system. The results derived from the experimental setup were exactly as expected and matched the simulation results.

A summary of Chapters 1 to 6 is presented below.

Chapter 1. In this chapter, emergency powers that can be used in blackout and emergencies were mentioned. The importance of electric cars and V2L, V2H, and V2G systems as one of the emergency powers are explained.

Chapter 2. In this chapter, the Future Building Laboratory (FBL), where the designed V2L system will be used, was presented. The electrical system and the loads of the FBL was presented. The transient and steady-state currents of some loads in the FBL are examined.

Chapter 3. In this chapter, the battery types used in electric vehicles are mentioned. The characteristics and modelling of the Nissan Leaf battery were examined. First and second-order battery models were examined and compared to the real Nissan Leaf battery's characteristics.

Chapter 4. In this chapter, the vehicle-to-load (V2L) circuit components were simulated and designed. A frequency domain analysis of the V2L circuit was conducted and the transfer functions of the system were obtained. Based on that, suitable proportional integral controllers were selected and designed. Finally, the whole system with the control part was simulated and the results were analyzed.

Chapter 5. In Chapter 5, the V2L circuit, which was designed and simulated in chapter 4, was experimentally tested in the PEER Group power laboratory. Experimental results were analyzed and compared with simulation results.

Chapter 6. In this chapter, the various V2L and V2H methods using Nissan Leaf at the solar house were explored. The ChAdeMO working principle and the enabling of EVs' discharging feature were dissuaded and explained.

7.2 Future Work

For the future work, the V2L and V2H experimental measurements at the solar house using a Nissan Leaf can be carried out as explained in Chapter 6. The integration of the V2H system with the other renewable energy sources at the FBL can be investigated. In addition, the closed-loop control technique proposed in chapter 4 can be tested experimentally via a DSP microcontroller.

8 References

[1] "Natural Hazards of Canada [Online]. Available: https://www.publicsafety.gc.ca/cnt/mrgnc-mngmnt/ntrl-hzrds/index-en.aspx [Accessed April 2023].

[2] Weather-Related Blackouts Doubled Since 2003: Report [Online]. Available: https://www.climatecentral.org/news/weather-related-blackouts-doubled-since-2003-report-17281 [Accessed April 2023].

[3] Top Five Backup Power Options for Your Home Electrical System [Online]. Available: https://trustedpros.ca/articles/electrical/top-five-backup-power-options-for-your-home-electrical-system [Accessed May 2023].

[4] Fuel Cells [Online]. Available: https://www.energy.gov/eere/fuelcells/fuelcells#:~:text=Fuel%20cells%20work%20like%20batteries,)—sandwiched%20around%20an%20electrolyte. [Accessed May 2023].

[5] Mousavi G., S. Mohammad & Faraji, Faramarz & Majazi, Abbas & Al-Haddad, Kamal. (2017). A comprehensive review of Flywheel Energy Storage System technology. Renewable and Sustainable Energy Reviews. 67. 477-490. 10.1016/j.rser.2016.09.060.

[6] Socaciu, Lavinia. (2012). Thermal energy storage: an overview. Appl Math Mech. 55. 785-793.

[7] Y. Zhou and X. Li, "Vehicle to grid technology: A review," 2015 34th Chinese Control Conference (CCC), Hangzhou, China, 2015, pp. 9031-9036, doi: 10.1109/ChiCC.2015.7261068.

[8] Tan, Kang & Ramachandaramurthy, Vigna K. & Yong, Jia Ying. (2016). Integration of electric vehicles in smart grid: A review on vehicle to grid technologies and optimization techniques. Renewable and Sustainable Energy Reviews. 53. 720-732. 10.1016/j.rser.2015.09.012.

[9] M. El Chehaly, O. Saadeh, C. Martinez and G. Joos, "Advantages and applications of vehicle to grid mode of operation in plug-in hybrid electric vehicles," 2009 IEEE Electrical Power & Energy Conference (EPEC), Montreal, QC, Canada, 2009, pp. 1-6, doi: 10.1109/EPEC.2009.5420958.

[10] Liu, C., Chau, K. T., Wu, D., & Gao, S. (2013). Opportunities and Challenges of Vehicle-to-Home, Vehicle-to-Vehicle, and Vehicle-to-Grid Technologies. Proceedings of the IEEE, 101(11), 2409–2427. doi:10.1109/jproc.2013.2271951

[11] The All-New 2023 Nissan Leaf [Online]. Available: https://www.nissan.ca/vehicles/electric-cars/leaf.html [Accessed April 2023].

[12] MITSUBISHI MOTORS IMPLEMENT FIRST 'VEHICLE TO GRID' PILOT ON DUTCH MARKET WITH MITSUBISHI OUTLANDER PHEV [Online]. Available: https://www.mitsubishi-motors.com/en/newsrelease/2017/detail1082.html [Accessed April 2023].

[13] What's Bidirectional Charging and Which EVs Offer It? [Online]. Available: https://www.cars.com/articles/whats-bidirectional-charging-and-which-evs-offer-it-457608/ [Accessed April 2023].

[14] Fazel Mohammadi, Mehrdad Saif, "A comprehensive overview of electric vehicle batteries market, "e-Prime - Advances in Electrical Engineering, Electronics and Energy,Volume 3,2023,100127,

[15] Ding, Y., Cano, Z.P., Yu, A. et al. Automotive Li-Ion Batteries: Current Status and Future Perspectives. Electrochem. Energ. Rev. 2, 1–28 (2019).

[16] How do electric car batteries work? [Online]. Available: https://www.energysage.com/electric-vehicles/101/how-do-electric-car-batteries-work/ [Accessed May 2023].

[17] Deng, Da. (2015). Li-ion batteries: basics, progress, and challenges. Energy Science & Engineering. 3. 10.1002/ese3.95.

[18] Tie, S. F., & Tan, C. W. (2013). A review of energy sources and energy management system in electric vehicles. Renewable and Sustainable Energy Reviews, 20, 82–102. doi:10.1016/j.rser.2012.11.077

[19] Burke, A. F. (2007). Batteries and Ultracapacitors for Electric, Hybrid, and Fuel Cell Vehicles. Proceedings of the IEEE, 95(4), 806–820. doi:10.1109/jproc.2007.892490

[20] Inside the race for a car battery that charges fast — and won't catch fire. [Online]. Available: https://www.washingtonpost.com/technology/2022/05/18/solid-state-batteries-electric-vehicles-race/ [Accessed June 2023].

[21] Li, C., Wang, Z., He, Z., Li, Y., Mao, J., Dai, K., … Zheng, J. (2021). An advance review of solid-state battery: Challenges, progress and prospects. Sustainable Materials and Technologies, 29, e00297. doi:10.1016/j.susmat.2021.e00297

[22] Manthiram, A., Chung, S.-H., & Zu, C. (2015). Lithium-Sulfur Batteries: Progress and Prospects. Advanced Materials, 27(12), 1980–2006. doi:10.1002/adma.201405115

[23] The 5 Most Common Types of EV Batteries Explained [Online]. Available: https://www.makeuseof.com/different-types-ev-batteries-explained/ [Accessed May 2023].

[24] Nissan Leaf [Online]. Available: https://ev-database.org/car/1106/Nissan-Leaf [Accessed May 2023].

[25] Nikola Rakanovic (2020). Modelling of lithium battery and V2G charger for degradation assessment [Unpublished bachelor's thesis]. Technical University of Denmark

[26] Varela Barreras, Jorge & Pinto, Cláudio & Castro, Ricardo & Schaltz, Erik & Swierczynski, Maciej & Andreasen, Søren & Araújo, Rui. (2015). An Improved Parameterization Method for Li-ion Linear Static Equivalent Circuit Battery Models Based on Direct Current Resistance Measurement. 10.1109/SMART.2015.7399223.

[27] Zhang, L., Peng, H., Ning, Z., Mu, Z., & Sun, C. (2017). Comparative Research on RC Equivalent Circuit Models for Lithium-Ion Batteries of Electric Vehicles. Applied Sciences, 7(10), 1002. doi:10.3390/app7101002

[28] Madani, Seyed Saeed & Schaltz, Erik & Kær, Søren. (2019). An Electrical Equivalent Circuit Model of a Lithium Titanate Oxide Battery. Batteries. 5. 31. 10.3390/batteries5010031.

[29] J. Wang, H. Wu, T. Yang, L. Zhang and Y. Xing, "Bidirectional Three-Phase DC–AC Converter With Embedded DC–DC Converter and Carrier-Based PWM Strategy for Wide Voltage Range Applications,"

in IEEE Transactions on Industrial Electronics, vol. 66, no. 6, pp. 4144-4155, June 2019, doi: 10.1109/TIE.2018.2866080.

[30] Zaohong Yang, "Bidirectional DC-to-AC inverter with improved performance," in IEEE Transactions on Aerospace and Electronic Systems, vol. 35, no. 2, pp. 533-542, April 1999, doi: 10.1109/7.766935.

[31] Z. Yu, A. Mohammed and I. Panahi, "A review of three PWM techniques," Proceedings of the 1997 American Control Conference (Cat. No.97CH36041), Albuquerque, NM, USA, 1997, pp. 257-261 vol.1, doi: 10.1109/ACC.1997.611797.

[32] Namboodiri, Anuja, and Harshal S. Wani. "Unipolar and bipolar PWM inverter." International Journal for Innovative Research in Science & Technology 1.7 (2014): 237-243.

[33] Wu, X.; Gao, X.; Wang, J.; Li, Z.; Du, S.; Gao, S.; Li, F.; Du, J.; Shchurov, N.I.; Zhang, X. Advances in Modeling and Suppression Methods of EMI in Power Electronic Converters of Third-Generation Semiconductor Devices. Electronics 2023, 12, 2348.

[34] S. G. Solanki, M. Ramasamy, S. Manzoor and U. K. R. Ganesalingam, "Design & Development for OFF grid Solar Inverter," 2018 IEEE 4th International Symposium in Robotics and Manufacturing Automation (ROMA), Perambalur, India, 2018, pp. 1-5, doi: 10.1109/ROMA46407.2018.8986709.

[35] A. A. Alrimali, A. Mohamed Aljehaimi, A. S. Hussein and P. Pillay, "Controller Design for an Off-Grid Photovoltaic Solar Inverter," 2021 IEEE 1st International Maghreb Meeting of the

[36] Kim, Hyosung, and Seung-Ki Sul. "A novel filter design for output LC filters of PWM inverters." Journal of Power Electronics 11.1 (2011): 74-81.

[37] Hurng-Liahng Jou, Kuen-Der Wu, Jinn-Chang Wu, Wen-Jung Chiang, “A three-phase four-wire power filter comprising a three-phase three- wire active power filter and a zig-zag transformer,” IEEE Transactions on Power Electronics, Vol.23, No.1, pp.252-259, Jan. 2008.

[38] J. Hobraiche, J. –P. Vilain, P. Macret, N. Patin, “A new PWM strategy to reduce the inverter input current ripples,” IEEE Transactions on Power Electronics, Vol.24, No.1, pp/172-180, Jan. 2009.

[39] N. M. Abdel-Rahim and J. E. Quaicoe, "Analysis and design of a multiple feedback loop control strategy for single-phase voltage-source UPS inverters," in IEEE Transactions on Power Electronics, vol. 11, no. 4, pp. 532-541, July 1996, doi: 10.1109/63.506118.

[40] Ghosh, A., Banerjee, S., Sarkar, M.K. and Dutta, P., 2016. "Design and implementation of type-II and type-III controller for DC-DC switched mode boost converter by using K-factor approach and optimisation techniques" . IET Power Electronics, 9(5), pp.938-950.

[41] Saurav, S., & Ghosh, A. (2021). Design and Analysis of PID, Type II and Type III controllers for Fourth Order Boost Converter. 2021 7th International Conference on Electrical Energy Systems (ICEES). doi:10.1109/icees51510.2021.93836

[42] Cherati, S. M., Azli, N. A., Ayob, S. M., & Mortezaei, A. (2011). Design of a current mode PI controller for a single-phase PWM inverter. 2011 IEEE Applied Power Electronics Colloquium (IAPEC). doi:10.1109/iapec.2011.5779864

[43] M. Yilmaz and P. T. Krein, "Review of Battery Charger Topologies, Charging Power Levels, and Infrastructure for Plug-In Electric and Hybrid Vehicles," in *IEEE Transactions on Power Electronics*, vol. 28, no. 5, pp. 2151-2169, May 2013, doi: 10.1109/TPEL.2012.2212917.

[44] Jar, Ben & Watson, Neville & Miller, Allan. (2016). Rapid EV Chargers: Implementation of a Charger.

[45] Anegawa, Takafumi. (2011). Safety design of CHAdeMO quick charging system. World Electric Vehicle Journal. 4. 855-859. 10.3390/wevj4040855.

[46] https://www.theverge.com/2022/9/12/23349971/nissan-leaf-bidirectional-charging-approved-v2h-v2g-fermata-energy

[47] A. A. Salunkhe, P. P. Kamble and R. Jadhav, "Design and implementation of CAN bus protocol for monitoring vehicle parameters," 2016 IEEE International Conference on Recent Trends in Electronics, Information & Communication Technology (RTEICT), Bangalore, India, 2016, pp. 301-304, doi: 10.1109/RTEICT.2016.7807831.

[48] https://www.setec-power.com/vehicle-to-home-v2h-6kw-charger/